



National Library
of Canada

Bibliothèque nationale
du Canada

Acquisitions and
Bibliographic Services Branch

Direction des acquisitions et
des services bibliographiques

395 Wellington Street
Ottawa, Ontario
K1A 0N4

395, rue Wellington
Ottawa (Ontario)
K1A 0N4

Voitelo - Votre référence

Cartão - Nota de referência

NOTICE

AVIS

The quality of this microform is heavily dependent upon the quality of the original thesis submitted for microfilming. Every effort has been made to ensure the highest quality of reproduction possible.

La qualité de cette microforme dépend grandement de la qualité de la thèse soumise au microfilmage. Nous avons tout fait pour assurer une qualité supérieure de reproduction.

If pages are missing, contact the university which granted the degree.

S'il manque des pages, veuillez communiquer avec l'université qui a conféré le grade.

Some pages may have indistinct print especially if the original pages were typed with a poor typewriter ribbon or if the university sent us an inferior photocopy.

La qualité d'impression de certaines pages peut laisser à désirer, surtout si les pages originales ont été dactylographiées à l'aide d'un ruban usé ou si l'université nous a fait parvenir une photocopie de qualité inférieure.

Reproduction in full or in part of this microform is governed by the Canadian Copyright Act, R.S.C. 1970, c. C-30, and subsequent amendments.

La reproduction, même partielle, de cette microforme est soumise à la Loi canadienne sur le droit d'auteur, SRC 1970, c. C-30, et ses amendements subséquents.

Canada

**Structural analysis of airborne flux traces and their link
to remote sensing of vegetation and surface temperature.**

by

Paulo Henrique Caramori

McGill University, Montreal

October, 1992

A thesis submitted to
the Faculty of Graduate Studies and Research
in partial fulfillment of the requirements for
the degree of Doctor of Philosophy

© Paulo Henrique Caramori, 1992



National Library
of Canada

Acquisitions and
Bibliographic Services Branch

395 Wellington Street
Ottawa, Ontario
K1A 0N4

Bibliothèque nationale
du Canada

Direction des acquisitions et
des services bibliographiques

395, rue Wellington
Ottawa (Ontario)
K1A 0N4

Your file / Votre référence

Our file / Notre référence

The author has granted an irrevocable non-exclusive licence allowing the National Library of Canada to reproduce, loan, distribute or sell copies of his/her thesis by any means and in any form or format, making this thesis available to interested persons.

L'auteur a accordé une licence irrévocable et non exclusive permettant à la Bibliothèque nationale du Canada de reproduire, prêter, distribuer ou vendre des copies de sa thèse de quelque manière et sous quelque forme que ce soit pour mettre des exemplaires de cette thèse à la disposition des personnes intéressées.

The author retains ownership of the copyright in his/her thesis. Neither the thesis nor substantial extracts from it may be printed or otherwise reproduced without his/her permission.

L'auteur conserve la propriété du droit d'auteur qui protège sa thèse. Ni la thèse ni des extraits substantiels de celle-ci ne doivent être imprimés ou autrement reproduits sans son autorisation.

ISBN 0-315-87848-7

Canada

Date: _____

Université McGill
FACULTÉ DES ÉTUDES SUPÉRIEURES ET DE LA RECHERCHE

NOM DE L'AUTEUR: _____

DÉPARTEMENT: _____ GRADE: _____

TITRE DE LA THÈSE: _____

Par la présente, l'auteur accorde à l'université McGill l'autorisation de mettre cette thèse à la disposition des lecteurs dans une bibliothèque de McGill ou une autre bibliothèque, soit sous la forme actuelle, soit sous forme d'une reproduction. L'auteur détient cependant les autres droits de publications. Il est entendu, par ailleurs, que ni la thèse, ni les longs extraits de cette thèse ne pourront être imprimés ou reproduits par d'autres moyens sans l'autorisation écrite de l'auteur. La présente autorisation entre en vigueur à la date indiquée ci-dessous à moins que l'auteur demande un délai d'une année lors de la soumission de la thèse.

Adresse permanente de l'auteur:

Signature de l'auteur: _____

Date: _____

Suggested short title:

Airborne flux traces versus remote sensing of the surface.

General Abstract

Paulo Henrique Caramori

This thesis examines the link between airborne flux estimates of CO₂, sensible heat, and water vapor, and surface parameters retrieved by remote sensing. **Chapter 1** analyses the relationship between surface temperature and vegetation indices, obtained from the Advanced Very High Resolution Radiometer on board of NOAA-9 and -10 satellites, and fluxes of sensible heat, latent heat, and CO₂, estimated from aircraft. Linear relationships between CO₂ and the Normalized Difference Vegetation Index (NDVI) or the Simple Ratio vegetation index (SR) are found on a daily basis, but a highly nonlinear relationship appears for the seasonal variation. Latent Heat fluxes showed the poorest correlations with surface parameters. A seasonal linear relationship appeared between sensible heat and NDVI. Local extreme flux values due to the intermittency of boundary layer dynamics largely contribute to lower the correlations; such variations are the reason for the difficulties in relating fluxes obtained from single overpasses and over short distances to fixed points at the surface. This problem is further examined in **Chapter 2**, in which conditional sampling of airborne flux estimates is used to characterize the turbulent structures that are carrying flux, and their link to the surface. The analysis confirms that few extreme events may carry a significant fraction of the flux. Missing or hitting one of these structures may translate into very large oscillations on the flux estimate that are often not directly coupled to surface characteristics. A much clearer surface 'signature' emerges when measurements are taken within the surface layer, since the reorganization of turbulent structures that takes place with increasing height will result in a merging of the signature that came from different sources at the surface. This helps to explain some of the poor correlations obtained in Chapter 1 and reinforces the need for a better understanding of the distributions of these turbulent structures over different ecosystems, their evolution with height and their dependence on boundary layer and/or

surface properties. This objective is approached in **Chapter 3**, in which the statistical distributions of the structures are described for three ecosystems and several heights within the boundary layer. It is found that structure diameter and spacing can be approximated by a lognormal distribution for all situations evaluated. The average plume diameter and spacing increase with height, whereas the number of plumes decreases as a power function of height. This is a result of intensive reorganization that takes place near the surface, with dissipation of weaker structures and merging of dominant plumes into larger ones. The results again show that at higher altitudes the information contained in a single plume may originate from several sources at the surface, and assigning such information to a given satellite pixel will result in poor correlations in many cases. The statistics presented in this chapter provide a unique database against which models of near-surface boundary layer structures can be verified.

Résumé

Le lien entre le flux aérien estimé de CO_2 , la chaleur sensible, la vapeur d'eau et des paramètres de surface obtenus par télédétection est examiné dans cette thèse. Le chapitre 1 analyse la relation entre la température de surface et des indices de végétation obtenus grâce au radiomètre à très haute résolution à bord des satellites NOAA-9 et -10, et les flux de chaleur sensible, chaleur latente et CO_2 mesurés à bord d'un avion. Des relations linéaires entre le CO_2 et l'indice de différence normalisé de végétation (NDVI) ont été trouvés sur une base journalière mais la relation est tout à fait non linéaire sur une base saisonnière. Les corrélations les plus mauvaises ont été obtenus entre les flux de chaleur latente et les paramètres de surface. Une relation linéaire entre la chaleur sensible et le NDVI a été trouvée. Des valeurs de flux local extrêmes dues à l'intermittances des turbulences ont largement contribué à l'abaissement des corrélations. De telles variations sont à la base des difficultés à relier les flux obtenus à partir de simples vols en avion faits sur de courtes distances à des points fixes de la surface. Ce problème est examiné plus en profondeur dans le chapitre 2, dans lequel un échantillonnage conditionnel de l'estimé des flux aériens est utilisé pour caractériser les structures turbulentes qui portent les flux et leurs liens avec la surface. L'analyse confirme que certains événements extrêmes peuvent porter une partie non négligeable du flux. Manquer ou rencontrer une de ces structures peut donner lieu à des oscillations très importantes de l'estimation du flux qui ne sont souvent pas directement associées aux caractéristiques de surface. Une signature de surface beaucoup plus claire apparaît quand les mesures sont prises à l'intérieur de la couche de surface puisque la réorganisation des structures turbulentes qui se fait quand la hauteur augmente entraîne un mélange des 'signatures' qui viennent de différentes sources à la surface. Ceci a permis d'expliquer certaines mauvaises corrélations obtenues dans le chapitre 1 et renforce le besoin d'une meilleure compréhension des distributions de ces structures turbulentes au dessus de différents écosystèmes ainsi que de leur évolution comme fonction de l'hauteur au dessus

du sol et de leur dépendance des couches limites et/ou des propriétés de surface. Ceci est l'objectif du chapitre 3 dans lequel les distributions statistiques des structures sont décrites pour trois différents écosystèmes et pour différentes hauteurs de la couche limite. Il y a été trouvé que le diamètre et la distance entre les structures peuvent être approximés par une distribution log-normale. Le diamètre moyen des structures et leur espacement augmente avec la hauteur mais le nombre de structures diminue en suivant une fonction de la hauteur. Ceci résulte de la réorganisation intensive qui se passe près de la surface et qui entraîne la dissipation des structures les plus faibles et le mélange des structures dominantes pour des structures très larges. A nouveau, les résultats montrent qu'à des altitudes plus grandes, l'information contenue dans une structure unique peut venir de plusieurs sources à la surface et assigner une telle information à un pixel de satellite donné donne de mauvaises corrélations dans de nombreux cas. Les statistiques présentées dans ce chapitre forment une base de données unique avec laquelle les modèles sur les structures des couches limites près de la surface peuvent être vérifiés.

Acknowledgements

First and foremost, I would like to express my sincere gratitude to Professor Peter H. Schuepp, for his invaluable support, encouragement, and assistance throughout the course of this study.

I also wish to extend my appreciation to the following key institutions and individuals who were fundamental for the completion of this project:

Instituto Agronômico do Paraná (IAPAR) for sanctioning my official study leave, and Empresa Brasileira de Pesquisa Agropecuária (EMBRAPA) and Inter-American Institute for Co-operation in Agriculture (IICA) for awarding me a scholarship grant. The efficient administration of my scholarship by Mr. Ernani Fiori, the representative of IICA in Canada, is greatly appreciated.

Dr. Raymond L. Desjardins from Agriculture Canada, Ottawa, for the encouraging discussions, suggestions, and support.

J. I. MacPherson from the Institute for Aerospace Research and the Twin Otter crew for collecting the unique database that I had the privilege to work with.

Dr. Josef Chilar and Canada Centre for Remote Sensing for the fruitful interactions and logistic support. The help from Manon Desforges and Davinder Manak on the satellite image processing is also highly acknowledged.

Many thanks to Anne Weill for helping to prepare the French summary.

My sincere thanks are also extended to all my friends and their families: Rogério, Mazé, Eider, Vanda, Perotto, Rosângela, Deli, Luci, Estelle, Xavier, Mariolga, Pepe, Clarete, Samuel, Lin, Guo Ya, Constance, and Mike Duncan, for all the entertaining moments and support provided during these years.

I have also high esteem and regard for my children Samantha and Thiago, my parents, and brothers, for their love, affection, invigorating messages, and understanding when I had to leave them to pursue my Ph.D. studies.

I am very thankful to Canada and all the friends we made during these years. Our two canadian children, Daniel and Fernando, certainly will have plenty of reasons to be proud of their country.

Finally, I wish to express my deepest gratitude to my dear wife Lázara and my sons Daniel and Fernando, for their profound love, joy and support that gave me strength to complete this project.

I wish to dedicate this thesis to the memory of
Dr. MAMDOUH FANOUS,
a great friend and excellent teacher.

Claims to Originality

The present thesis provides the following original contributions to knowledge:

1) The relationship between CO₂ uptake and vegetation indices, based on analyses of the most extensive database published to date, proved to be highly nonlinear over very active vegetating surfaces. This goes against previously held opinion, as exemplified by the findings of Sellers et al. (1987), which was generally based on a few measured values.

2) This is the first work to analyze the relationship between vegetation indices and CO₂ flux on a seasonal basis.

3) This is the first work to analyze systematically the link between surface characteristics and coherent turbulent structures within the atmospheric boundary layer over different ecosystems.

4) The statistical analysis performed on an extensive database of rising plumes and spacing between plumes of water vapor and sensible heat, over different ecosystems and at several heights within the atmospheric boundary layer, show for the first time the broad validity of approximations based on the lognormal distribution.

5) Extensive statistical analysis of the coherent turbulent structures that dominate transfer over the ecosystems investigated in these studies show remarkable consistency, suggesting that such structures may be determined more by boundary layer dynamics than surface characteristics.

Thesis statement

This thesis is divided into three main topics presented in separated chapters, with relevant literature review incorporated within each Chapter.

The analyses of CO₂ flux versus vegetation indices presented in Chapter 1 have been published. The paper reference is: Cihlar, J., Caramori, P. H., Schuepp, P. H., Desjardins, R. L., and MacPherson, J. I. Relationship between satellite-based vegetation indices and aircraft-based CO₂ measurements Journal of Geophysical Research, 97(D17):18,515-18,522, 1992. Dr. Cihlar supervised the satellite image processing, which was done by this author and a summer student. All the analyses, including aircraft data processing, interpretation, and relationship to satellite parameters, were performed by this author. The analyses referring to sensible heat and water vapor fluxes within this chapter were done by this author and have not been published yet.

The content of Chapter 2 has been submitted as a paper to the Journal of Climate (accepted subject to minor revisions); all the analyses were performed by this author. The paper is co-authored by this author, P.H. Schuepp, R.L. Desjardins, and J.I. MacPherson. Dr. Desjardins and MacPherson helped in the discussions and data collection, and Dr. Schuepp contributed with discussions and editing.

The content of chapter 3 was entirely prepared by this author.

Professor P. H. Schuepp has supervised all the work presented in this thesis.

Table of contents

General Abstract	ii
Résumé	iv
Acknowledgements	vi
Claims to Originality	ix
Thesis statement	x
List of Tables	xiv
List of figures	xv
General Introduction	1
References	2
Chapter 1:	4
Abstract	4
1.1. INTRODUCTION	6
1.2. METHODOLOGY	7
1.2.1. Description of the study area	7
1.2.2. Satellite Data	7
1.2.2.1. Processing and calibration	7
1.2.3. Footprint correction	13
1.2.4. Aircraft Data	16
1.2.4.1. Data collection	16
1.2.4.2. Smoothing of RR flux data	17
1.2.4.3. Long wavelength contribution to the flux	19
1.2.5. Estimation of regional evapotranspiration	22

1.3. RESULTS	26
1.3.1. CO ₂ Flux versus NDVI and SR	26
1.3.2. Sensible and Latent Heat flux versus NDVI and Surface Temperature (TS)	32
1.4. DISCUSSION	40
1.5. SUMMARY AND CONCLUSIONS	45
1.6. REFERENCES	46
 Connecting Statement	 50
 Chapter 2	 51
Abstract	51
2.1. INTRODUCTION	53
2.2. MATERIALS AND METHODS	55
2.2.1. Aircraft instrumentation and data collection	55
2.2.2. Eddy correlation technique and quadrant analysis	56
2.2.3. Defragmentation	59
2.2.4. Definition of 'extreme events'	61
2.2.5. Linear vs. non-linear detrending	64
2.3. RESULTS AND DISCUSSION	67
2.3.1. Effect of detrending	67
2.3.2. Quadrant contribution to the flux	72
2.3.3. Structure size and flux contribution	75
2.3.4. Spacing between structures	82
2.3.5. Flight altitude vs. flux 'signature'	82

2.4. SUMMARY AND CONCLUSIONS	92
2.5. REFERENCES	94
Connecting Statement	98
Chapter 3	99
Abstract	99
3.1. INTRODUCTION	101
3.2. MATERIALS AND METHODS	103
3.2.1. Aircraft instrumentation and data processing	103
3.2.2. Threshold values vs flux	105
3.2.3. Distribution of plume diameter and spacing	111
3.3. RESULTS AND DISCUSSION	113
3.3.1. Distributions of plume diameter and spacing	113
3.3.2. Mean plume diameter versus height	113
3.3.3. Stability versus plume size	119
3.3.4. Line Density of Plumes	121
3.3.5. Mean spacing versus height	124
3.3.6. Flux contribution versus height	124
3.4. SUMMARY AND CONCLUSIONS	130
3.5. REFERENCES	132
General Conclusions	135
Suggestions for future studies	137
Appendix	138

List of Tables

Table 1.1. Description of satellite data used	9
Table 1.2. Summary of the aircraft data used	9
Table 1.3. Linear equations and regression coefficients (r) for the relationships between Sensible and latent heat fluxes versus surface temperature (TS) and Normalized Difference Vegetation Index (NDVI)	33
Table 2.1. Summary of the run characteristics: site, flight ID, start time, mean flight altitude (z), incident shortwave radiation ($K\downarrow$), friction velocity (u_*), stability (z/L), and ratio of flight level to boundary layer height (z/z_i) ...	57
Table 2.2. Summary of 'quadrant' analysis: site, quadrant (1 = excess up, 2 = excess down, 3 = deficit down, 4 = deficit up), frequency and flux/time fractions of events in each quadrant. Standard deviations are given in brackets. The runs specified in Table 2.1 were used in the calculations	75
Table 3.1. Site, average flight height, combined run length, shortwave solar radiation ($k\downarrow$), sensible heat flux (H), sensible heat flux (LE), stability parameter (z/L), and ratio of flight level to boundary layer height (z/z_i). The range of values observed for $K\downarrow$, H , LE , and z/L are given	104

List of Figures

Figure 1.1. Location of the study area. The F-West and F-East are end-points of the regional runs.	8
Figure 1.2. Relative contribution from upwind pixels for the flying height of 150m above ground.	15
Figure 1.3. Cospectra of (a) CO ₂ flux, (b) sensible heat flux, and (c) water vapor flux for the regional runs on four days	20
Figure 1.4. Percentage of flux remaining after filtering at 3 km	21
Figure 1.5. Satellite NDVI versus aircraft CO ₂ flux on four days in 1987 ...	28
Figure 1.6. Satellite Normalized difference vegetation index (NDVI) versus aircraft CO ₂ flux for all days combined	29
Figure 1.7. Satellite Simple ratio vegetation index (SR) versus aircraft CO ₂ flux for the regional runs. Data from all days are combined	30
Figure 1.8. Satellite SR versus aircraft CO ₂ flux for the regional runs on four dates in 1987	31
Figure 1.9. Relationship between Radiative surface temperature (TS) and the Normalized difference vegetation index (NDVI) on three combined dates in 1987	35
Figure 1.10. a) Relationship between Sensible heat flux and Radiative surface temperature (TS) during three dates in 1987. b) Relationship between Latent heat flux and TS	36
Figure 1.11. a) Seasonal relationship between Sensible heat flux and Normalized difference vegetation index (NDVI). b) Seasonal relationship between Latent heat flux and NDVI	37
Figure 1.12. Regional variability of Latent heat fluxes on three different dates. Date represent an area of 75 by 10 km	38
Figure 2.1. Scatter plot of vertical wind fluctuation (w') versus water vapor	

concentration fluctuation (q')	60
Figure 2.2. Cumulative flux contribution versus threshold function ϕ (values are sorted in ascending order). Threshold at 95% of flux fraction is indicated by straight lines	63
Figure 2.3. Normalized Difference Vegetation Index (NDVI) over the FIFE site on July 28, 1989. Data were obtained from the afternoon overpass of the NOAA-9 satellite. Notice pronounced contrast between SW (dry) and SE (moist) corners	64
Figure 2.4. Mixing ratio of water vapor over a 15 km run at the S end of the FIFE site on July 28, 1989 (run JL281 in Table 1). Linear (least squares) and non-linear (Fourier approximation with truncation after the 2nd term) detrending are illustrated	68
Figure 2.5. Effect of detrending on structural analysis of run JL281 (Fig. 2.4). The distribution of structures within the four modes of transport (excess up/down, deficit up/down) is plotted along with contributions to the mean flux estimate after detrending	69
Figure 2.6. Effect of detrending of water vapor concentration on mean flux estimates over the FIFE site	70
Figure 2.7. Linear correlation between flux fraction of thermal plumes and Normalized Difference Vegetation Index (NDVI) over the FIFE site on July 28, 1989. Each point represents the cumulative flux fraction from the excess-up mode over a 5-km segment, from either the SW (dry) or the SE (moist) end of the runs	73
Figure 2.8. Frequency distribution of structure sizes over wet and dry areas of the FIFE and Wetland sites. FIFE data are separated into W (dry) and E (moist) sections.	77
Figure 2.9. Frequency distribution of structure sizes over irrigated (moist) and non-irrigated (dry) areas of the San Joaquin Valley	78
Figure 2.10. Relative contribution from all four modes of transport (excess up/down, deficit up/down) versus structure size; (a) over moist and dry areas of the FIFE site and (b) over irrigated and non-irrigated areas of the San Joaquin Valley	80

Figure 2.11. Relative flux contribution from moisture plumes (excess up) versus structure size over wet and dry areas of the FIFE site	81
Figure 2.12. Spacing (m) between moisture plumes over the FIFE site	83
Figure 2.13. Ratio of Infrared (IR) over Red (R) reflected solar radiation (VI), difference between radiative surface temperature and air temperature ($T_s - T_a$), and distribution of thermal and moisture plumes over a 15-km mixed grassland and agricultural land near the FIFE site. Mean flight altitude is 150 m. (Width of plume 'box' indicates duration, and area the relative flux contribution)	88
Figure 2.14. Surface characteristics and plume distribution (as defined in Figure 2.13) for a 15-km run over the S end of the FIFE site. Mean flight altitude is 90 m.	89
Figure 2.15. Surface characteristics and plume distribution for a 12-km run over the San Joaquin Valley. Mean flight altitude is 30 m	87
Figure 2.16. Difference between radiative surface temperature and air temperature ($T_s - T_a$), Ratio of Infrared (IR) over Red (R) reflected solar radiation (VI), and distribution of thermal and moist plumes for a 12-km run over the San Joaquin Valley. Mean flight altitude is 30m	90
Figure 2.17. Difference between radiative surface temperature and air temperature ($T_s - T_a$), Ratio of Infrared (R) over Red (R) reflected solar radiation (VI), and distribution of thermal and moist plumes for a 12-km run over the San Joaquin Valley. Mean flight altitude is 100 m	90
Figure 3.1. Effect of different threshold levels defined as fractions of the standard deviation (rms) of the flux. The rms value is calculated including all datapoints of the given run	107
Figure 3.2. Water vapor flux along a run segment over the wetland, showing the threshold of ± 0.2 rms (solid lines) and ± 1 rms (dashed lines). Datapoints within the \pm line for a given threshold level are eliminated .	108
Figure 3.3. A moisture plume with weak tails. The solid lines represent the size of the structure after the application of thresholds equivalent to 0.2 rms and 1 rms	109
Figure 3.4. A moisture plume with many small flux values. Solid lines	

represent plume diameter after application of the thresholds of 0.0, 0.2 rms, and 1 rms	110
Figure 3.5. Lognormal distributions of diameter and spacing of thermal and moisture plumes at different heights above wetland. Structures that contributed less than 0.2% to the total flux within a given run are not included. The relative frequency functions (F(x)) are plotted as symbols and the incremental probability functions (p(x)) are plotted as solid lines	114
Figure 3.6. Lognormal distributions of diameter and spacing of thermal and moisture plumes at different heights above grassland (FIFE). Structures that contributed less than 0.2% to the total flux within a given run are not included. The relative frequency functions (F(x)) are plotted as symbols and the incremental probability functions (p(x)) are plotted as solid lines	115
Figure 3.7. Lognormal distributions of diameter and spacing of thermal and moisture plumes at different heights above partially irrigated agricultural land. Structures that contributed less than 0.2% to the total flux within a given run are not included. The relative frequency functions (F(x)) are plotted as symbols and the incremental probability functions (p(x)) are plotted as solid lines	116
Figure 3.8. Mean diameter of thermal and moisture plumes at different heights above wetland	117
Figure 3.9. Mean diameter of thermal and moisture plumes above grassland (FIFE)	118
Figure 3.10. Plume diameter as a function of the negative of the Obukhov length (-L) for wetland and partially irrigated agricultural land.	120
Figure 3.11. Line density of thermal and moisture plumes as a function of height above wetland	122
Figure 3.12. Line density of thermal and moisture plumes as a function of height above grassland	123
Figure 3.13. Mean spacing of thermal and moisture plumes at different heights above wetland	126

Figure 3.14. Mean spacing of thermal and moisture plumes at different heights above grassland 127

Figure 3.15. Flux contributions from different classes of diameter of thermal and moisture plumes, at four heights above wetland 128

Figure 3.16. Flux contributions from different classes of diameter of thermal and moisture plumes, at four heights above grassland 129

General Introduction

There has been a growing emphasis in recent years on regional and global models of the energy or mass balance. This has been partly a response to growing concern over greenhouse gas emission as an agent in global climate change and partly due to the perceived need for a better understanding of the link between the atmosphere and the biosphere in global circulation models (GCMs). In particular, the flux boundary conditions for energy and mass at the earth-atmosphere interface for GCMs need to be better defined.

Several attempts have been made to evaluate flux estimates on a regional scale using either aircraft or satellite-based observations (e.g. Soer 1980, Price 1982, Nieuwenhuis et al. 1985, Taconet et al. 1986, Schuepp et al. 1987, Desjardins et al. 1988, Mack et al. 1990). In general, satellites are viewed as a promising tool for large-scale monitoring of environmental characteristics, and aircraft as the most suitable near-surface platform to collect information for the verification of satellite-based models on a comparable scale.

Instrumented aircraft have the advantage of being able to probe the atmosphere over a wide range of scales, from local (of the order of km) to regional (up to a few hundred km), providing information about the spatial variation of flux estimates. While the availability of onboard fast, accurate sensors have made possible reliable measurements of atmospheric properties, the interpretation of such measurements and their link to the surface is still not well understood. A meaningful interpretation of airborne observations must be based on a more profound understanding of boundary-layer dynamics, of surface characteristics and processes, and of the interaction between them.

As a first attempt to verify the feasibility of using aircraft observations to test satellite-based algorithms for estimation of earth-atmosphere exchange processes, Chapter 1 of this thesis evaluates the relationship between airborne flux estimates of sensible heat, water vapour and CO₂, and surface parameters retrieved by satellite. Some of the problems and limitations inherent in these analyses reinforce the need for a better interpretation of aircraft-based flux estimates, in order to make them relevant to comparisons against satellite-based observations. In Chapter 2, conditional sampling of aircraft-based flux observations is used to analyze the link between surface characteristics and fluxes estimated at different heights within the boundary layer, and in Chapter 3 the statistical properties of the turbulent structures are described above different ecosystems. The findings help to explain some of the limitations encountered in Chapter 1. They contribute to an objective definition of sampling criteria for airborne flux observations at different heights and provide a unique database against which models of boundary layer structure may be verified.

References

- Desjardins, R.L., J.I. MacPherson, P.H. Schuepp, and F. Karanja. An evaluation of aircraft flux measurements of CO₂, water vapor and sensible heat. Bound.-Layer Meteor., 47, 55-70, 1988.
- Mack, A.R., R.L. Desjardins, J.I. MacPherson, and P.H. Schuepp, 1990: Relative photosynthetic activity of agricultural lands from airborne carbon dioxide and satellite data. Int. J. Rem. Sens., 11(2), 237-251, 1990.
- Nieuwenhuis, G.J.A., E.H. Smidt, and H.A.M. Thunnissen. Estimation of regional

evapotranspiration of arable crops from thermal infrared images. Int. J. Remote Sensing, 6, 1319-1344, 1985.

Price, J.C.. On the use of satellite data to infer surface fluxes at meteorological scales. J. Appl. Meteor., 21, 1111-1122, 1982.

Schuepp, P.H., R.L. Desjardins, J.I. MacPherson, J. Boisvert, and L.B. Austin. Airborne determination of regional water use efficiency and evapotranspiration: present capabilities and initial field tests. Agric. For. Meteorol., 41, 1-19, 1987.

Soer, G.J.R., 1980: Estimation of regional evapotranspiration and soil moisture conditions using remotely sensed crop surface temperatures. Remote Sensing Environ., 9, 27-45, 1980.

Taconet, O., Bernard, R., and Vidal-Madjar, D., 1986: Evapotranspiration over an agricultural region using a surface flux/temperature model based on NOAA/AVRR data. J. Clim. Appl. Meteor., 25, 284-307, 1986.

Chapter 1:

Relationship between satellite-derived parameters and aircraft-based measurements of CO₂, sensible heat, and water vapor fluxes.

Abstract

Aircraft-based flux estimates of sensible heat, latent heat, and CO₂, are compared against satellite-derived surface temperature and vegetation index, to explore the possibility of using a single aircraft overpass as a basis for fitting satellite-based models. The study area was located southwest of the site of the FIFE project that took place over the Konza prairie and adjacent areas in Kansas during 1987. Data were obtained from 75 km regional runs between the FIFE site and Salina, with the National Research Council of Canada's Twin Otter research aircraft, in June, July, August, and October of 1987. One third of the area was mainly grassland, with cultivated land predominating in the remaining portion of the transect. Normalized difference vegetation index (NDVI), simple ratio vegetation index (SR), and surface temperature, were computed for the same area and adjacent upwind pixels from NOAA advanced very high resolution radiometer (AVHRR). Aircraft and satellite data were processed to obtain spatially coincident and locally representative flux values. Results show a linear relationship between NDVI or SR and CO₂ uptake during single days; however, a nonlinear relationship emerged when all data sets were combined. Overall, about 60% and 72% of total

variability in CO₂ flux was accounted for by the NDVI and SR, respectively. Water vapor fluxes were least correlated with surface temperature or NDVI. The feasibility of parameterizing sensible heat flux using satellite-based surface temperature is also evaluated. The latter could then be used in the energy balance equation to obtain regional evapotranspiration.

1.1. INTRODUCTION

Land surface and vegetation play an important, but insufficiently understood, role in the biogeochemical cycles of the earth. In particular, the transfer of heat, CO_2 and H_2O between the soil and the atmosphere is now recognized as a key link between the biosphere and the atmosphere, and substantial research efforts in this area are planned as part of the International Geosphere-Biosphere Programme (IGBP) (1990).

The exchange between the earth's surface and the atmosphere is basically determined by the available energy and the status of vegetation and, as such, it varies spatially as well as temporally. During daytime and unstable conditions, a vegetated surface is normally a source for sensible heat and water vapor, and a sink for CO_2 which is taken up in photosynthesis. A moveable platform such as an aircraft will measure the net flux to or from the surface during the time of its overpass. Since it is not practical to measure these exchanges repeatedly and over large areas, the feasibility of using satellite observations to estimate surface exchange is an important research issue. As part of measurements taken during the First International Field Experiment (FIFE) of the Satellite Land Surface Climatology Project (ISLSCP) (Sellers et al., 1988), a study was undertaken over Kansas grasslands and agricultural lands to assess the relationship between satellite radiance measurements and aircraft-based estimates of fluxes of CO_2 , sensible heat and latent heat.

1.2. METHODOLOGY

1.2.1. Description of the study area

The regional runs (RR) in this study were flown between the aircraft base near Salina and the FIFE site. The Eastern third of the run (adjacent to the FIFE site) was mainly grassland, with cultivated land predominating in the remaining portion of the transect. The agricultural land was a mixture of plowed land, crops at different growing stages, woods, and pasture. Vegetation activity was generally smaller over this part of the transect. The coordinates of the RR are shown in Figure 1.1.

1.2.2. Satellite Data

1.2.2.1. Processing and calibration. Images from the NOAA-9 and -10 Advanced Very High Resolution Radiometer (AVHRR) over the area of study were obtained by NASA. Subscenes measuring 256 lines x 256 pixels (16 bits) were extracted from the raw full scenes and archived in the FIFE Information System (FIS). The extracted data covered both the grassland of the FIFE test site and the RR (Figure 1.1). Raw images (Level 0 product) from numerous dates were provided by FIS. Following quality and cloud cover review of images obtained near the dates at which aircraft flux measurements were made, four images were selected for processing and analysis (Table 1.1). The satellite image obtained on July 14 was used for comparison with aircraft measurements taken on July 11,

Figure 1.1. Location of the study area. The F-West and F-East are end-points of the regional runs.

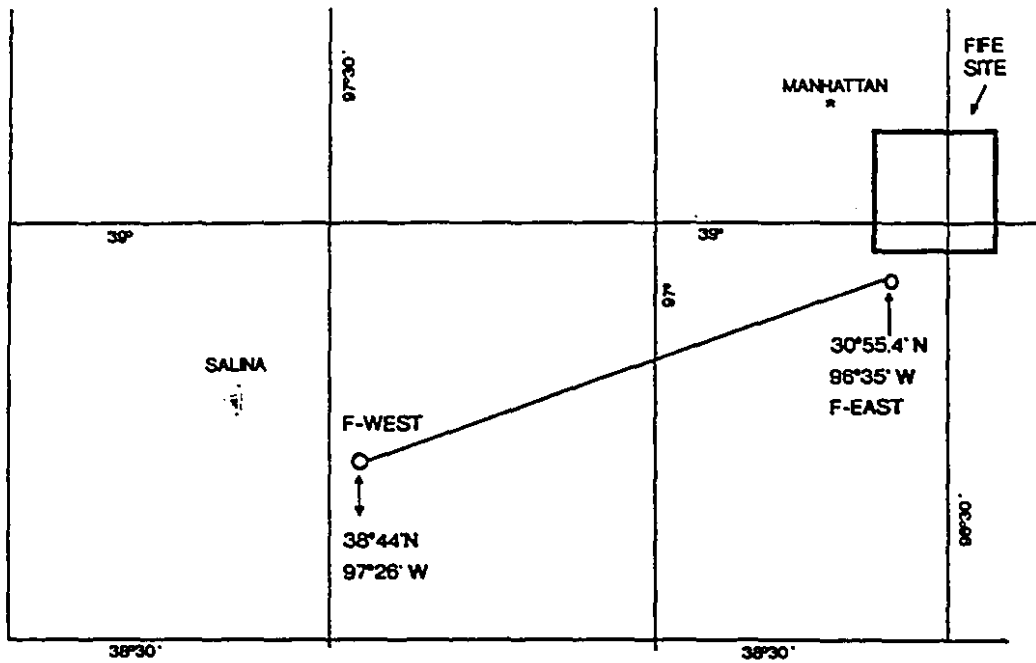


Table 1.1. Description of satellite data used

Satellite	Date	Time (GMT, HH:MM)	Sun Angle (θ_{sun})	Sensor Angle (θ_{sun})	$\Delta\phi$
NOAA-9	87/06/28	21:00	35.3	22.0	175.8
NOAA-10	87/07/14	14:09	58.1	33.7	14.7
NOAA-9	87/08/15	20:45	38.6	44.1	160.1
NOAA-9	87/10/07	21:16	61.4	10.3	155.7

* $\Delta\phi$ is the difference between sun and sensor azimuth angles.

Table 1.2. Summary of the aircraft data used.

Flight date (1987)	Start G.M.T. (HH:MM)	End G.M.T. (HH:MM)	Radiation (W m^{-2})	Wind speed (m s^{-1})	Wind direction
June 28	21:47	22:09	524	3.38	S
July 11	21:25	21:47	474	14.60	S
August 15	21:58	22:18	486	12.54	S
October 7	16:18	16:36	595	3.12	N

since no clear image was available for July 11.

Using 10 ground control points whose coordinates were extracted from a topographic map, individual images were registered and resampled to 1-km pixel size, using a standard map projection. The end points of the regional run and the outlines of the FIFE site were located on each image. Digital values for AVHRR channels 1, 2, 4, and 5 were extracted into separate files for pixels over an area covering the aircraft flight line and extending upwind of it for 10 km. These data files (separated according to channel/date combinations) were transferred to a spreadsheet program for further processing.

Radiometric sensor calibration and atmospheric corrections were applied to raw radiance values in each channel. Sensor calibration constants (gain, offset) were obtained from FIS for each satellite/channel combination; in the case of NOAA 9, sensor degradation corrections were also introduced (based on standard NOAA procedures). Atmospheric corrections were computed using the 5S program (Tanré et al., 1990) for a standard summer, temperate latitude and continental atmosphere. The raw radiance measurements for channels 1 and 2 were converted to reflectance through the following formulas (Teillet et al, 1990):

$$\theta_{(i,j)} = \frac{Y_{(i,j)}}{[1 + Y_{(i,j)} S_{(i)}]} \quad (1)$$

$$Y_{(i)} = A_{(i)}L^*_{(i,j)} + B(i) \quad (2)$$

$$L^* = \frac{[Q_{(i,j)} - O_{(i)}]}{G_{(i)}} \quad (3)$$

$$G_{(i)} = aD + b \quad (4)$$

$$O_{(i)} = cD^2 + dD + e \quad (5)$$

where,

θ is the surface reflectance of pixel j in channel i ;

S is the spherical albedo;

L^* is the apparent radiance at the sensor ($\text{mW m}^{-2} \text{sr}^{-1}$);

Q is the raw digital count;

G is the gain;

O is the offset;

D is the number of days since launch;

A, B, a, b, c, d, e are coefficients.

The values for A , B , and S (for an altitude of 0.34 km) were calculated using the 5S model.

The normalized difference vegetation index (NDVI) and the simple ratio vegetation index (SR) were computed for each pixel (i, j) as follows:

$$NDVI_{(i,j)} = \frac{[\theta_{(2,j)} - \theta_{(1,j)}]}{[\theta_{(2,j)} + \theta_{(1,j)}]} \quad (6)$$

$$SR_{(i,j)} = \frac{\theta_{(2,j)}}{\theta_{(1,j)}} \quad (7)$$

The result of these steps were matrices of NDVI or SR values for each date covering the Regional Run plus a margin of the 10 1-km² pixels upwind.

Channels 4 and 5 of NOAA-9 were used to retrieve surface temperature, through the following equations:

$$Q_i = \frac{G (DN)_i}{O_i} \quad (8)$$

$$T_i = \frac{c_2 v}{\ln \frac{(1 + c_1 v^3)}{Q_i}} \quad (9)$$

where,

Q_i is the apparent raw radiance at the sensor for the channel i ;

$(DN)_i$ is the raw digital count for the channel i ;

O is the offset;

T_i is the surface temperature for the channel i ;

c_1 is the first Planck's constant (1.1910659E-05 mW m⁻² sr⁻¹ cm⁻⁴);

c_2 is the second Planck's constant (1.438844 cm K);

ν is the central wavenumber for each channel.

Finally, the surface temperature was obtained using the following expression provided by NOAA:

$$T_s = 3.6569T_4 - 2.6705T_5 - 268.93 \quad (10)$$

where,

T_s is the radiative surface temperature,

T_4 is the surface temperature obtained from channel 4,

T_5 is the surface temperature obtained from channel 5.

The operations described above produced maps of NDVI and radiative surface temperatures for the area of interest along the flight trajectories.

1.2.3. Footprint correction. Since fluxes were measured at the relatively high average height of 150 m above ground, it is important to identify the area (pixels) that actually contributed to the flux measured by the aircraft sensors. With aircraft trajectories generally along the E-W direction, and the wind approximately perpendicular (S or N) to the flight line for the runs examined in this study (Table 1.1), the effective upwind source areas were located S and N of the flight track. To account for the dominant contributions from upwind sources, the footprint function described by Schuepp et al. (1990), adjusted to the numerical Lagrangian simulations of Leclerc and Thurtell (1990), was used to generate weighted values of vegetation indices and surface temperature within the 10 upwind pixels from the

flight line. It was assumed that any contribution beyond this distance would be negligible, in agreement with predictions of the footprint function. The flight line was assumed to be centered on the first pixel. The weighted values for vegetation indices and surface temperature for each pixel k along the flight line was obtained through the expression

$$\alpha_k = \sum_{i=1}^n \alpha_i \left[e^{\sigma(z-d)/(ku_*x)} \right]_{x_{i-1}}^{x_i} \quad (11)$$

where:

$\alpha_{(i)}$ = NDVI, SR, or surface temperature value, of i th pixel upwind;

U = mean wind speed between the ground and level z (m s^{-1});

u_* = friction velocity (m s^{-1});

x_i, x_{i-1} = upwind and downwind displacements from the flight line of the i th pixel (in meters) where $x_0 = 0$;

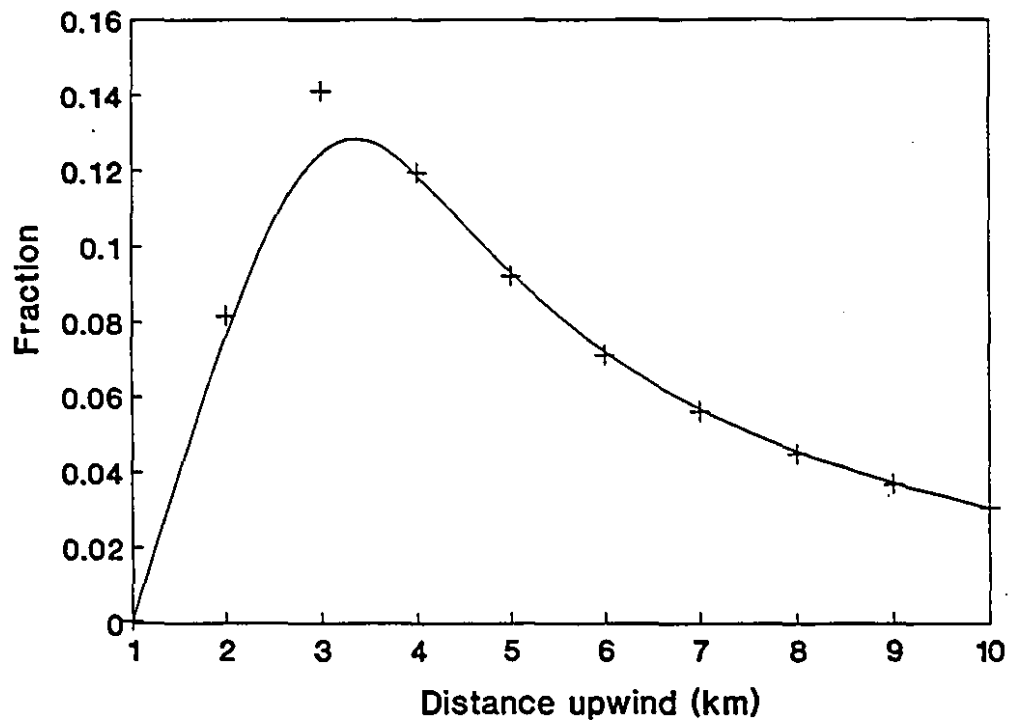
Z = flight altitude (m);

d = displacement height (assumed = 0);

k = von Karman constant (0.4).

Figure 1.2 shows the relative contribution to the flux measured at 150 m, estimated to originate from the pixels located up to 10 km upwind of the flight trajectory. The ratio U/u_* was assumed to be equal to 10 for both cases, based on preliminary analysis of the FIFE aircraft data. This value may be somewhat high, based on subsequent adjustment of the footprint function over the FIFE site (Schuepp et al., 1992), but it is unlikely that a smaller value would invalidate our

Figure 1.2. Relative contribution from upwind pixels for the flying height of 150m above ground, for an assumed U/u ratio of 10.



findings. The footprint-weighted values of NDVI and surface temperature were averaged over 3 km segments of the RR, giving a total of 25 values along the 75 km run.

1.2.4. Aircraft Data

1.2.4.1. Data collection. The airborne flux data were obtained by the National Research Council Twin Otter atmospheric research aircraft along the regional run during transit to and from the base at Salina (see Figure 1.1 and Table 1.2). The flight lines were approximately 75 km long and flown at constant pressure altitude, corresponding to a mean altitude of 150 m. The aircraft was equipped to measure the contributions to the flux densities of momentum, CO₂, and sensible and latent heat (MacPherson, 1988). Airspeed, angles of attack, and sideslip were measured through pressure sensors in the aircraft's nose-mounted boom. The inertial velocity of the aircraft was determined by complementary filtering technique based on data from accelerometers, rate gyros, and Doppler radar. The three components of the air motion were then derived from the difference between air velocity relative to the aircraft and the aircraft velocity relative to the ground. They were resolved into earth-fixed axes using aircraft heading and attitude signals.

A fast-response infrared analyzer (wavelengths 4.28, 2.58, and 3.90 μm with the last wavelength used as a reference) was used to measure fluctuations of CO₂ and H₂O in the ambient air. It had a sensitivity of 0.01 g m⁻³ for H₂O and 0.0002

g m⁻³ for CO₂. The air was taken from a 122 cm² inlet located 15.2 cm above the fuselage. The analyzer was located in the rear cabin, about 12 m from the nose boom, but this horizontal displacement was accounted for during data processing. The flux estimates are based on 64 analog signals digitized at 16 Hz, passed through anti-aliasing low-pass filters with a breakpoint set to 5 Hz. At a true airspeed of 60 m s⁻¹, this filtering results in a short wavelength limit of the aircraft measurements of approximately 12 m.

1.2.4.2. Smoothing of RR flux data. To optimize the correspondence between airborne flux measurements and surface distribution of CO₂ sources or sinks, it was necessary to correct for extreme local flux contributions. Such singularities are present as inherent features of the intermittency of boundary layer dynamics. They are real in the sense that they portray physical transfer that has occurred, but they cannot be assumed to realistically represent the actual source or sink strength immediately upwind of their point of observation. The approach of Schuepp et al. (1989) was used to smooth flux estimates. This method considers that the flux estimate may be described by

$$F_c = r_{wc} \sigma_w \sigma_c \quad (12)$$

where r_{wc} is the correlation between vertical wind and the concentration of the property been analyzed (sensible heat, water vapor, or CO₂), and σ_w and σ_c are the standard deviations of vertical wind and the scalar property.

The smoothing procedure is based on the assumption that any measurement performed over a given surface with its physical, meteorological and vegetative conditions will have, on the average, expected values for σ_w , σ_c , and r . Local overestimation of the flux by the eddy correlation technique (e.g. as a result of a convective plume) will therefore appear as an excessively high recorded value for one or more of these parameters. If the time series for r , σ_w , and σ_c along a flight is described by Fourier series, it is possible to preserve the characteristic variation of these parameters along the line through the lower terms in the series. Correction for small-scale (local) deviations can then be made on the basis of the departure of local values for r , σ_w , and σ_c from the expected values, represented by a truncated Fourier series. The degree of resolution of this analysis, i.e. the scales over which r , σ_w , and σ_c values are expected to represent averaged source/sink strength of underlying terrain rather than local boundary layer structure, can be selected through the level of truncation. The corrected, smoothed flux estimate for a segment i will then become

$$F_k = (F_r F_w F_c)_i \quad (13)$$

where F stands for the Fourier Series approximations of σ_w , σ_c and r .

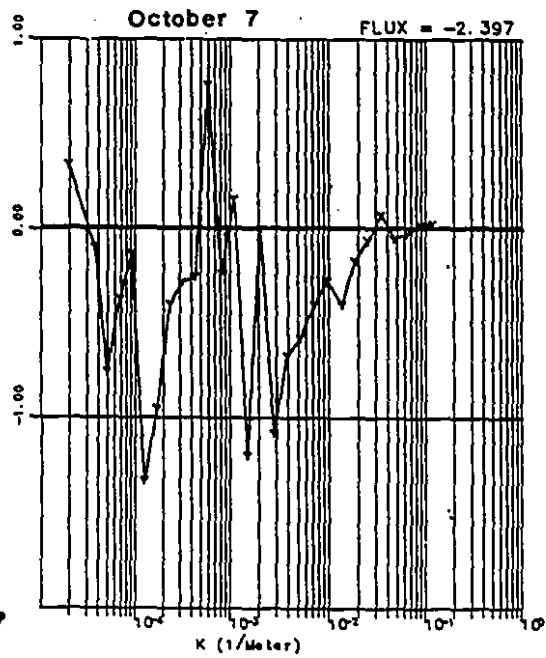
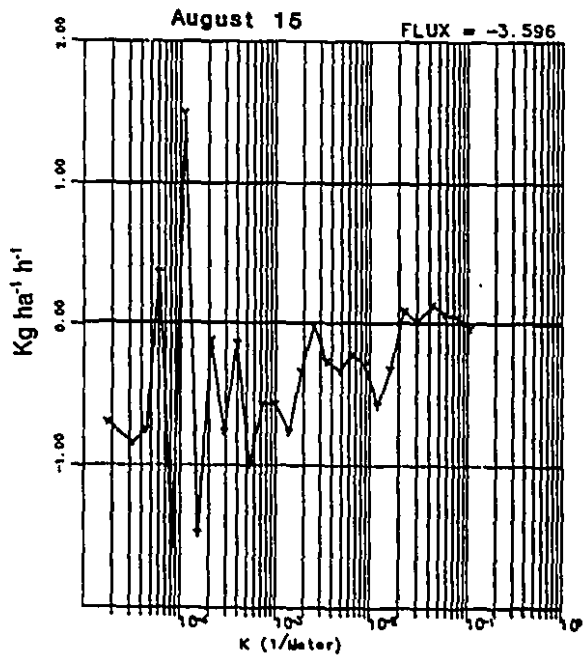
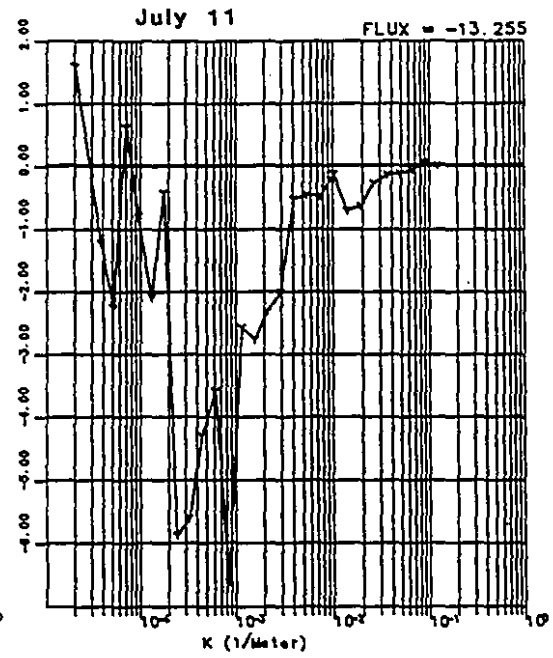
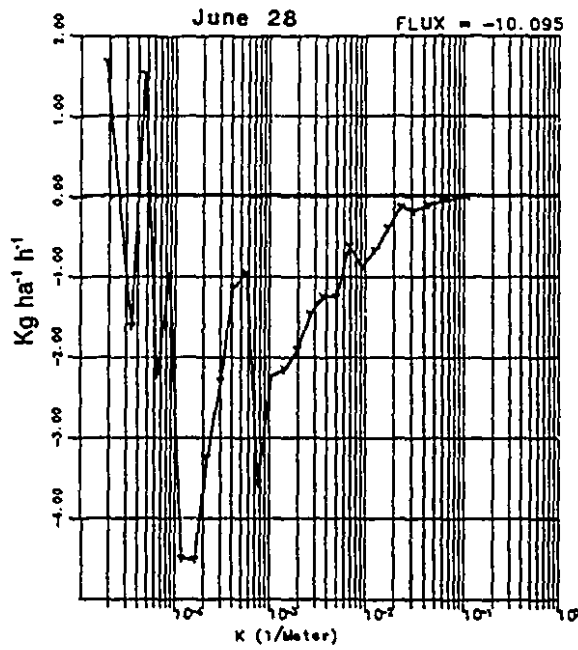
While this procedure may reduce the flux relative to that obtained by averaging over longer sections of the RR, it avoids the potential error of interpreting a transient, coherent turbulent structure as a permanent excessive

local source in the mapping procedure.

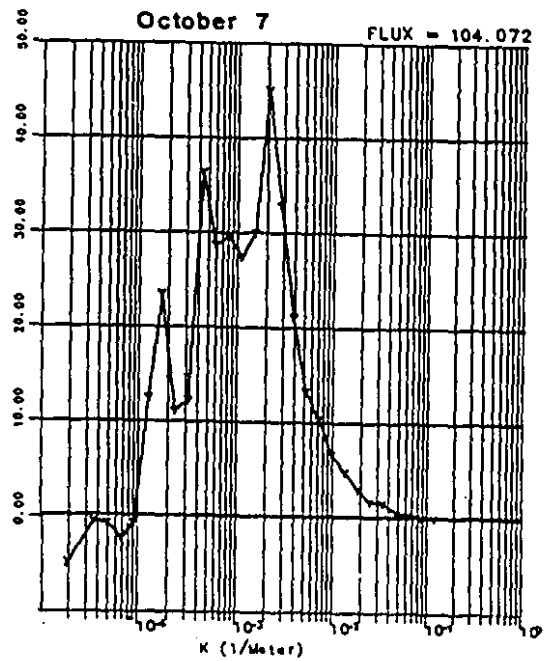
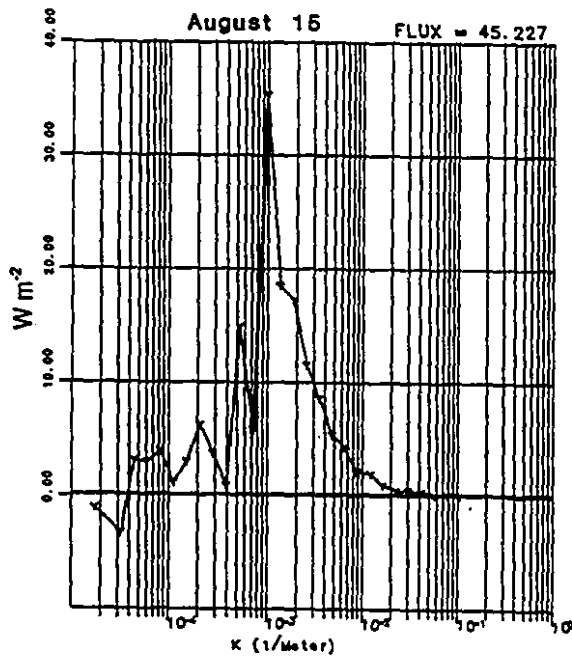
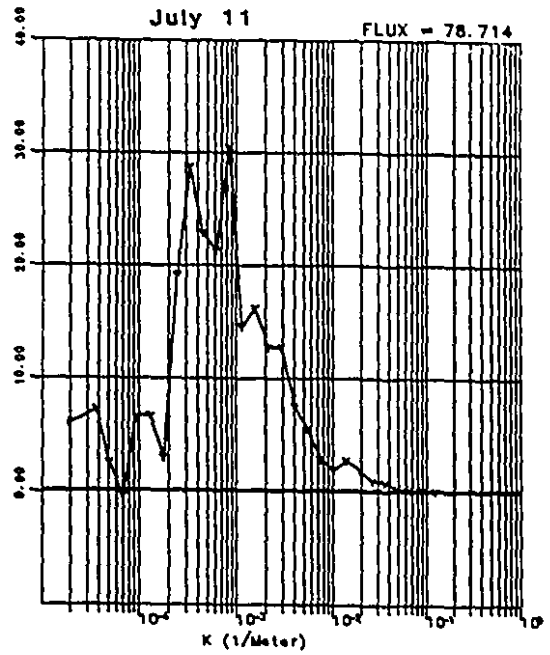
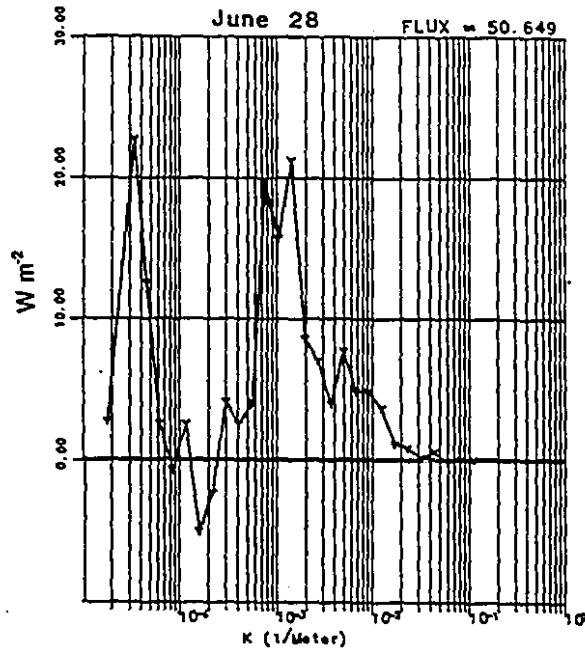
1.2.4.3. Long wavelength contribution to the flux. Since flux estimates were calculated over 3 km, the longer wavelength contributions to the flux would be excluded from the analysis, resulting in a lowering of flux estimates. To quantify this potential reduction, cospectral analysis was performed along the RR for each flight. The results for CO₂, sensible heat, and water vapor are shown in Figure 1.3.a, 1.3.b, and 1.3.c, respectively. Irregularities in the form of the cospectra, particularly for CO₂ on August 15 and October 7 may be partly explained from experimental conditions: CO₂ fluxes were much smaller on August 15 and October 7, due to lower photosynthetic activity on those days, with associated difficulties in measuring small fluxes reliably. On August 15 all the area was very dry, which may have caused respiration to be very high. The lower values observed on October 7 are due to advanced senescence of the vegetation. By integrating the cospectra over wavenumbers from 0.1 m⁻¹ to 3.33E-04 m⁻¹ (or 1.3E-05 m⁻¹), corresponding to integration over wavelengths from 10 m to 3 km (or 75 km), an estimate of the flux based on 3 km can be compared to one based on all wavelengths. Results showed that scales smaller than 40 m (wave number 2.5 x 10⁻² m⁻¹) did not contribute significantly to the flux. Figure 1.4 shows the percentage of the flux remaining after filtering at 3 km for the 4 RR observation days. It is evident that a significant portion (25% to 50%) of the flux contributions during these flights at 150 m must be attributed to longer wavelengths. To correct

Figure 1.3. Cospectra of (a) CO₂ flux, (b) sensible heat flux, and (c) water vapor flux for the regional runs on four days.

CO2



Sensible Heat



Water Vapor

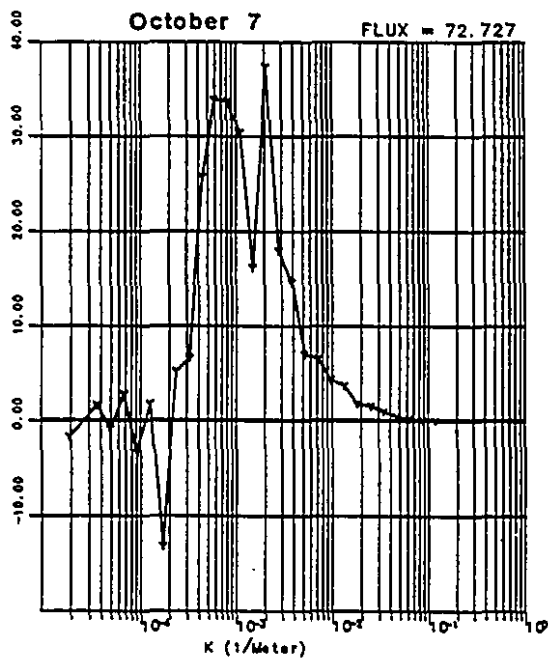
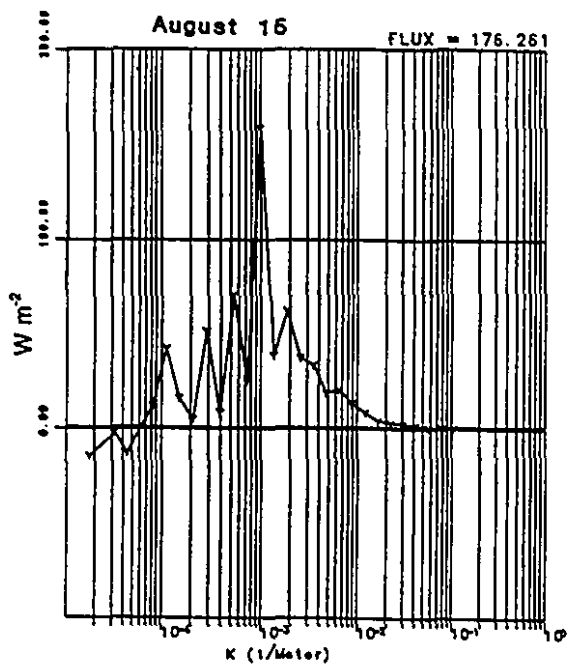
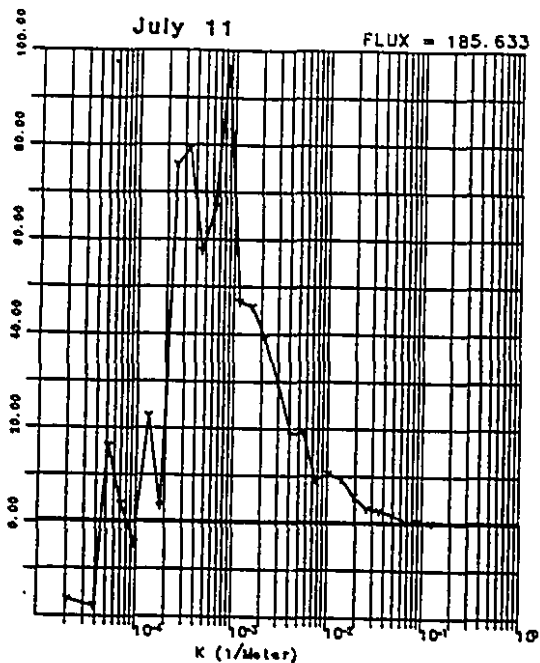
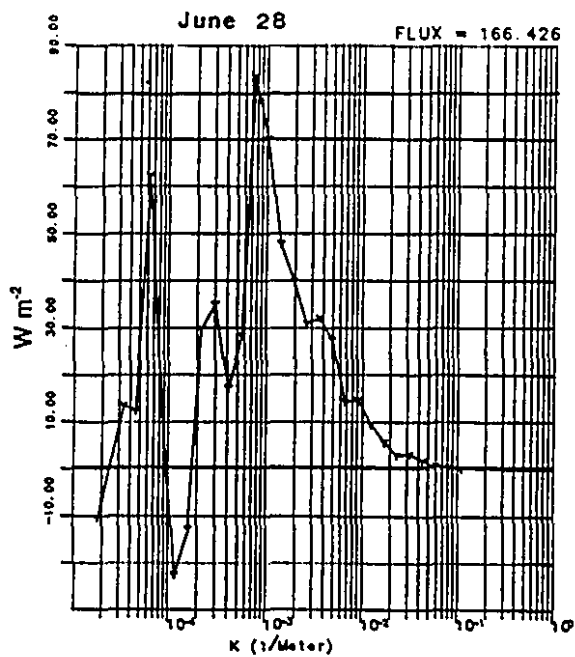
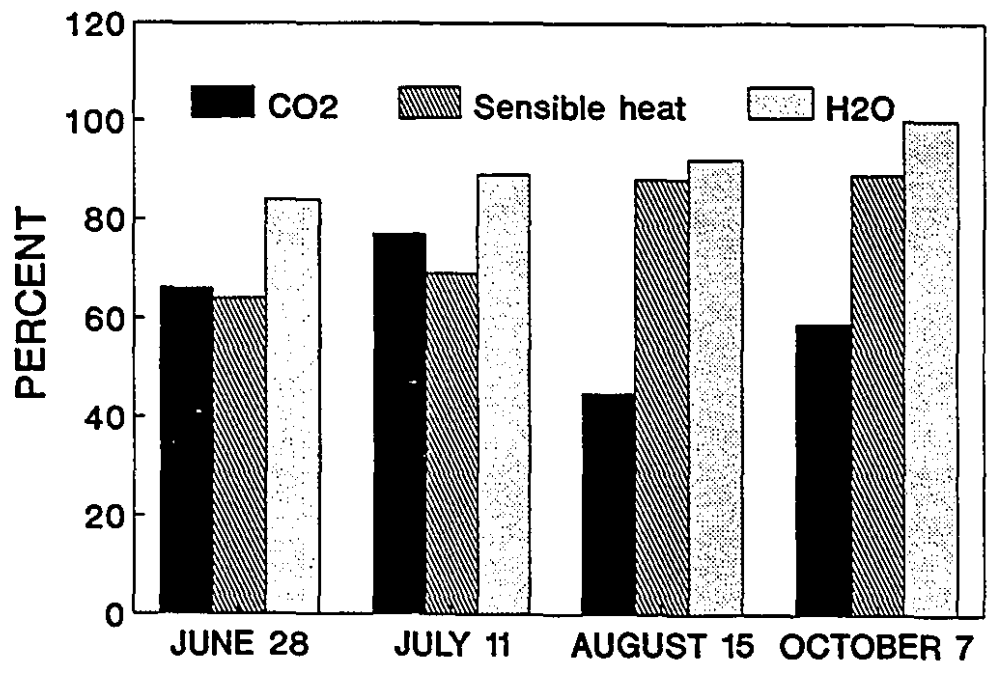


Figure 1.4. Percentage of flux remaining after filtering at 3 km.



for this underestimation, the percentage of the flux lost on the day under consideration was added to the final estimate for each 3 km segment. It should be noted that a further 10% loss has also been estimated in all 1987 FIFE data due to the wind measuring equipment used (MacPherson, 1990). This effect was not accounted for in the processing of the 1987 flux data. The flux divergence with height was also not considered in the present analyses since information from only one height was available for these runs. Betts et al. (1989) have described budget studies over the FIFE site in which the flux divergence has been evaluated.

1.2.5. Estimation of regional evapotranspiration

The energy balance equation for a given surface, assuming negligible advection, storage, and biological synthesis, is given by:

$$RN + G + H + LE = 0 \quad (14)$$

where:

RN = net radiation;

G = soil heat flux;

H = sensible heat flux;

LE = latent heat flux.

All fluxes are normally expressed in $W.m^{-2}$. If RN, G, and H can be measured or estimated, equation (14) can be solved for LE. The sensible heat can be

estimated through the following bulk transfer equation:

$$H = \frac{-\rho c_p (TS - Ta)}{ra} \quad (15)$$

where,

ρc_p = volumetric heat capacity ($J m^{-3} K^{-1}$);

TS = surface temperature (K);

Ta = air temperature (K);

ra = aerodynamic resistance to heat transfer (sm^{-1}); it can be approximated by the aerodynamic resistance to momentum transfer (Monteith, 1981) as

$$ra = \frac{\left[\ln\left(\frac{z}{z_0}\right) - \psi_m \right]^2}{k^2 U} \quad (16)$$

z_0 = roughness length (m);

ψ_m = stability correction for momentum transfer;

If the surface conditions are very uniform, net radiation, air temperature and windspeed can be measured at a ground station and assumed to be more or less constant over the region of study (Gash, 1986). For partial canopy and over extended areas, measurements representing the various types of soil cover should be used, if a more realistic estimation is to be obtained. In the present analyses,

we used the Twin Otter as a moveable platform to obtain mean values of energy balance components and surface parameters for each 3 km segment along the RR as follows: sensible heat flux through eddy correlations of vertical wind and temperature signals; incoming (K_{\downarrow}) and reflected (K_{\uparrow}) shortwave solar radiation from a Kipp and Zonen and an Eppley pyranometer, respectively; surface temperature measured with a Barnes PRT-5 radiation thermometer. With these measurements, it is possible to obtain an estimation of the regional net radiation through the simple balance with upward (Ld_{\uparrow}) and downward (Ld_{\downarrow}) longwave radiation as

$$RN = K_{\downarrow} - K_{\uparrow} + Ld_{\downarrow} - Ld_{\uparrow} \quad (17)$$

The term Ld_{\downarrow} can be estimated from the Stefan-Boltzmann Law:

$$Ld_{\downarrow} = \epsilon_{ac} \sigma T^4 \quad (18)$$

where

T = air temperature (K);

σ = Stefan-Boltzmann constant ($5.67 \times 10^{-8} \text{ W m}^{-2} \text{ K}^{-4}$);

ϵ_{ac} = atmospheric emissivity under clear skies, which can be estimated empirically through the expression of Idso and Jackson (1969):

$$\epsilon_{ac} = 1 - 0.261 \exp[-7.77 \cdot 10^{-4} (273 - T)^2] \quad (19)$$

Ld_{\uparrow} is estimated from the surface temperature and surface emissivity ϵ

(approximately 0.98):

$$Ldt = e \sigma T^4 \quad (20)$$

The soil heat flux is assumed to represent 10% of the net radiation, based on observed values over the FIFE site. With it, and the approximations presented above, the latent heat flux can be estimated for each satellite pixel from equation (14).

1.3. RESULTS

1.3.1. CO₂ Flux versus NDVI and SR

Figure 1.5 shows the relationship between NDVI and CO₂ for four time periods (dates) during the 1987 growing season (Table 1.2). CO₂ flux downward (corresponding to photosynthetic activity) is considered positive. Overall the estimated CO₂ fluxes are within the range of values obtained in previous works (e.g. Desjardins et al. 1982, Austin et al. 1987, Mack et al. 1990). At any given date, increased NDVI resulted in increased CO₂ uptake at the surface, as expected, with an approximately linear relationship between the two parameters. The scatter of points around the regression line was appreciable for all dates. This can be expected considering the highly intermittent nature of CO₂ exchange. The sensitivity of CO₂ uptake to NDVI changes and the ranges of NDVI and fluxes differed significantly between observation days. June and August data are broadly similar, and October showed the expected reduction in NDVI and flux. The July CO₂ measurements were much higher than those for the other periods, particularly in the eastern part of the RR (grassland SW of the FIFE site). Overall, there is a suggestion of linearity between NDVI and CO₂ flux, although nonlinearity could be masked by the scatter of individual points. The local time of overpass was different for the July data (Table 1.1), but the NDVI consistency with other data sets suggests that the time of satellite overpass was not the principal reason for the difference in the NDVI-CO₂ flux relationship.

Figure 1.6 shows the combined data from the four dates. Most of the data again conform to a linear relationship between NDVI and CO₂ flux, with exception of the eastern part of the July RR where very high fluxes were measured. The wide range of flux values (15-35 kg ha⁻¹ h⁻¹) associated with a narrow range of NDVIs (0.67-0.71) suggests that the NDVI reached saturation.

Since the relationship between simple ratio vegetation index (SR) and CO₂ flux is expected to be linear (Sellers et al. 1987), we also examined it for all dates combined; the results are presented on Figure 1.7. Overall, the linearity increased in comparison to that presented in Figure 1.6 (R = 0.72 for CO₂ flux vs SR against R = 0.64 for CO₂ flux vs NDVI), but the nonlinearity of the July data is still evident. The relationship between SR and CO₂ flux along the RR is shown for each day in Figure 1.8. We can see that most of the points fall within the same cluster, with the exception of the east end on July 14, where the nonlinearity occurred. One possible explanation for such high values could be sought in the occurrence of extreme turbulent events, that could have been sampled within the 3-km run segments. But analyses performed on another day with similar conditions (July 9) show similarly high CO₂ flux values over the same area, which lead us to believe that these fluxes reflect a much more active vegetation rather than a momentarily excess caused by local boundary layer dynamics.

On the basis of least square fit of exponential equations, 61% of the total variability in CO₂ flux was explained by NDVI, and 72% by SR. Undoubtedly, part

Figure 1.5. Satellite NDVI versus aircraft CO₂ flux on four days in 1987.

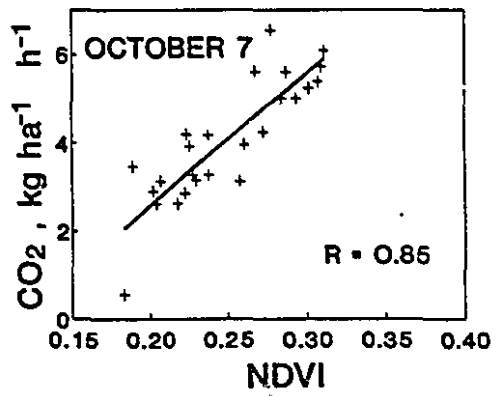
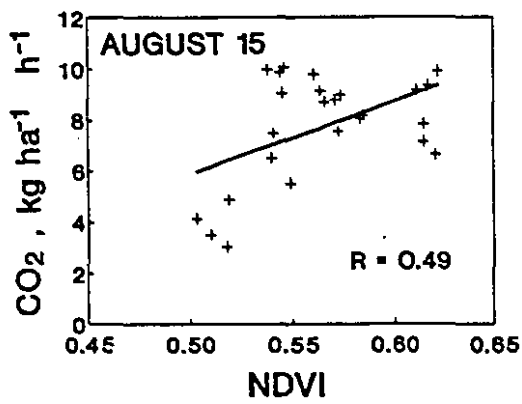
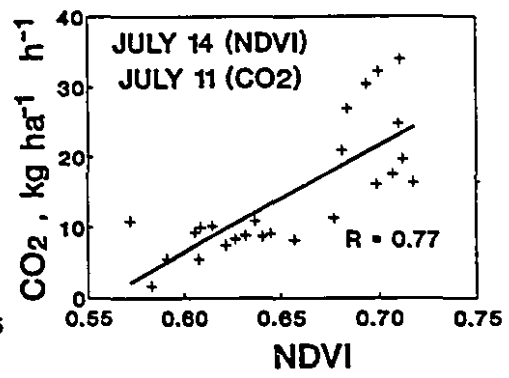
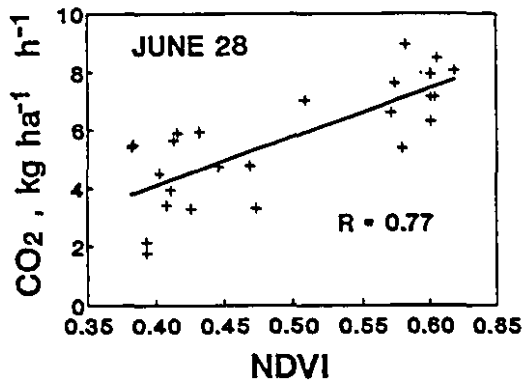


Figure 1.6. Satellite Normalized difference vegetation index (NDVI) versus aircraft CO₂ flux for all days combined.

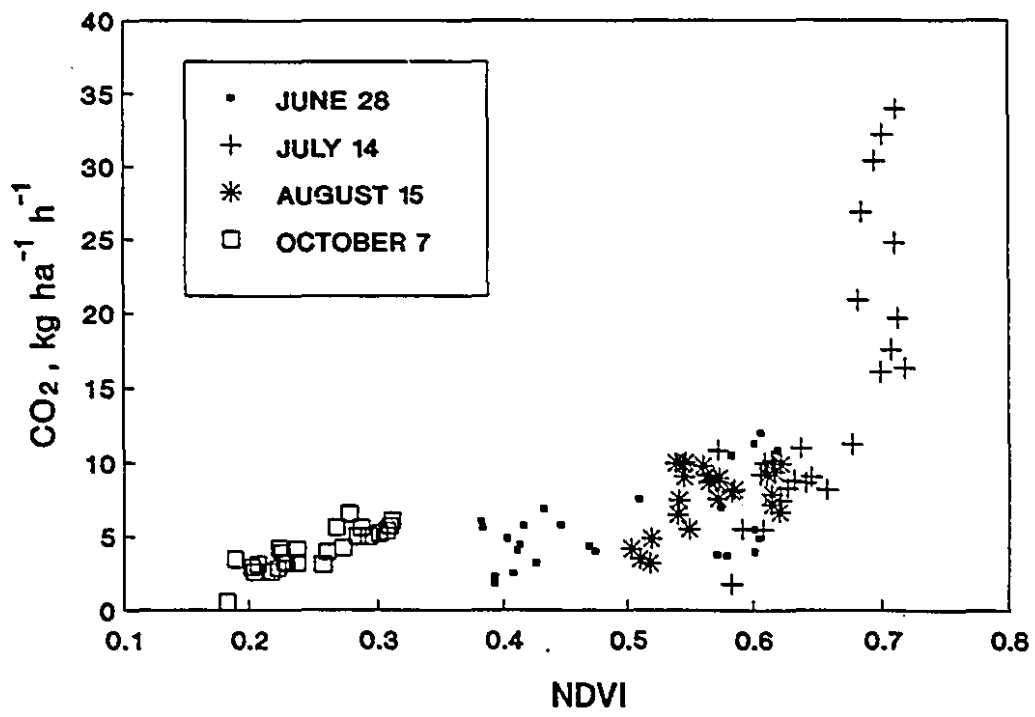


Figure 1.7. Satellite Simple Ratio vegetation index (SR) versus aircraft CO₂ flux for the regional runs. Data from all days are combined.

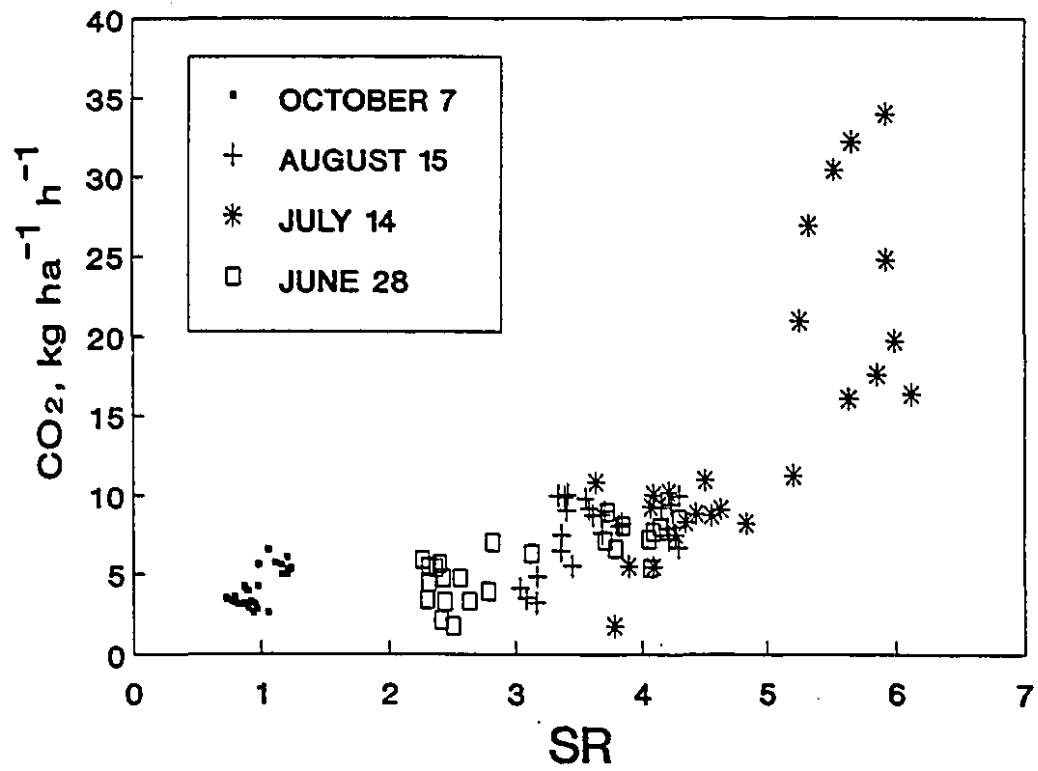
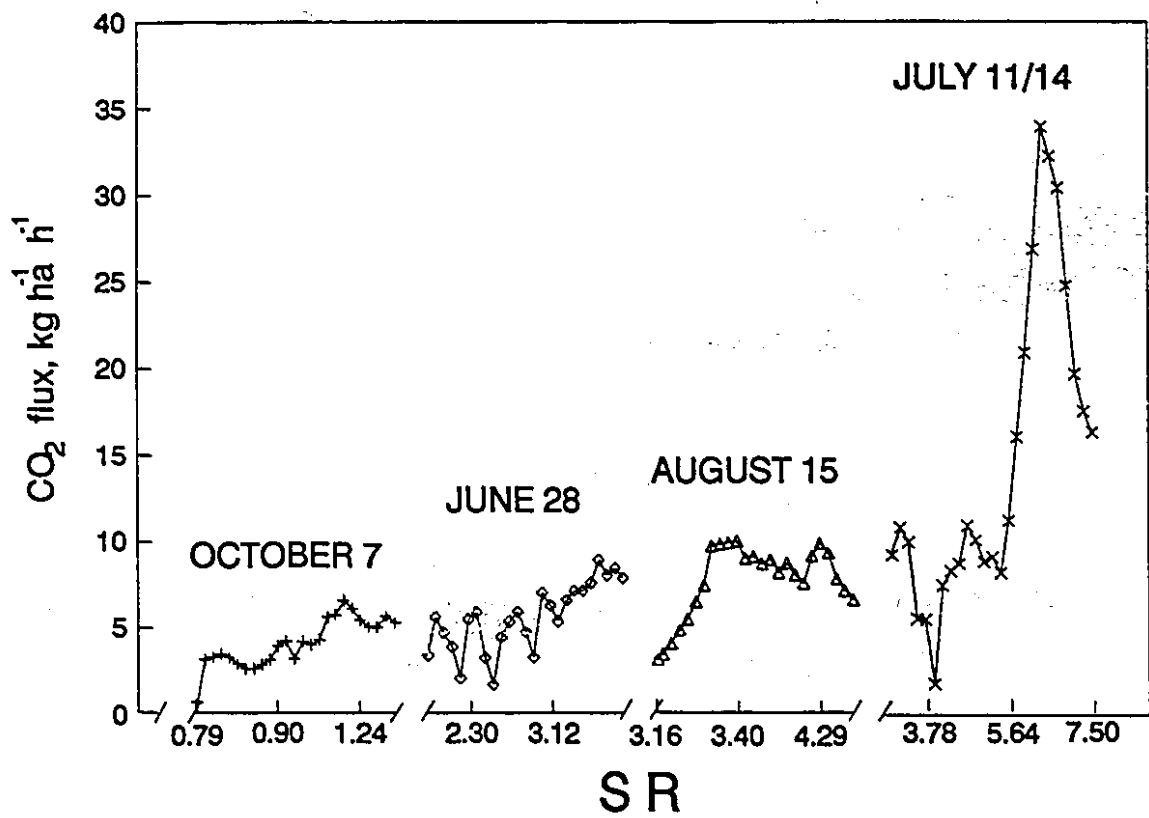


Figure 1.8. Satellite SR versus aircraft CO₂ flux for the regional runs on four dates in 1987.



of the remaining variability is caused by the random nature of boundary layer turbulence which remained after processing the aircraft data at high spatial resolution. Although the aircraft data were all collected under somewhat different radiation conditions (Table 1.2), normalization of the flux values by the incident radiation did not reduce the scatter significantly.

1.3.2. Sensible and Latent Heat flux vs NDVI and Surface Temperature (TS)

Results shown in Figure 1.9 exhibit the expected inverse relationship between NDVI and TS, with the summer data (June 28 and August 15) clustering separately from the fall data (October 7). This illustrates the important role of vegetation status in the energy partitioning at the earth's surface. Greener, more active vegetation is expected to be cooler as a result of transpiration. The significant correlation between NDVI and TS under the studied conditions also suggests that, in principle, both parameters should be efficient indicators of energy transfer away from the surface. The same cannot be expected for a crop fully covering the surface, where NDVI would be a poorer indicator of heat transfer, since it would not differentiate as effectively between stressed and unstressed vegetation.

Figure 1.10 a,b shows the relationships between surface temperature (TS) and sensible and latent heat flux for the three dates in 1987 where NOAA-9 data were available. The fitted linear equations and correlation coefficients are given in Table 1.3.

Table 1.3. Linear equations and regression coefficients (r) for the relationships between Sensible and latent heat fluxes versus surface temperature (TS) and Normalized Difference Vegetation Index (NDVI).

Sensible Heat	Latent Heat
<p>October 7</p> <p>$H = -94.7 + 7.8 \text{ TS}, r = 0.72$</p> <p>$H = 174.3 - 329.3 \text{ NDVI}, r = 0.73$</p>	<p>October 7</p> <p>$H = 192.0 - 4.0\text{TS}, r = 0.34$</p> <p>$H = 77.5 + 71.6\text{NDVI}, r = 0.14$</p>
<p>August 15</p> <p>$H = -289.2 + 9.3 \text{ TS}, r = 0.68$</p> <p>$H = 33.6 - 23.4 \text{ NDVI}, r = 0.53$</p>	<p>August 15</p> <p>$H = 821.6 - 20.0\text{TS}, r = 0.41$</p> <p>$H = -215 + 631.9\text{NDVI}, r = 0.53$</p>
<p>June 28</p> <p>$H = -365.5 + 11.1 \text{ TS}, r = 0.89$</p> <p>$H = 193.3 - 309.9 \text{ NDVI}, r = 0.78$</p>	<p>June 28</p> <p>$H = 175.4 - 0.78\text{TS}, r = 0.06$</p> <p>$H = 169 - 45.8\text{NDVI}, r = 0.10$</p>
<p>Seasonal</p> <p>$H = -24.1 + 2.62 \text{ TS}, r = 0.46$</p> <p>$H = 143.1 - 196.9 \text{ NDVI}, r = 0.87$</p>	<p>Seasonal</p> <p>$H = 20.5 + 3.4\text{TS}, r = 0.48$</p> <p>$H = 65 + 145.9\text{NDVI}, r = 0.51$</p>

The seasonal equation in this table is given by the three dates combined. Positive linear relationships were observed between sensible heat and surface temperature, as expected, and negative correlations for latent heat, with considerable scatter. Overall, a better fit is obtained between TS and sensible heat. The data from June 28 and August 15 fall within the same cluster, whereas the data from October 7 appear totally different. Although surface temperatures were considerably smaller in October 7, the sensible heat flux is higher than in June 28 and August 15. This can be explained by factors such as the pronounced

temperature gradients on that day, the lower plant physiological activity in October and possible lower surface moisture, causing most of the available energy to be converted into sensible heat.

The relationship between NDVI and sensible or latent heat flux is presented in Figure 1.11 a,b. The best-fit linear equations with respective correlation coefficients are given in Table 1.3. Again, sensible heat flux shows better correlation with NDVI than latent heat. The sensible heat flux data for June 28 appear more scattered, suggesting a nonlinear response as the NDVI approaches lower values. This could be physically real, linked to areas with partial canopy and generally higher variability in NDVI at that time of the year, which could contribute to very high values of sensible heat flux. Nevertheless, the possibility of scattering caused by inclusion or exclusion of very extreme events within each 3-km segment cannot be eliminated. A strong, negative linear relationship between NDVI and sensible heat flux is observed in the seasonal data, highlighting again the role of vegetation in the energy transfer.

Using the least-square linear fit between sensible heat flux and TS for each day, the sensible heat flux was estimated for each satellite pixel along the flight line and nine pixels upwind. These values were used in the energy balance equation to obtain the corresponding estimated evapotranspiration for each satellite

Figure 1.9. Relationship between Radiative surface temperature (TS) and the Normalized difference vegetation index (NDVI) on three combined dates in 1987.

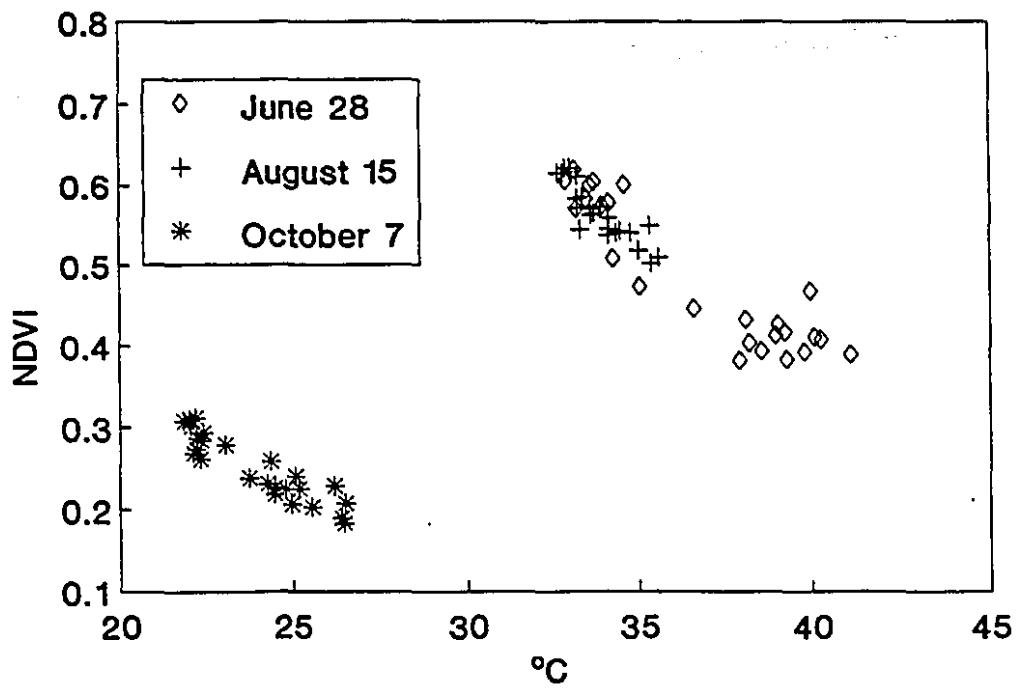


Figure 1.10. a) Relationship between Sensible heat flux and Radiative surface temperature (TS) during three dates in 1987. b) Relationship between Latent heat flux and TS.

• June 28 + October 7 * August 15

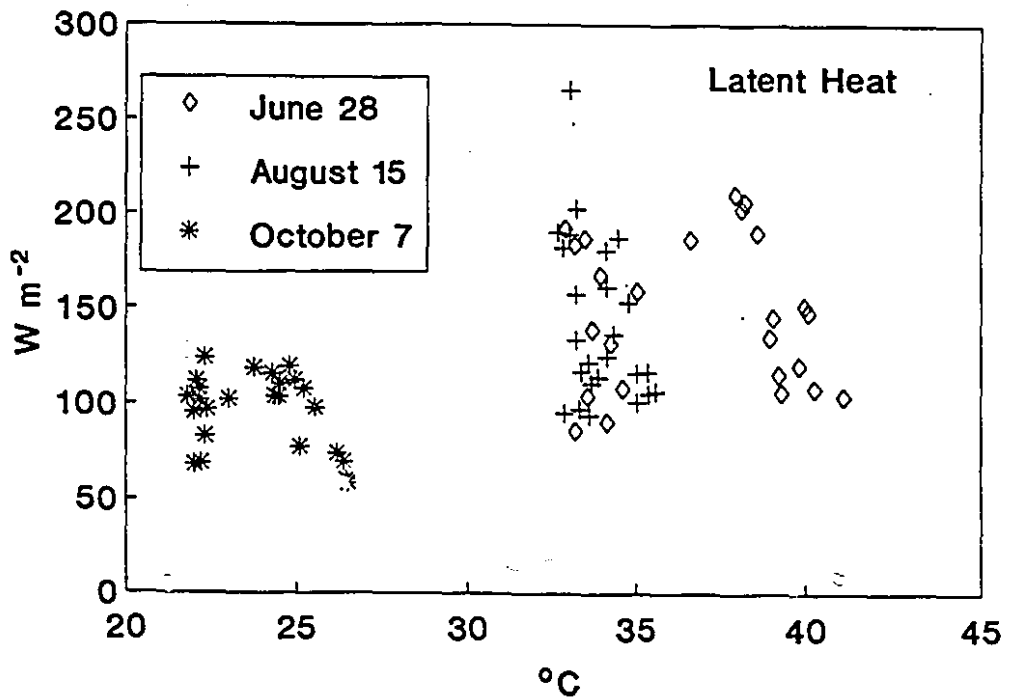
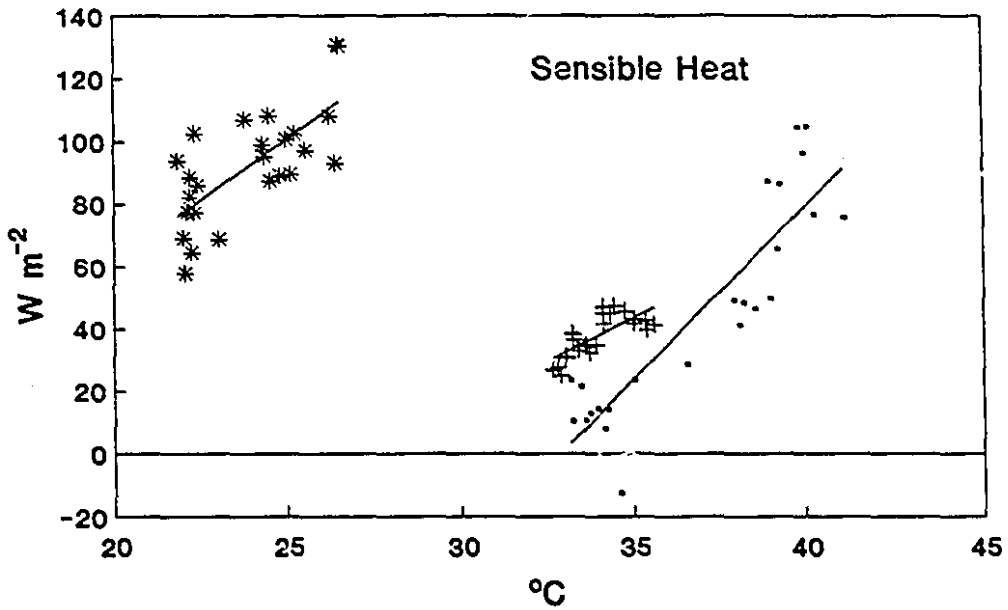


Figure 1.11. a) Seasonal relationship between Sensible heat flux and Normalized difference vegetation index (NDVI). b) Seasonal relationship between Latent heat flux and NDVI.

◇ June 28 + August 15 * October 7

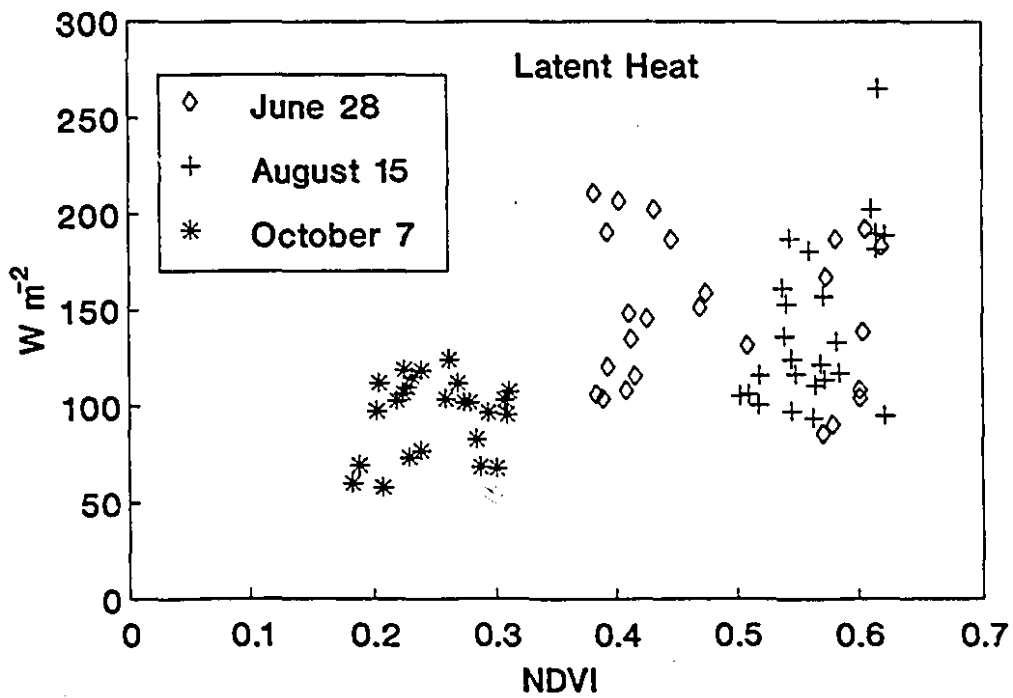
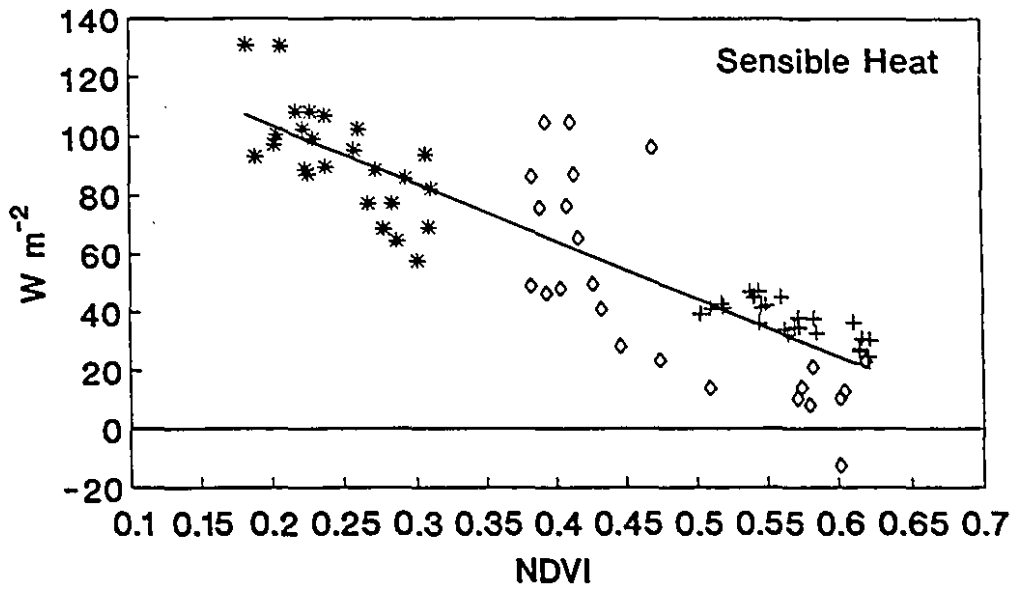
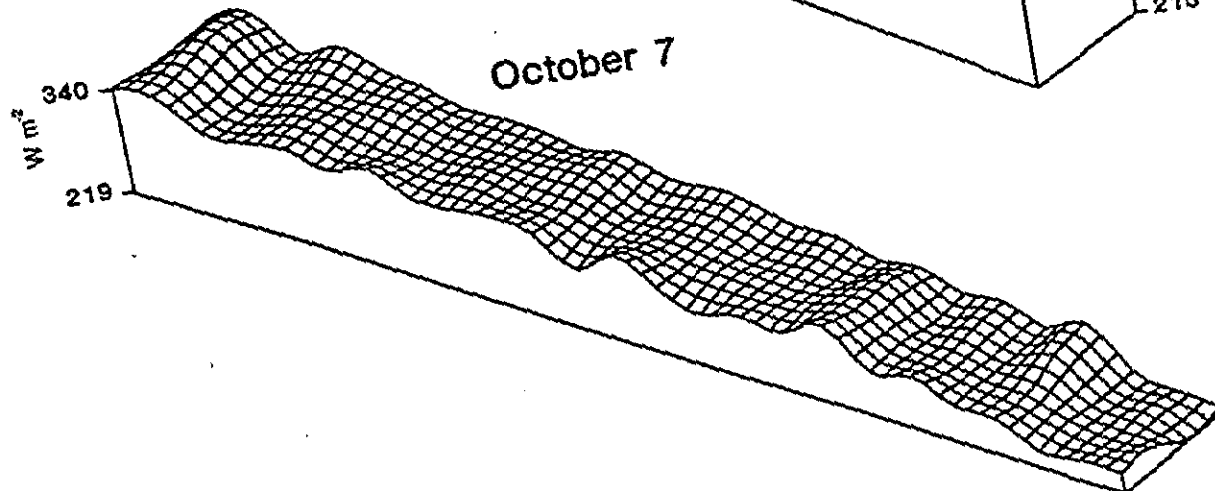
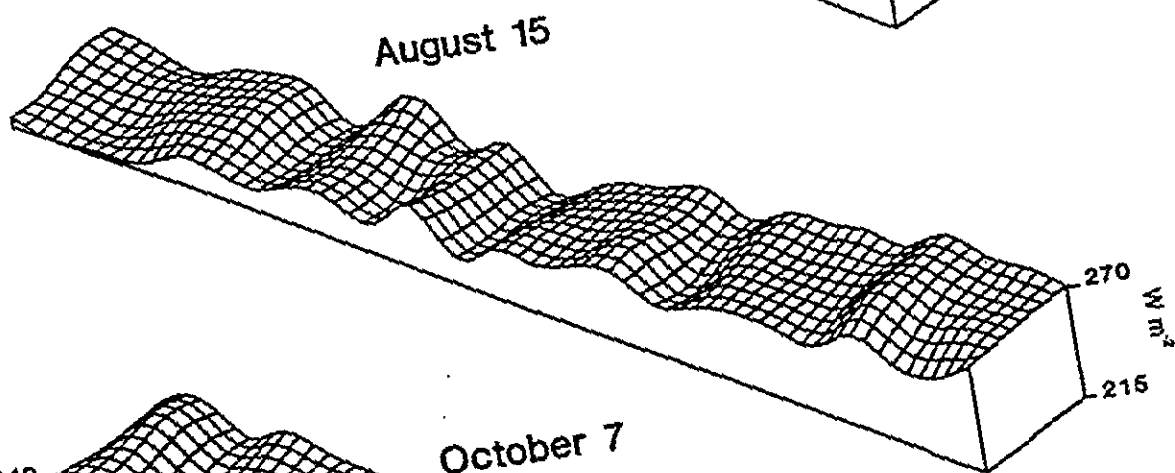
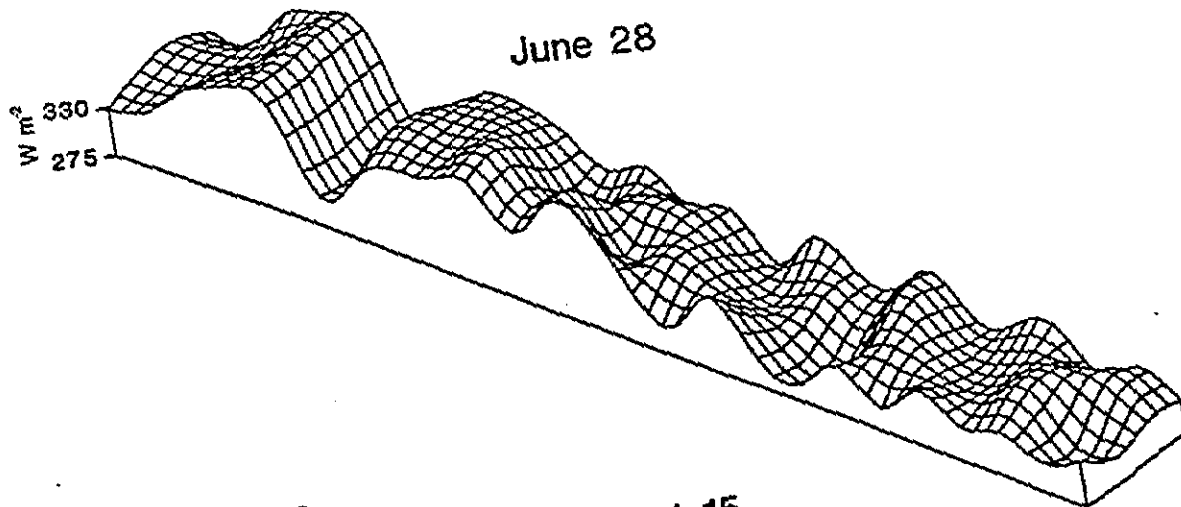


Figure 1.12. Regional variability of Latent heat fluxes ($W m^{-2}$) on three different dates. Data represent an area of 75 by 10 km.



pixel covering the same area. The results for June 28, August 15, and October 7 are presented in Figure 1.12. The data from June 28 and October 7 show higher evapotranspiration values over the grassland area, whereas on August 15 the agricultural land exhibits higher values. This behaviour can be attributed to variability in surface moisture due to irregular local rainfall distribution, illustrating the importance of accounting for local variations of the energy balance in estimating regional fluxes.

1.4. DISCUSSION

In recent years, considerable progress has been achieved in relating flux estimates from aircraft to spectrally derived data. Desjardins et al. (1989) demonstrated the feasibility of using airborne CO₂ flux measurements to characterize biomass production. Mack et al. (1990) showed that CO₂ fluxes measured with airborne sensors can be meaningfully related to vegetation indices derived from LANDSAT data in so far as a linear relationship could be established over agricultural land in Manitoba during the peak green period in July. Schuepp et al. (1992) and Desjardins et al. (1992) obtained very good correlation between airborne flux estimates of CO₂, sensible heat, and latent heat, and independently observed data on TS-Tair difference and greenness (SR), after correcting for the downwind displacement between surface source area and airborne sampling location (footprint correction).

The substantial scatter of points found in the present analyses (Figures 1.5 and 1.6 for CO₂, 1.10 and 1.11 for sensible and latent heat) is consistent with studies on the natural variability of boundary layer processes (e.g. Wyngaard et al. 1978, Wyngaard 1983, Lenschow and Stankov 1986, Saucier et al. 1991). Using Twin Otter flux observations, Austin et al. (1987) concluded that CO₂ flux discrepancies with scale lengths of 3 km can only be distinguished if the discrepancy is of the order of 10 kg ha⁻¹ h⁻¹ or more; eight passes would be

needed to delineate 1 km scale features. Part of the problem is undoubtedly due to the intermittency of the atmospheric boundary layer transfer, which was not sampled adequately enough within each 3 km run segment. At the flight altitude of 150 m (out of the surface layer), structural details related to surface exchange might already have been lost due to reorganization within the boundary layer. Scattering could also be due to inherent limitations of the NDVI, which may be affected by factors that alter soil background optical properties, such as the moisture status of the surface, soil roughness and textural variations (Huete and Warrick, 1990).

The argument for linearity of NDVI versus CO_2 uptake is usually made in terms of the analysis by Sellers (1985, 1987). Sellers, using a combination of models and experimental data, concluded that the simple ratio vegetation index is linearly related to the area-averaged photosynthetic capacity of the vegetation canopy. This linear relationship is caused by the complementary effect of two nonlinear responses, photosynthesis versus absorbed radiation (related to the leaf area index, LAI) and LAI versus the SR. It should be noted that the NDVI versus SR relationship itself is somewhat nonlinear. At high LAI values, the NDVI reaches saturation, so that further LAI increases are not reflected in the NDVI. Nevertheless, higher LAI can further increase the biomass accumulation rate, as in the July data. Experimental confirmation of this linearity has usually been based on relatively narrow ranges of CO_2 flux values; in this study also, it only appears

to apply over a limited range of conditions. The nonlinear nature of the NDVI versus CO₂ relationship on a seasonal basis may be surprising, but it appears real. The high CO₂ fluxes in July are similar to values measured by Mack et al. (1990) over an agricultural/grassland area in Manitoba. The explanation for the nonlinearity remains to be found.

Three factors are likely involved, all time-dependent in the growing season: (1) the intensity of the photosynthetic activity; (2) the intensity of respiration; and (3) the proportion of green vegetation within an AVHRR pixel. The diurnal CO₂ exchange between vegetation, soil and atmosphere encompasses CO₂ uptake by plants through photosynthesis, as well as CO₂ release from plants (respiration) and the soil (decomposition of organic matter). Both uptake and release exhibit a diurnal trend, but only the difference between the two is measured from an aircraft platform. A successful extrapolation to the total budget would have to rely on ancillary information (photosynthetically active radiation, air temperature, moisture availability/stress, etc.). An important prerequisite for this extrapolation would be a soil respiration model, preferably one driven by satellite data.

The higher scattering of latent heat flux data versus TS or NDVI is certainly related to the mechanism of water dynamics within the soil-plant complex. Idso et al. (1974, 1975) using albedo measurements, classified the drying process of the soil in three stages: (1) wet soil surface at potential evaporation, (2) transition between wet and dry with variable evaporation, and (3) dry soil surface with nearly

constant, low evaporation. Under field conditions all situations may be found over short distances (within a satellite pixel), given the high spatial variability of rainfall distribution, soil properties, and vegetation cover. Since evaporative demand may easily exceed the upward soil moisture flux, a wet soil may dry rapidly at the surface, while containing high moisture content in the root zone. Under conditions of partial canopy or bare soil, therefore, remote sensing of the surface may give a false idea of moisture availability.

A reliable parameterization of sensible heat flux over areas with nonuniform vegetation cover based on data from aircraft or satellite is an important research issue. Previous attempts to parameterize sensible heat flux based on radiative surface temperature (TS) over areas with partial canopy have given poor results (e.g. Stewart, 1989). This is due to the fact that TS may not represent the active interface between plant and atmosphere where most of the energy is transferred. A satellite sensor will provide an integrated value of surface temperature that includes bare soil and vegetation. The real aerodynamic surface temperature can be estimated from reliable measurement of sensible heat flux, air temperature and wind speed, solving equation 15 for TS. Under unstable conditions and partial canopy, the aerodynamic surface temperature is normally much smaller than TS.

The estimation of surface roughness presents another challenge to this approach. Considering the variations in vegetation cover and terrain topography, a reliable estimation for this parameter may be difficult (Lettau 1969, Thompson

1978). Our approach avoids these problems by using measured fluxes over the area of study. The results are preliminary, but promising for large-scale monitoring of energy exchange conditions at the surface. If reference sites are used to collect data representative of the region of interest, a reliable relationship between TS and sensible heat flux can be obtained and fluxes can be estimated with some confidence. The fact that the summer and fall data cluster very differently indicates that such relationships must be obtained for different periods of the year to account for differences in energy availability.

1.5. SUMMARY AND CONCLUSIONS

A study of the relationship between the vegetation index derived from AVHRR data and aircraft-based flux measurements from the NRC aircraft was undertaken in Kansas during the 1987 growing season. The study site consisted of a 75 km transect between Manhattan and Salina. A linear relationship between NDVI or SR versus CO₂ flux was found for any single date, but on a seasonal basis the relationship was nonlinear. This result is tentatively attributed to three seasonally varying functions within the AVHRR pixel, viz. intensity of photosynthetic activity, intensity of respiration, and proportion of green vegetation. Latent heat generally showed the poorest correlation with surface parameters. A linear seasonal relationship was found between NDVI and sensible heat.

The present study is the first to examine the relationship of AVHRR data to CO₂ uptake and fluxes of sensible heat and latent heat on a seasonal basis. The use of data over a large portion of the growing season provides an indication of the complexities inherent in the relationship between fluxes and surface parameters. In spite of the fairly substantial 1987 data set, the results must be considered tentative. Additional data sets including different types of soil cover and vegetation conditions, with repeated runs over the same area and within the atmospheric surface layer, would be required to confirm our findings. This illustrates the challenges involved in developing reliable models for inverting satellite data to meaningful biophysical parameters.

1.6. REFERENCES

- Austin, L. B., P. H. Schuepp, and R. L. Desjardins. The feasibility of using airborne CO₂ flux measurements for the imaging of the rate of biomass production, Agric. For. Meteorol., 39, 13-23, 1987.
- Betts, A. K., R. L. Desjardins, J. I. MacPherson, and R. D. Kelly. Boundary-layer heat and moisture budgets from FIFE. Boundary Layer Meteorol., 50, 109-137, 1990.
- Desjardins, R. L., E. J. Brach, P. Alvo, and P. H. Schuepp. Aircraft monitoring of surface carbon dioxide exchange. Science, 216, 733-735, 1982.
- Desjardins, R. L., J. I. MacPherson, P. H. Schuepp, and F. Karanja. An evaluation of aircraft flux measurements of CO₂, water vapour and sensible heat, Boundary Layer Meteorol., 47, 55-69, 1989.
- Desjardins, R. L., P. H. Schuepp, J. I. MacPherson, and D. J. Buckley. Spatial and temporal variation of the fluxes of carbon dioxide and sensible and latent heat over the FIFE site, J. Geophys. Res., 97,(d17), 18,467-18,476, 1992.
- Gash, J. H. C.. An analytical framework for extrapolating evaporation measurements by remote sensing surface temperature. Int. J. Remote Sens., 8(8), 1245-1249, 1986.
- Huete, A. R. and A. W. Warrick. Assessment of vegetation and soil water regimes in partial canopies with optical remotely sensed data. Remote Sens. Environ., 32, 155-167, 1990.
- Idso, S. B. and R. D. Jackson. Thermal radiation from the atmosphere. J. Geoph. Res., 74, 5397-5403, 1969.
- Idso, S. B., R. J. Reginato, R. D. Jackson, B. A. Kimball, and F. S. Nakayama. The three stages of drying of field soil. Soil Sci Soc. Am. Proc., 38, 831-837, 1974.

- Idso, S. B., R. D. Jackson, R. J. Reginato, B. A. Kinball, and F. S. Nakayama. The dependence of bare soil albedo on soil water content. J. Appl. Meteorol., 14, 109-113, 1975.
- International Geosphere-Biosphere Programme, The International Geosphere-Biosphere Programme: A Study of Global Change, The Initial Core Projects, Rep. 12, 1990.
- Leclerc, M. Y. and G. W. Thurtell. Footprint prediction of scalar fluxes using a Markovian analysis, Boundary Layer Meteorol., 52, 247-258, 1990.
- Lenschow, D. H. and B. B. Stankov. Length scales in the convective boundary layer, J. Atmos. Sci., 43(12), 1198-1209, 1986.
- Lettau, H.. Note on aerodynamic roughness-parameter estimation on the basis of roughness-element description, J. Appl. Meteorol., 8, 828-832, 1969.
- Mack, A. R., R. L. Desjardins, J. I. MacPherson, and P.H. Schuepp. Relative photosynthetic activity of agricultural lands from airborne carbon dioxide and satellite data, Int. J. Remote Sens., 11, 237-251, 1990.
- MacPherson, J.I.. NAE Twin Otter operations in FIFE, Lab. Tech. Rep. LTR-FR-104, 49 pp., Natl. Res. Counc. Canada, Ottawa, Canada, 1988.
- MacPherson, J.I.. NAE Twin Otter operations in FIFE, Lab. Tech. Rep. LTR-FR-113, 80 pp., Natl. Res. Counc. Canada, Ottawa, 1990.
- Monteith, J. L.. Evaporation and surface temperature. Quart. J. R. Met. Soc. 107, 1-27, 1981.
- Saucier, A., M. R. Duncan, and G. L. Austin. Mean flux estimation and cospectra of airborne carbon dioxide and water vapour eddy flux measurements in the planetary surface layer, Boundary Layer Meteorol. 55, 227-254, 1991.

- Schuepp, P. H., R. L. Desjardins, J. I. MacPherson, J. B. Boisvert, and L. B. Austin. Interpretation of airborne estimates of evapotranspiration, Estimation of Areal Evapotranspiration, IAHS Publ. 177, pp. 185-196, 1989.
- Schuepp, P. H., M. Y. Leclerc, J. I. MacPherson, and R. L. Desjardins. Footprint prediction of scalar fluxes from analytical solutions of the diffusion equation, Boundary Layer Meteorol., 50, 355-373, 1990.
- Schuepp, P. H., J. I. MacPherson, and R. L. Desjardins. Adjustment of footprint correction for airborne flux mapping over the FIFE site, J. Geophys. Res., 97(d17), 18,455-18,466, 1992.
- Sellers, P. J.. Canopy reflectance, photosynthesis and respiration, Int. J. Remote Sens., 6, 1335-1372, 1985.
- Sellers, P. J.. Canopy reflectance, photosynthesis and transpiration, II. The role of biophysics in the linearity of their interdependence, Remote Sens. Environ., 21, 143-183, 1987.
- Sellers, P. J., F. G. Hall, G. Asrar, D. Strebel, and R. E. Murphy. The First ISLSCP Field Experiment (FIFE), Bull.Am. Meteorol.Soc., 69, 22-27, 1988.
- Stewart, J. B., W. J. Shuttleworth, K. Blith, and C. R. Lloyd. FIFE, a comparison between aerodynamic surface temperature and radiometric surface temperature over sparse prairie grass. Proc. 19th Conf. Agric. and Forest Met. and Ninth Conf. Biomet. and Aerobiol., Charleston, S. Carolina, p.144-146, Amer. Met. Soc., 1989.
- Tanré, D., C. Deroo, M. Herman, and J. Morcrette. Description of a computer code to simulate the satellite signal in the solar spectrum: The 5S code, Int. J. Remote Sens., 11(4), 659-668, 1990.
- Teillet, P.M.. Surface reflectance retrieval using atmospheric correction algorithms, Proceedings of the IGARSS'89, 12th Canadian Symposium on Remote Sensing,

Vancouver, B.C., p.864-866, Can. Soc. Remote Sensing, 1989.

Thompson, R. S.. Note on the aerodynamic roughness length for complex terrain, J. Appl. Meteorol., 17, 1402-1403, 1978.

Wyngaard, J. C.. Lectures on the planetary boundary layer, in: Mesoscale Meteorology - Theories, Observations and Models, edited by D. K. Lilly and T. Gal-Chen, pp. 603-650, pp. 216-224, D. Reidel, Norwell, Mass., 1983.

Wyngaard, J. C., W. T. Pennell, D. H. Lenschow, and M. A. Lemone. The temperature-humidity covariance budget in the convective boundary layer, J. Atmos. Sci., 35, 47-58, 1978.

Connecting Statement

In Chapter 1 we explored the feasibility of using single aircraft overpasses as a basis for fitting satellite-based information. It was observed that a considerable part of the variability in the relationships between NDVI and surface temperature versus sensible heat, water vapor and CO₂ fluxes remained unexplained, due to the intermittent nature of turbulence. This problem is further explored in Chapter 2, in which we use conditional sampling of aircraft-based flux estimates of sensible heat and water vapor to isolate individual turbulent structures that dominate transport, and to examine their link to surface characteristics.

Chapter 2:

STRUCTURAL ANALYSIS OF AIRBORNE FLUX ESTIMATES OVER DIFFERENT ECOSYSTEMS

Abstract

Aircraft-based observations of the turbulent fields of velocity and scalars are used to study those coherent turbulent structures that dominate turbulent transfer of moisture and heat above three different ecosystems. Flux traces are defragmented, to reconstruct the presumed full size (along the sampled transect) of these structures, and flux traces simplified by elimination of those that contribute negligibly to the flux estimate. Structures are analyzed in terms of size, spatial distribution and contribution to the flux, in the four 'quadrant' modes of eddy-covariance transfer (excess up/down and deficit up/down). The effect of non-linear detrending of moisture and temperature data on this 'structural analysis', over surfaces with heterogeneous surface wetness, is also examined. Results over grassland, wetland and wet and dry agricultural land, show that non-linear detrending appears to provide a physically more realistic description of structures than linear detrending. Significant differences were observed between structure size and associated relative flux contribution, between moist and dry areas, with smaller structures playing a more important role over the moist areas. Structure

size generally increases with height, as spatial reorganisation from smaller structures into larger ones takes place. This coincides with a gradual loss of surface 'signature' (position and clustering of plumes above localized source areas), in accordance with the concept of the 'blending height'. Data are expected to provide a basis for an eventual statistical description of boundary-layer transfer events, and help to interpret the link between boundary-layer transfer and surface source distributions.

2.1. INTRODUCTION

In Chapter 1 of this thesis, the relationships between airborne flux estimates over 3 km run segments, and remote sensing of vegetation (NDVI) and surface temperature, showed significant scatter, particularly for water vapor. Part of the observed scatter may be attributed to (1) the intermittent nature of turbulence, not adequately sampled in a single aircraft overpass, and (2) the flight altitude of 150 m. The latter exceeds the surface layer where fluxes are expected to be approximately constant and closely related to underlying surface characteristics. Over the FIFE site, Brutsaert and Sugita (1990) have shown that the maximum height for validity of the Monin-Obukhov similarity was around 100 m.

In this chapter, conditional sampling of the turbulent structures that carry fluxes is used to isolate individual events along flight lines and to study their link to surface characteristics. These analyses deal with the specific application of aircraft-based observations to estimate fluxes of moisture and sensible heat by the eddy correlation technique.

Several authors have used conditional sampling of airborne data to analyze the properties of updrafts and downdrafts in the atmospheric boundary layer (e.g. Manton 1977, Coulman 1980, Lenschow and Stephens 1980, Mahrt and Palmier 1984, Grossman 1984, Shaw and Businger 1985, Duncan and Schuepp 1992). It groups data from many turbulent 'events', with application of threshold criteria, into

specific modes of transport, providing quantitative information about size, frequency, and distribution of events (Greenhut and Khalsa 1982). An introduction to 'quadrant' techniques, where turbulent transport is represented in terms of excess up/down or deficit up/down modes is provided by Antonia (1981), Shaw (1985) and Grant et al. (1986), among others.

In the present study we analyze the time series of airborne observations on transport of moisture and sensible heat, to identify those coherent turbulent events that are contributing significantly to the flux estimate. In particular, the size of these events, their distribution in space and their relative contribution to the flux are examined. The effect of detrending on results of this analysis is addressed, and the question to what extent the physical characteristics of these events are determined by boundary layer dynamics rather than surface properties, such as the spatial distribution of surface moisture and temperature. Results may contribute to a better definition of airborne sampling criteria above different ecosystems under different conditions of atmospheric stability. They may also be of interest to boundary layer modellers as a statistical description of real events against which models of turbulent transfer can be tested. In so far as this chapter summarizes results obtained over different ecosystems, the findings may help to improve description of the link between the hydrological balance and atmospheric circulation models.

2.2. MATERIALS AND METHODS

2.2.1. Aircraft instrumentation and data collection

The Canadian Twin Otter research aircraft is equipped to measure the three wind components, air and surface temperature, CO₂ and water vapor concentration, incident and surface-reflected short wave radiation, among many other parameters. Turbulence is measured at the nose of the aircraft, using a gust boom incorporating a Rosemount 5-hole probe and associated pressure transducers. Air temperature is also sensed at the nose using a Rosemount fast-response heated probe, and surface temperature by PRT-5 radiation thermometer. CO₂ and water vapor concentrations are measured by an infrared gas analyzer installed in a duct through the cabin from a 120 cm² inlet on the top of the fuselage. All data are digitized at the rate of 16 Hz, giving a resolution of 3.75 m per data point at the mean aircraft speed of 60 m.s⁻¹. A more detailed description of instrumentation and data processing is presented in Chapter 1 and elsewhere (MacPherson, 1988, 1990).

The database analyzed in the present study includes information collected during the FIFE Experiment over grassland in Kansas in the summer of 1989 (Sellers and Hall 1988), the Canadian Northern Wetland Study (NOWES) in the Hudson Bay - James Bay lowlands in Northern Ontario in the summer of 1990, and the California Ozone Deposition Study (CODE) in the San Joaquin Valley in

the summer of 1991 (MacPherson, 1992). Dates and a summary of runs analyzed for this database are presented in Table 2.1.

2.2.2. Eddy correlation technique and quadrant analysis

A general definition of a turbulent coherent event, such as a thermal or plume, is not yet available (see review by Schulmann and Moeng 1991). Possibilities include the use of threshold values of temperature, updraft velocity, humidity and turbulence intensity, but no single parameter can be expected to provide a satisfactory definition (Lenschow and Stephens 1980). Grossman (1984) pointed out that the combination of moisture and vertical wind would be more adequate to describe convective cells. The present analysis follows this idea, and an approach similar to that of Duncan and Schuepp (1991) (hereafter referred to as **DS**), in which eddy correlations of vertical wind and scalar admixture (sensible heat, water vapor) are used to identify the different modes of transport. In the eddy correlation technique (Swinbank 1951), fluxes are estimated from space/time averages of fluctuations of vertical wind (w') and scalar property (c') over a given sampling run.

It is important to realize that a physically meaningful definition of fluctuations must be based on a realistic definition of the mean. The question of convergence of the mean of observations in the turbulent boundary layer, in connection with analysis of the variability of airborne flux estimates, has been addressed elsewhere

Table 2.1. Summary of the run characteristics: site, flight ID, start time, mean flight altitude (z), incident shortwave radiation ($K\downarrow$), friction velocity (u.), stability (z/L), and ratio of flight level to boundary layer height (z/zi).

SITE	FLIGHT ID (*)	START TIME (LOCAL)	z(m)	$K\downarrow$ (wm^{-2})	u. (ms^{-1})	z/L (**)	z/zi
FIFE	JL2801	11:43:59	80	634	0.29	-4.44	0.07
	JL2802	11:50:24	80	738	0.40	-1.58	
	JL2803	11:57:40	89	658	0.34	-1.71	
	JL2804	12:03:39	92	759	0.44	-2.22	
	JL2814	13:01:42	92	799	0.26	-8.01	
	JL2815	13:08:06	92	871	0.28	-6.99	
	JL2816	13:14:14	87	779	0.40	-2.75	
	JL2817	13:21:11	84	853	0.32	-1.74	0.08
	AU0405	14:03:07	95	853	1.07	-0.05	
	AU0407	14:16:06	91	845	1.37	-0.04	0.04
	AU1207	12:32:05	97	810	0.37	-3.25	
	AU1210	13:17:38	96	817	0.45	-1.58	
WETLAND	JL1408	15:57:52	97	750	0.47	-1.04	0.02
	JL1411	16:15:00	96	768	0.57	-0.60	
	JL1705	15:25:19	97	725	0.24	-0.42	
	JL1706	15:31:22	99	734	0.19	-0.31	
	JL1711	16:01:55	97	762	0.44	-0.24	
	JL1712	16:07:04	98	770	0.23	-0.14	
SAN JOAQUIN VALLEY	JL1301	15:15:04	30	882	0.33	-1.33	0.04
	JL1302	15:18:25	30	871	0.21	-1.79	
	JL1303	15:21:46	30	864	0.17	-6.72	
	JL1307	16:37:11	30	738	0.13	-4.96	
	JL1308	16:40:23	30	735	0.19	-0.44	
	JL1309	16:43:35	30	721	0.18	-4.76	

(*) First two digits = month (JL = July, AU = August), third and fourth digits = day, last two digits = run number.
(**) z is the flight altitude (m) and L is the Obukhov length (m).

in principle (e.g. Wyngaard et al. 1978, Wyngard 1983, Lenschow and Stankov 1986), as well as in terms of the Twin Otter airborne observations (Austin et al. 1987, Schuepp et al. 1989). It becomes particularly relevant over terrain with non-homogeneous distribution of surface characteristics, where mean quantities of scalars may be spatially variable. Filtering or detrending will generally be advisable in this case, but the effect of such procedures on the resulting analysis must be explored.

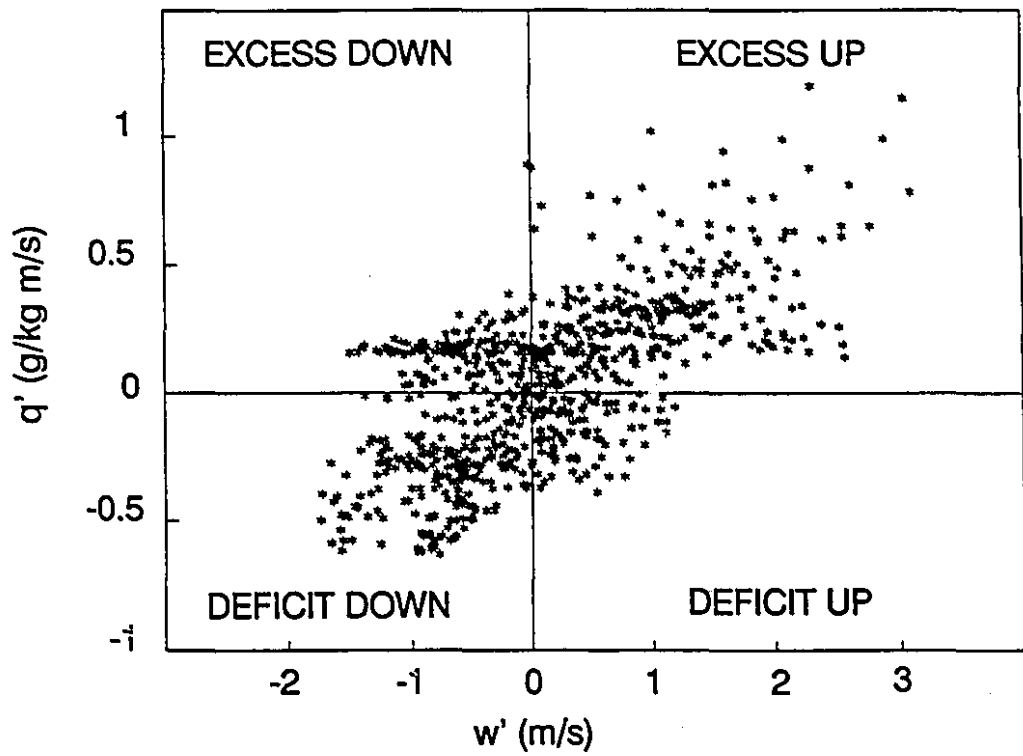
If the fluctuations of vertical wind and concentration are correlated, i.e. if upward and downward air motions preferentially contain an excess or deficit of concentration, the average of such products is non-vanishing. All studies of turbulent flux generally show that the turbulent transfer processes reflected by these fluctuations are not regularly distributed in space. Instead, transfer is effected by a number of more or less localized 'coherent events', which express the physical connection between vertical motion and the concentration field. For simplicity, such events will be called 'structures'. Structures would be characterized by duration (time fraction along a given run), intensity (fractional contribution to the total flux estimate), and spacing. A plume is a typical example of a structure, combining, for example, upward air motion ($w'^{(\uparrow)}$) with moisture excess ($q'^{(\uparrow)}$) (here called **excess up**). Similarly, the other three modes of transport would be **excess down**, **deficit down**, and **deficit up**. Figure 2.1 shows a representative case of a scatter plot of $w'q'$, in terms of these four quadrants, along a 5 km run segment

over the FIFE site. It illustrates that moisture transfer is primarily effected in the expected excess-up and deficit-down ('gradient') modes, although 'counter-gradient' events in the opposite quadrants are also present. It also shows, not surprisingly, noticeable asymmetry between opposing quadrants of gradient transfer, with a preponderance of extreme events in the excess-up, relative to the deficit-down, mode.

2.2.3. Defragmentation

The successful delineation in time or space of coherent structures that contribute to the flux estimate in turbulent flow, depends on the correct identification of sectors within the data vector where any one of the four modes of transport takes place. The occurrence of internal fluctuations (e.g. in q), may give short-term excursions into different quadrants that produce 'fragmented' structures. This problem is particularly acute when structures are weak, and near the tail-ends of structures. It may be caused, for example, by dry pockets enclosed inside a moist plume. A so-called 'defragmentation procedure', similar to that of **DS**, is used to recognize and restore the dominant structures. In this procedure, every datapoint is assigned a number corresponding to one of the four quadrants (as indicated in Figure 2.1), and a sequence of numbers representing the respective quadrant is generated along the run. Structures with a sequence of less than 8 datapoints in the same quadrant (30 m) are either eliminated from the database,

Figure 2.1. Scatter plot of vertical wind fluctuation (w') versus water vapor concentration fluctuation (q').



based on the fact that cospectral analysis showed negligible contribution to the flux estimates from such structures at flight levels (Alvo et al. 1984, Desjardins et al. 1991), or incorporated into a 'dominant' structure if the latter shows a gap equivalent to the eliminated structure. This approach differs from that of **DS** at the tail-ends of structures, where **DS** defragmented each given structure without considering characteristics of the subsequent one in the time series. In our analysis, the interface between any two structures is examined and the defragmentation based on consideration of both structures, with the one with higher flux value considered the dominant one. This procedure generally resulted in elimination of $\leq 3\%$ of the total flux estimate along a run.

2.2.4. Definition of 'extreme events'

Many (fragmented or defragmented) structures along a given run contribute very little to the flux; they complicate the 'flux signature' while carrying little significant information. A clearer picture of structures that primarily carry the flux can be obtained if a threshold is applied to eliminate non-significant events. This is accomplished by using a threshold function similar to that of **DS**. It is based on the product of the mean flux of each structure ($F_{s,i}$) along the run, and its fractional contribution to the total flux (F), i.e. in essence a quadratic function of flux contribution divided by the time fraction occupied by the structure along the run. The intensity of each structure is then defined by

$$\phi = F_{st} F \quad (1)$$

with

$$F_{st} = \frac{1}{x_{st}} \sum_{i=1}^{x_{st}} (w'q')_i$$

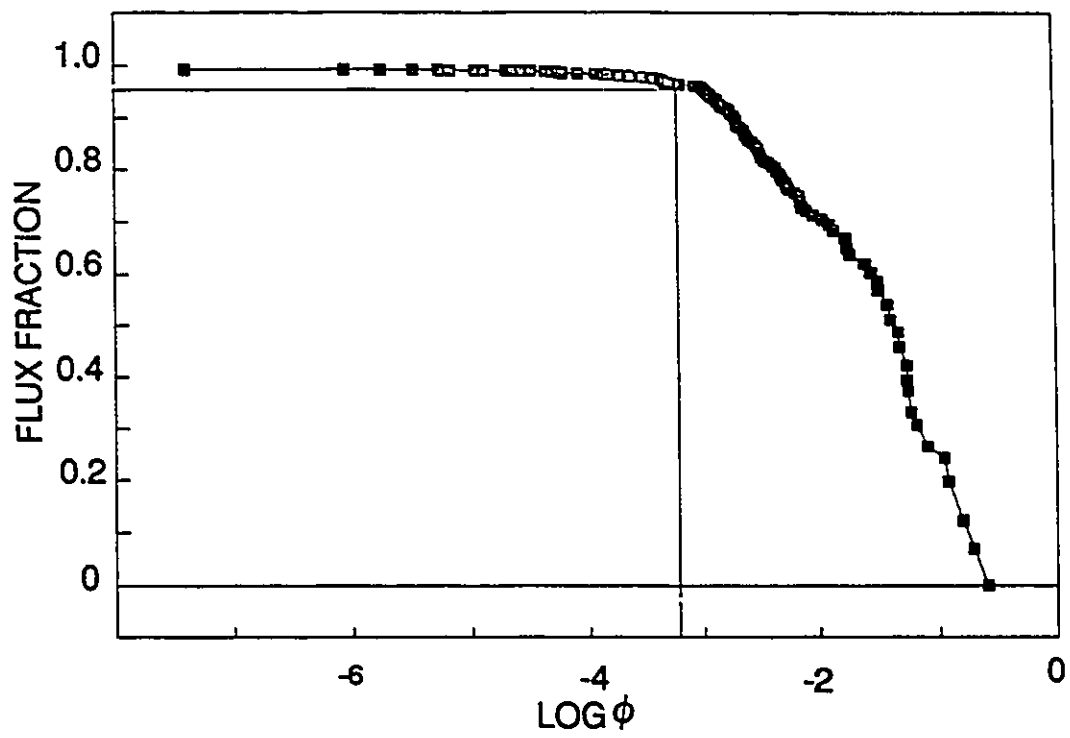
and

$$F = \frac{\sum_{i=1}^{x_r} |(w'q')_i|}{\sum_{j=1}^{x_r} |(w'q')_j|}$$

Terms and symbols in (1) are defined as follows: x is the number of data points, with subscripts st and r denoting 'structure' and 'run', respectively. Current datapoints within structures and runs are indicated by i and j , respectively. There may be an element of arbitrariness in the definition of this threshold procedure, but ϕ will provide a convenient threshold criterion.

The highly non-linear relationship between increasing threshold values ϕ , and the cumulative flux fraction of those events that exceed the given threshold (Figure 2.2), confirms that extreme 'events' are carrying much of the flux along the run. The question remains how to properly establish a threshold that separates these events from those of little significance. In our study we arbitrarily imposed a threshold value of ϕ in such a way that elimination of all structures below the threshold reduces the cumulative flux of the remaining structures to 95% of the flux

Figure 2.2. Cumulative flux contribution versus threshold function ϕ (values are sorted in ascending order). Threshold at 95% of flux fraction is indicated by straight lines.



estimate. The threshold is applied to the structures after defragmentation, which itself reduces the flux estimate by 2 to 3%. This procedure eliminated between 20 and 40 % of all structures along a typical run. The threshold is generally aligned around the point of maximum curvature of the plot of flux fraction vs. $\log \phi$ (Figure 2.2.).

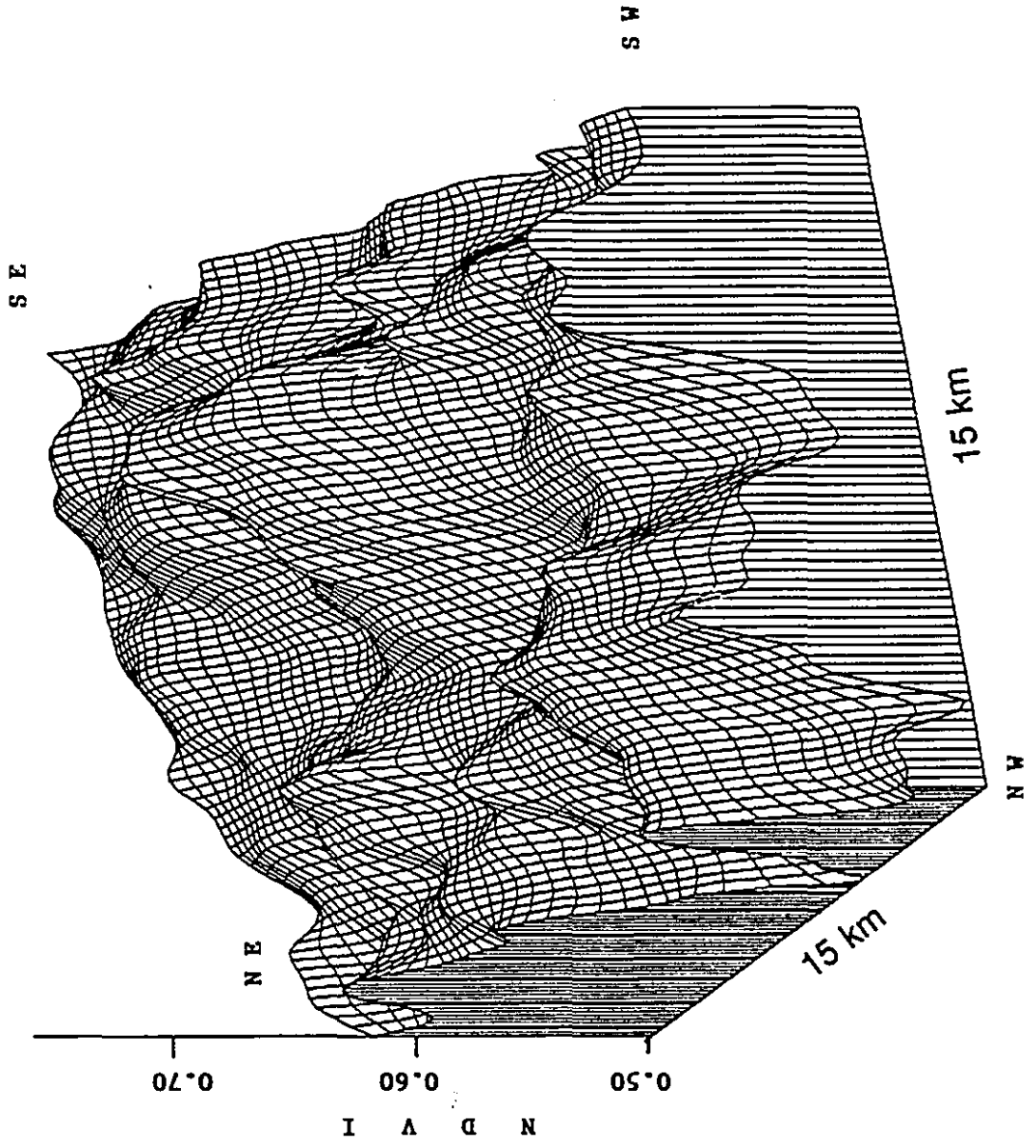
2.2.5. Linear vs. non-linear detrending

Since eddy correlation estimates and structural analysis are based on fluctuations, i.e. deviations from the mean, the results become very dependent on how the mean is defined. This problem is more serious for airborne techniques than for ground-based ones, because mean values often show trends over the extended areas that must be sampled for a reliable flux estimate; it is also much more acute over land than over oceans. Although linear detrending may be adequate for many homogeneous areas, it can be quite inadequate in situations where the mean concentration of the scalar property (e.g. water vapor) changes non-linearly along the run. In such cases, deviations computed against a physically incorrect mean could lead to the appearance of spurious structures, and unreliable flux estimates. On the other hand, non-linear detrending represents a high-pass filtering technique whose effects on the magnitude of the flux estimate cannot be deduced a priori.

The FIFE site in 1989 was characterized by pronounced moisture gradients,

associated with a dry area along the western end of the site and a green, moist area at the SE corner. This is illustrated in Figure 2.3, which shows the values of NDVI from NOAA-9 over the site for July 28. Some of the grid runs executed over this area were used to examine the sensitivity of structural analysis and flux estimates to the procedure of detrending of water vapor concentration. Two different detrending models are evaluated: linear (least squares) and non-linear (by Fourier series approximation with truncation after different terms).

Figure 2.3. Normalized Difference Vegetation Index (NDVI) over the FIFE site on July 28, 1989. Data were obtained from the afternoon overpass of the NOAA-9 satellite. Notice pronounced contrast between SW (dry) and SE (moist) corners.



2.3. RESULTS AND DISCUSSION

2.3.1. Effect of detrending

Figure 2.4 shows a pattern of water vapor concentration trends typical for all runs analyzed. It is clear that a straight line fit to the series will interpret both ends of the run primarily as excess, and the center portion as deficit. The non-linear detrending, using a Fourier approximation with truncation after the second term, provides an adequate fit to most of the analyzed data. A better fit is obtained with three terms when there is a pronounced change of concentration from the dry to the moist area, such as observed on August 4 and August 12. The spatial allocation of the turbulent structures along the run for both linear and non-linear detrending is given in Figure 2.5. The range of flux ($w'q'$) is shown on the right y axis, and the respective quadrant mode (excess \uparrow , excess \downarrow , deficit \downarrow , deficit \uparrow) is plotted against the left y axis. As the flux contribution shifts from one quadrant to another, a vertical line is displayed if the next structure occurs above the specified threshold level. If data is eliminated between structures, a blank space appears between dominant structures. We can observe that linear detrending in such cases leads to identification of excess-up (moist plumes) as the predominant positive contributions to the flux at the beginning and near the end, while deficit-down prevails in the center part of the run. Non-linear detrending, on the other hand, produces a more uniform distribution of plumes along the run. This appears more

Figure 2.4. Mixing ratio of water vapor over a 15 km run at the S end of the FIFE site on July 28, 1989 (run JL281 in Table 1). Linear (least squares) and non-linear (Fourier approximation with truncation after the 2nd term) detrending are illustrated.

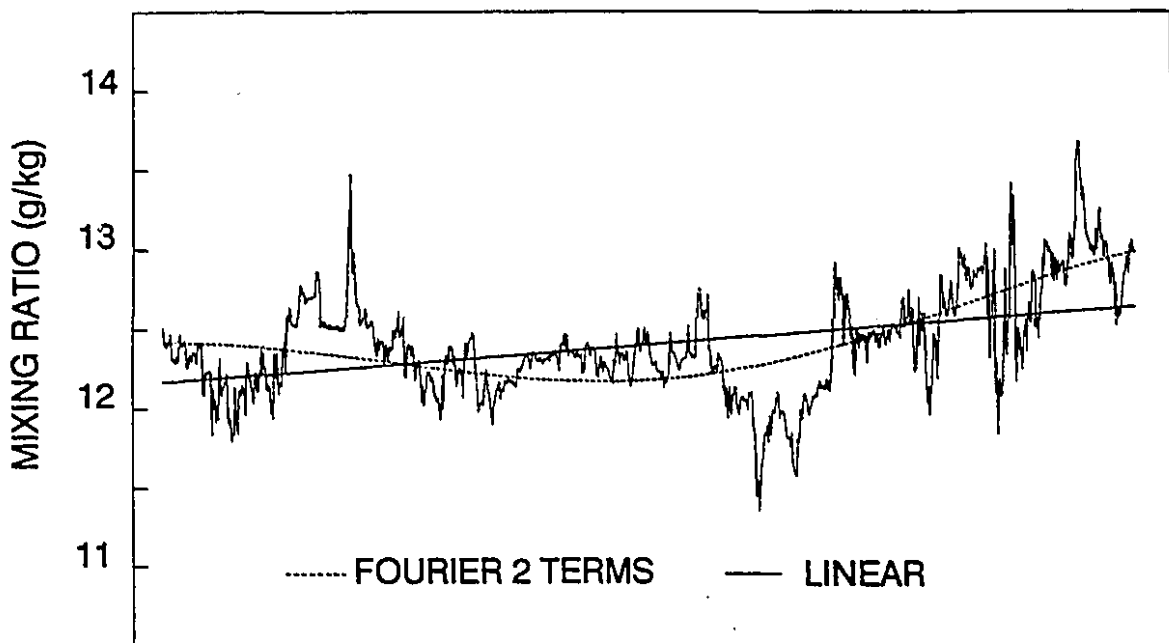


Figure 2.5. Effect of detrending on structural analysis of run JL281 (Fig. 2.4). The distribution of structures within the four modes of transport (excess up/down, deficit up/down) is plotted along with contributions to the mean flux estimate after detrending.

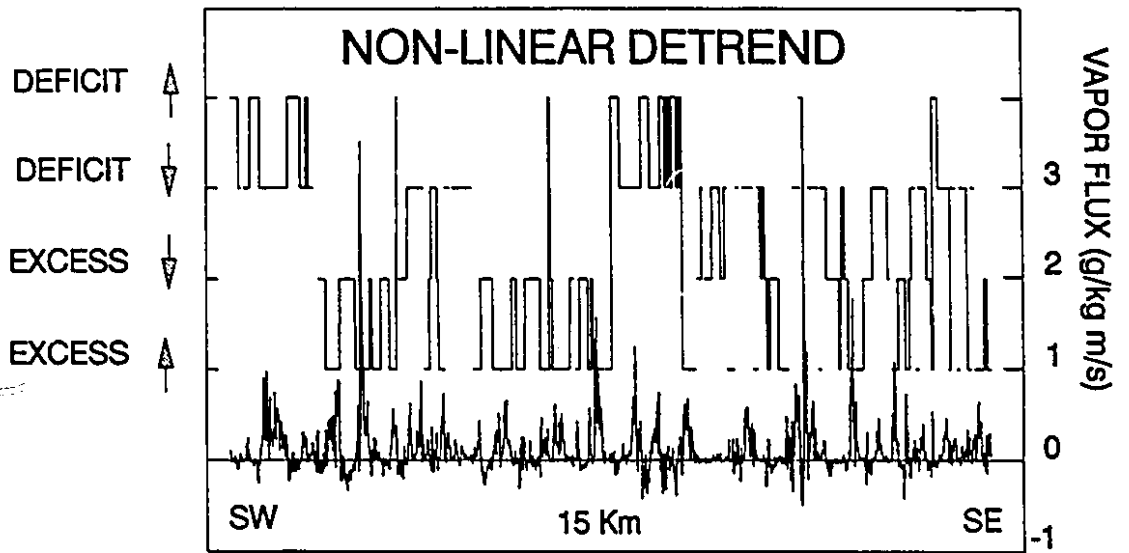
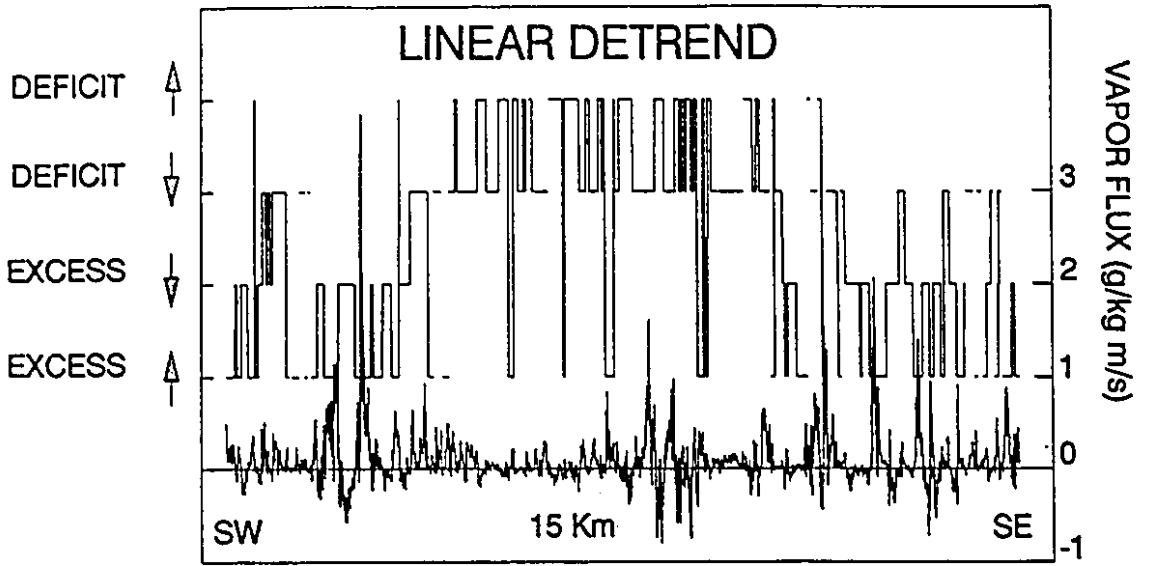
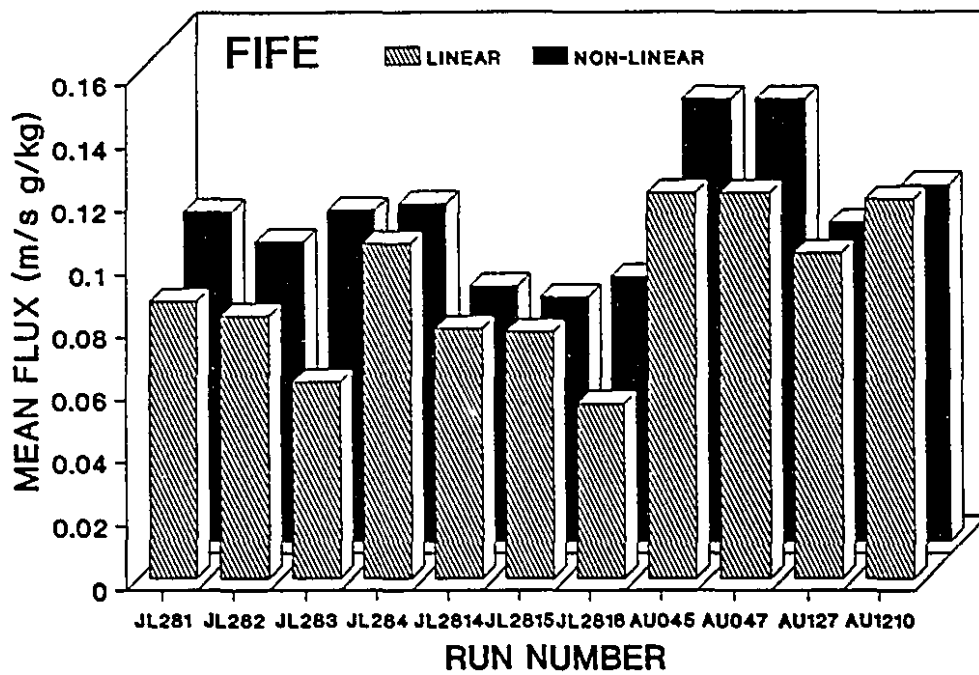


Figure 2.6. Effect of detrending of water vapor concentration on mean flux estimates over the FIFE site.



realistic, since it would be hard to formulate a physically convincing hypothesis for predominant downward dry air entrainment over the center of the FIFE site under prevailing surface and boundary-layer conditions. The same extreme plumes are identified by both procedures, although with altered relative magnitude. In terms of the mean flux estimates, significant differences were observed, as seen in Figure 2.6. Linear detrending generally underestimated the mean flux compared to non-linear detrending, with differences ranging from 20 to 40 % on some of the runs to negligible on others. Such underestimation may contribute to the occasionally observed underestimations of airborne fluxes relative to ground based observations over the FIFE site (Desjardins et al. 1992).

The fact that non-linear detrending tends to enhance the airborne flux estimate over that obtained under linear detrending is significant in so far as its high-pass filtering effect might be expected to reduce the overall flux estimate. It suggests that the potential loss of long-wavelength contributions is more than compensated, on the average, by a gain in physical realism. This argument is based on the implicit assumption that a physically incorrect manipulation will not consistently increase the correlation between two 'random' time series that are physically linked. Our analysis does not permit, at this stage, to document a convincing general argument in favor of non-linear detrending over that of filtering, for routine flux estimates. We feel, however, that non-linear detrending may provide a sensitive and flexible means of adjusting structural analysis to flux traces of

unfiltered data over complex ecosystems, where the precise mode of detrending may have to be chosen on a case by case basis.

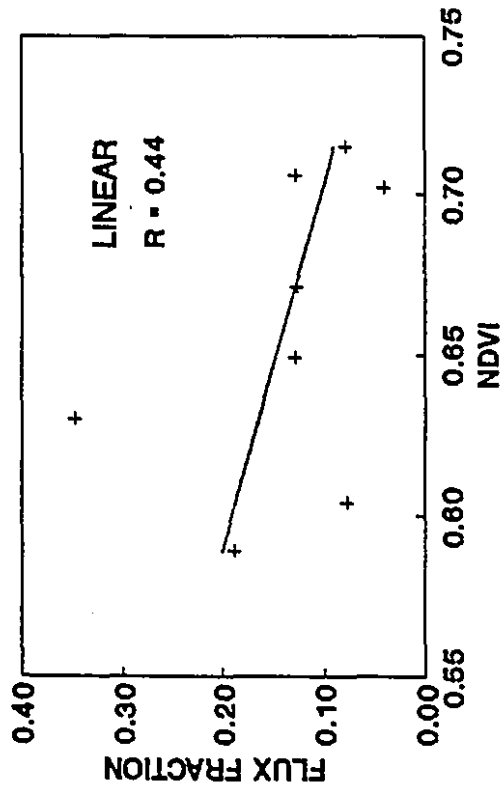
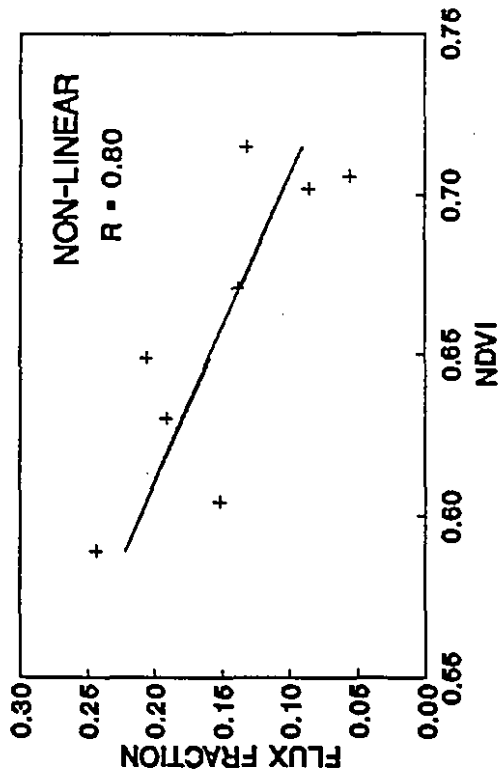
The quality of linear vs. non-linear detrending may be further examined by correlating the occurrence of structures along the run with surface features such as vegetation, surface moisture, or surface temperature. This analysis is demonstrated for greenness and thermal plumes, which would be expected to be negatively correlated. Figure 2.7 presents the correlation between the Normalized Difference Vegetation Index (NDVI) from the afternoon overpass of the NOAA-9 satellite on July 28, and the sensible heat flux fraction from the excess-up quadrant. Each point represents a 5 km average from either the W (dry) or E (moist) areas, from four different runs. The non-linearly detrended data show a higher correlation ($R = 0.80$) than the linearly detrended ($R = 0.44$), suggesting that the non-linear procedure provided more adequate reflection of surface 'signatures'.

2.3.2. Quadrant contribution to the flux

Comparative information for moisture transfer from the three ecosystems under consideration is presented in Table 2.2 for each quadrant, in terms of frequency of events and their associated flux and time fractions.

Flux and time fractions are defined here as the summation of flux contributions or time-duration for all events in each quadrant, after the defragmentation

Figure 2.7. Linear correlation between flux fraction of thermal plumes and Normalized Difference Vegetation Index (NDVI) over the FIFE site on July 28, 1989. Each point represents the cumulative flux fraction from the excess-up mode over a 5-km segment, from either the SW (dry) or the SE (moist) end of the runs.



run. Each value represents an average over all runs for each ecosystem, with standard deviations given in brackets. The data from FIFE (grassland) and from the Northern Wetland appear similar in terms of relative importance of the four quadrants. For these surfaces, quadrant 1 (moist plumes/excess up) is the most important mode of transport, accounting for an average of 45% of absolute contributions to the flux estimate, occupying about 31% of the time. Downward entrainment of dry air contributes about 35%, and the remaining 20% (in absolute values) represent counter-gradient transport modes (excess down and deficit up). Since our analysis deals with whole structures, often with relatively weak 'tail ends', these time fractions must not be confused with time fractions given for threshold procedures based on so-called hyperbolic holes in the quadrant plot. The latter progressively eliminate portions of all structures that fall below a given flux intensity threshold. Previous application of hyperbolic hole techniques to the FIFE data base has shown consistently that the most intense portions within all structures, which occupy about 20% of the time fraction along a run, contribute about 80% to the total flux estimate (Duncan et al. 1989, Duncan 1990).

Although the data from irrigated and dry California agricultural land (San Joaquin Valley) were taken at a lower average flight height, the mean value of z/z_i is within the same range of the other two ecosystems (Table 2.1). In this case, quadrants 1 and 3 are equally important in terms of flux contribution (about 35%), but quadrant 3 exhibits more structures and occupies a larger time fraction. It is

Table 2.2. Summary of 'quadrant' analysis: site, quadrant (1 = excess up, 2 = excess down, 3 = deficit down, 4 = deficit up), frequency and flux/time fractions of events in each quadrant. Standard deviations are given in brackets. The runs specified in Table 2.1 were used in the calculations.

LOCAL	QUADRANT	FREQUENCY OF EVENTS (%)	FLUX FRACTION (%)	TIME FRACTION (%)
FIFE	1	32.5(3.38)	45.1(2.38)	31.2(1.99)
	2	23.5(3.49)	12.2(1.11)	22.2(2.69)
	3	28.1(3.20)	32.1(3.19)	27.8(3.36)
	4	16.1(3.94)	8.5(1.36)	14.9(1.93)
WETLAND	1	31.6(2.07)	44.7(3.70)	31.3(2.55)
	2	22.0(2.52)	11.4(3.15)	19.6(1.94)
	3	26.7(2.75)	36.0(1.28)	33.0(2.10)
	4	19.7(3.20)	6.8(2.30)	13.4(3.11)
SAN JOAQUIN VALLEY	1	26.9(3.65)	35.9(3.73)	26.0(1.24)
	2	18.2(3.30)	10.7(2.59)	16.0(3.09)
	3	31.4(3.92)	34.6(3.12)	34.6(2.93)
	4	23.5(2.30)	16.3(2.77)	17.9(2.51)

yet possible to determine to what degree this difference is attributable to height or surface characteristics. It does suggest the possibility of a certain influence of the very atypical surface moisture distribution in this highly manipulated ecosystem.

2.3.3. Structure size and flux contribution

It is important to stress that the one-dimensional sampling of structures by aircraft trajectories cannot reveal the real size of structures except in an average, statistical sense that reflects essentially random transects through three-

dimensional structures. In the subsequent analysis, observations are presented in terms of frequency distributions of structure diameters for each run, averaged over the different intervals of class. Mahrt and Palmier (1984) have used average not values in a similar way to analyze quadrant contributions to heat transport in the atmospheric boundary layer, based on the argument that single runs are vulnerable to sampling problems.

Figure 2.8 shows average frequency of sampled structure sizes for all four modes of transport, for the FIFE and Wetland sites and Figure 2.9 presents similar information for the San Joaquin Valley. In order to explore potential differences between structure size over moist and dry areas, data are presented separately for primarily moist and dry sections of the FIFE and San Joaquin runs. The FIFE runs were split into E and W segments (moist and dry) and the San Joaquin data are based on 12 km segments of more or less uniform irrigated cropland (moist) and bare soil or senescent vegetation (dry).

The frequency of structures decreases approximately exponentially with increasing average size in all cases. Although comparisons with other studies must be approached with caution due to differences in criteria for defining structures, these findings are qualitatively similar to those of Manton (1977). There is an indication of a higher frequency of small plumes over moist areas, and of more frequent occurrence of larger structures over dry areas. This would be expected, considering that water vapor is less dense than dry air. Therefore, for a given

Figure 2.8. Frequency distribution of structure sizes over wet and dry areas of the FIFE and Wetland sites. FIFE data are separated into W (dry) and E (moist) sections.

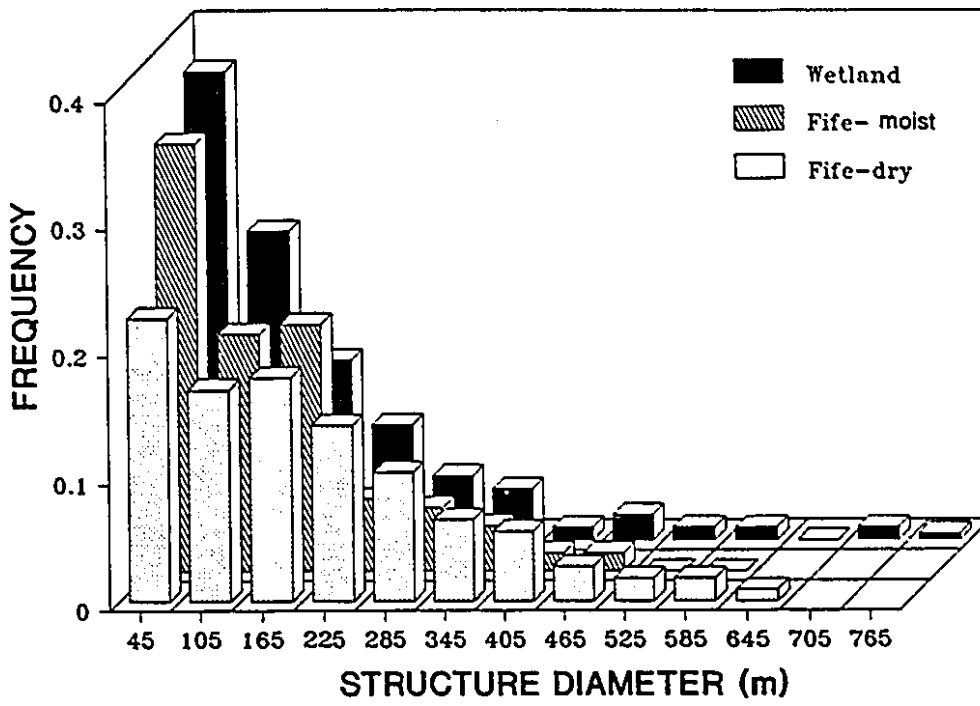
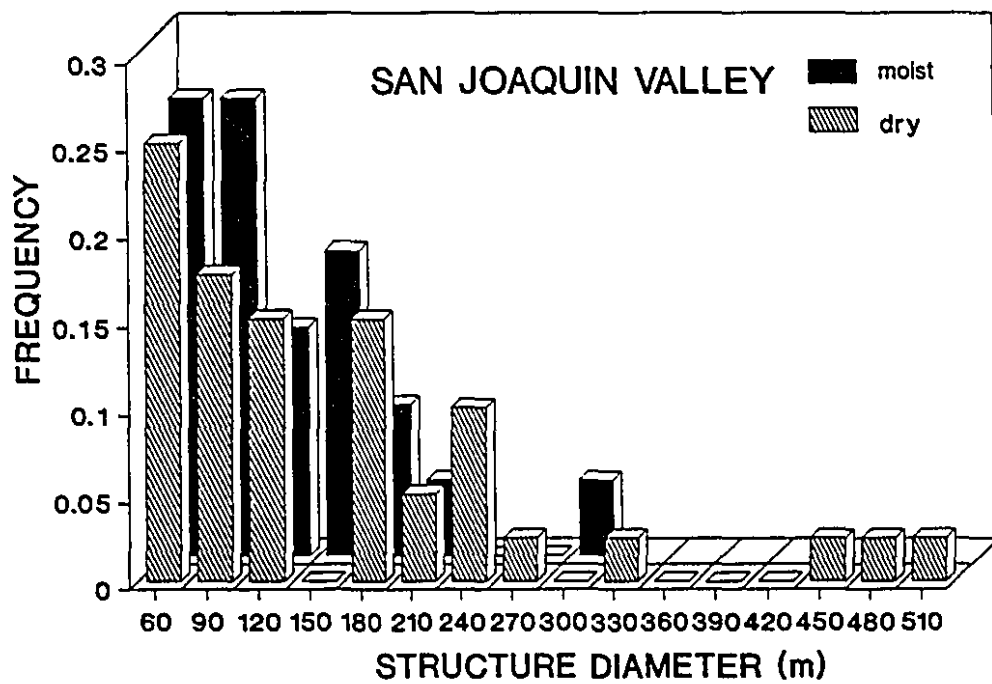


Figure 2.9. Frequency distribution of structure sizes over irrigated (moist) and non-irrigated (dry) areas of the San Joaquin Valley.



surface heating, a rising parcel of dry air is likely to generate plumes of larger size than a rising plume of moist air. No information is provided for structures with less than 30 metres, because of the previously mentioned demonstration of insignificant contribution to the flux from such structures at flight levels.

The relative contribution to the flux from different structure sizes is given in Figure 2.10, for the FIFE and San Joaquin Data separated as above into moist and dry areas. It considers all four modes of transport. Figure 2.11 presents the same information for the FIFE data, but only for the moist plumes. One may notice a significant difference in the range of structure diameters with maximum contribution to the flux, between moist and dry areas. Smaller structures generally contribute more strongly over the wet areas. Structure sizes are smaller for the San Joaquin Valley data, most likely attributable to the lower flight altitude of 30 m, suggesting merging of structures to form larger plumes with height. Structures with sizes of up to about 1 km were found both over the FIFE and Wetland sites. In such cases, individual structures can contribute up to between 10 and 20 % of the total flux along the run if they are in the excess-up quadrant, and their inclusion or exclusion along runs provides much of the observed run-to-run variability of flux estimates. A reliable statistical description of such extreme structures cannot easily be provided due to their sporadic appearance in this limited set of runs.

Figure 2.10. Relative contribution from all four modes of transport (excess up/down, deficit up/down) versus structure size; (a) over moist and dry areas of the FIFE site and (b) over irrigated and non-irrigated areas of the San Joaquin Valley.

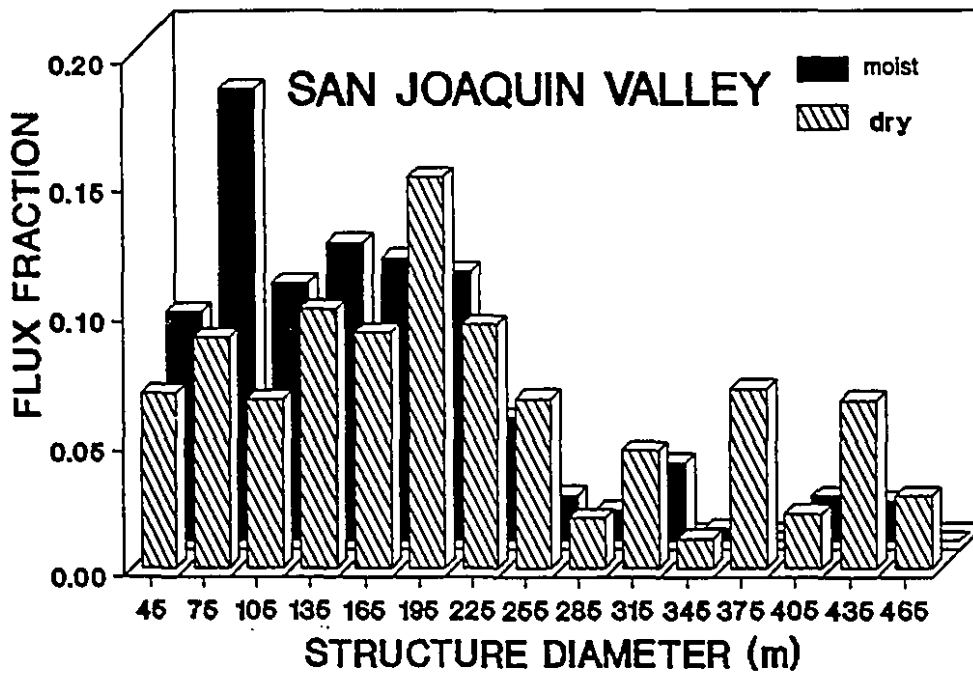
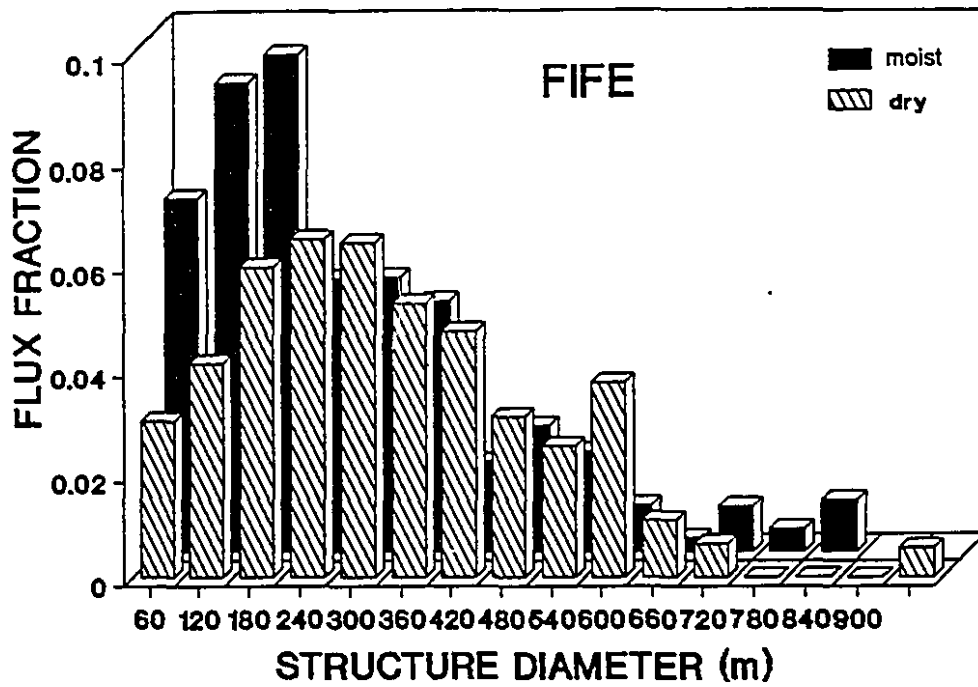
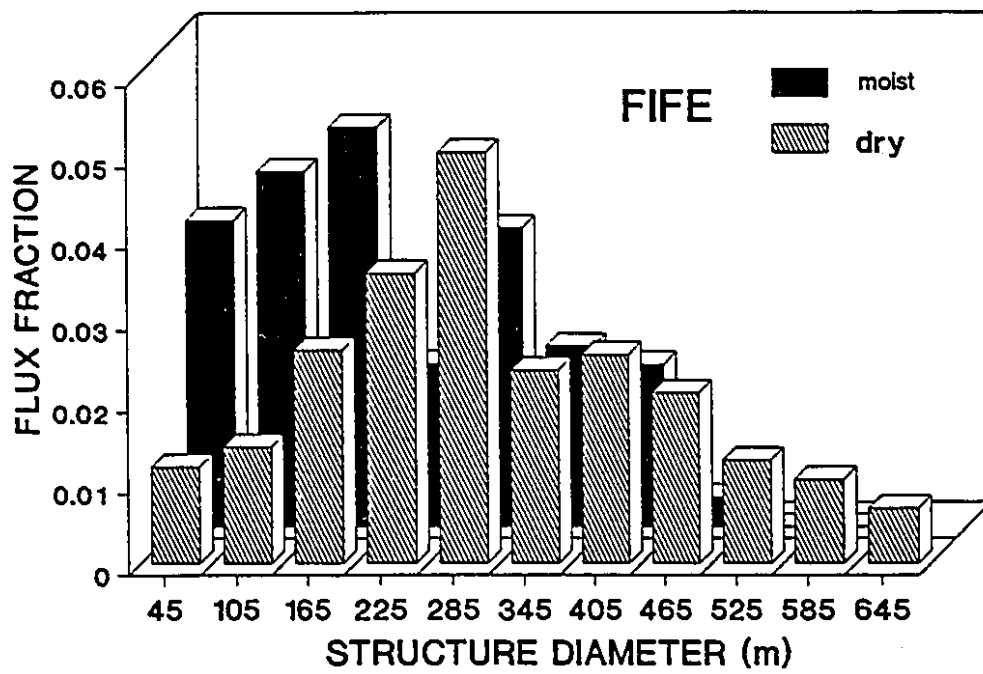


Figure 2.11. Relative flux contribution from moisture plumes (excess up) versus structure size over moist and dry areas of the FIFE site.



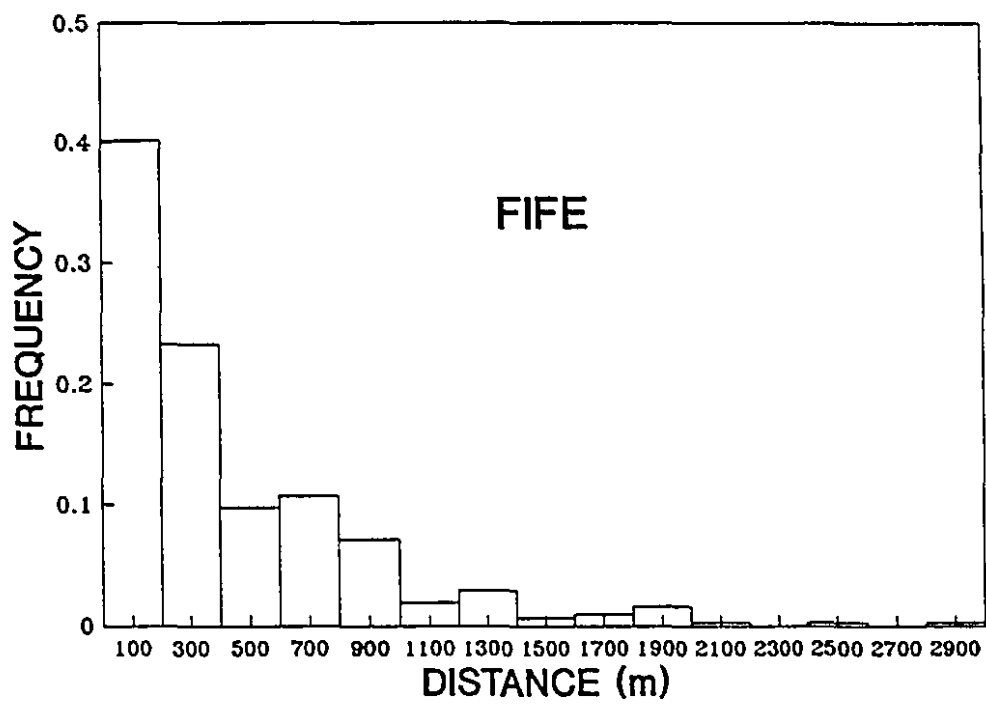
2.3.4. Spacing between structures

The intermittency of the turbulent transfer process in the atmosphere is a complicating factor in any attempt to relate flux observations to underlying surface characteristics, and it is a main factor in the design of sampling strategies. In our study we deal only with the patchiness of turbulence or global intermittency which is due to organization on scales larger than the main coherent eddies (Mahrt 1989). An eventual statistical model for the description of turbulent events, in space and time would also have to quantify spacings between structures. Figure 2.12 shows the distribution of spacing between 'significant' (i.e. above-the-threshold) wet plumes over the FIFE site in classes of 100 m of distance. About 95 % of structures are spaced between 0 to 1000 m, but gaps of up to 3 km were observed over this particular ecosystem. It must be remembered, that structures in our analysis are either rejected or retained as a whole, so that the spacing between structures may differ from that between 'intensive cores' of structures retained by other threshold techniques. Such conditions illustrate, at any rate, the difficulty of obtaining a representative flux estimate from limited sampling runs (as discussed e.g. by Lenschow and Stankov, 1986) and to obtain a clear signature of the surface from single overpasses such as used in Chapter 1.

2.3.5. Flight altitude vs. flux 'signature'

Any attempt to link airborne flux observations to surface source distributions

Figure 2.12. Spacing (m) between moisture plumes over the FIFE site.



must consider (a) the downwind displacement of the emitted source material between surface and flight level and (b) the degree of spatial organization in plume structure that may have occurred between those levels. Question (a) has been addressed in studies on 'footprint corrections' (Leclerc and Thurtell 1990, Schuepp et al. 1990, Cihlar et al. 1992, Wilson and Swaters 1991, Schuepp et al. 1992, Horst and Weil 1992). They generally work with parameterized diffusivity in the vertical and have not yet successfully solved the problem of the 'inverse footprint correction' (deducing effective upwind source strength distribution from airborne observations) except by a heuristic approximation (Schuepp et al. 1992) applicable only to strong, large-scale gradients in surface transfer. Our study addresses question (b) through preliminary comparative analysis of structures at different heights. Wieringa (1986) has introduced the concept of the 'blending height', i.e. the height (of typically 70 to 100 m) over a non-uniform terrain where flow becomes more or less independent of horizontal position. It must be expected that flux 'signatures' from localized, distinct surface elements will be difficult or impossible to identify at or above this height.

Case study 1: Our tentative analysis compares three situations: a) a 15-km segment of a regional run at an altitude of 150 m over grassland near the FIFE site; b) a 15 km run over the S end of the FIFE site at an altitude of approximately 100 m; c) a 12 km run over the San Joaquin Valley at an altitude of about 30 m. The difference between surface and air temperatures and the simple ratio

vegetation index for the three cases are plotted as surface characteristics, along with thermal and moist plumes, in Figures 2.13, 2.14, and 2.15. Situation (a) (Figure 2.13) shows that distribution of structures at greater heights even over homogeneous surfaces is very non-uniform, reflecting the strong degree of spatial reorganization into prominent plumes. This makes it extremely difficult to determine surface distributions of source strength from airborne sampling. Situation (b) (Figure 2.14) shows that where large-scale gradients (e.g. in surface temperature or vegetation index exists), the frequency of occurrence of plumes at 100 m generally reflects the overall distribution, although it might be unrealistic to expect resolution of pronounced local gradients. Situation (c) (Figure 2.15) shows that strong discontinuities in surface source strength or temperature are reflected in the distribution of structures sampled at heights well within the surface boundary layer.

Case study 2: In this case we analyzed the surface 'signature' of thermal and moisture plumes at 30 and 100 m over the San Joaquin Valley, along run segments of approximately 12 km over an area with transition between vegetation and bare soil/dead vegetation. Both the temperature and the humidity signal showed a nonlinear trend along the run, which was eliminated using Fourier series truncated after the second term. Figures 2.16 and 2.17 show simultaneous plots of $(T_s - T_a)$, greenness, thermal plumes, and moisture plumes, over the area. At 30 m, we see very intensive and wider plumes over the dry area, as a result of more

intensive surface heating. All the major moisture plumes are driven by the thermal plumes. Notice the very intensive thermal plume occurring around the location of the irrigation canal (where $T_s - T_a$ vanishes), driving an intensive local moisture plume. At 100m (Fig. 2.17) we see fewer thermal and moisture plumes, evidence of the merging of turbulent structures with increasing height. Most of the weak moisture plumes that were detected at 30 m are not present at 100 m.

Figure 2.13. Ratio of Infrared (IR) over red (R) reflected solar radiation (VI), difference between radiative surface temperature and air temperature ($T_s - T_a$), and distribution of thermal and moisture plumes over a 15-km mixed grassland and agricultural land near the FIFE site. Mean flight altitude is 150 m. (Width of plume 'box' indicates duration, and area the relative flux contribution).

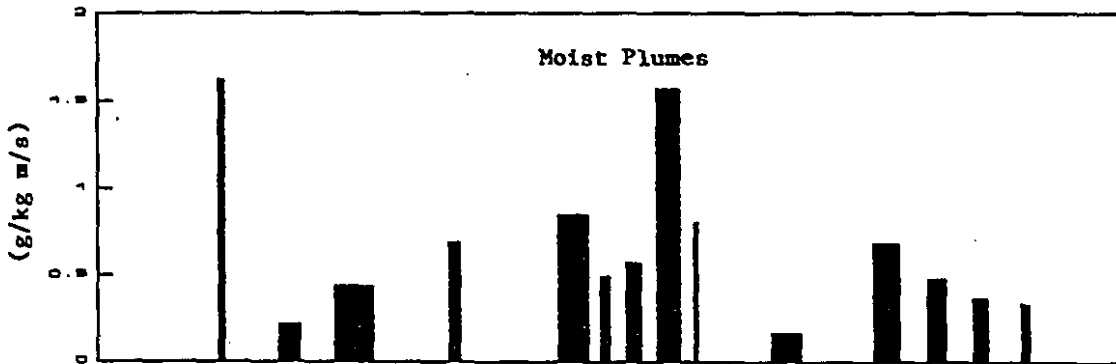
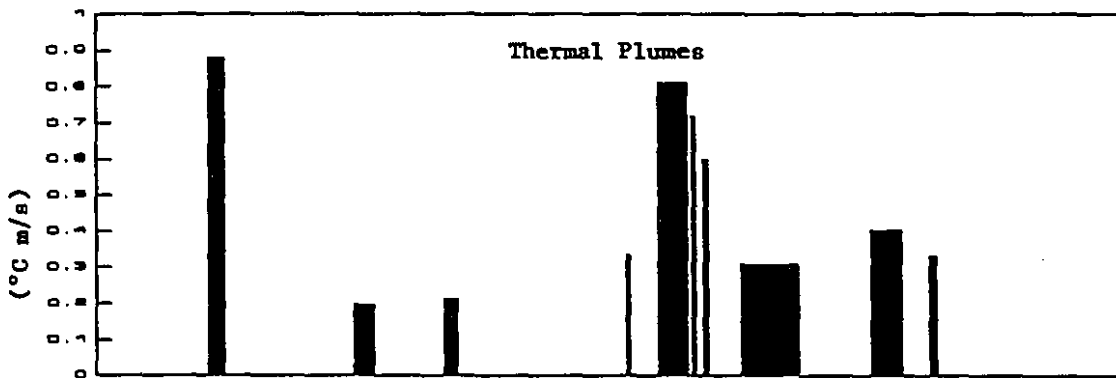
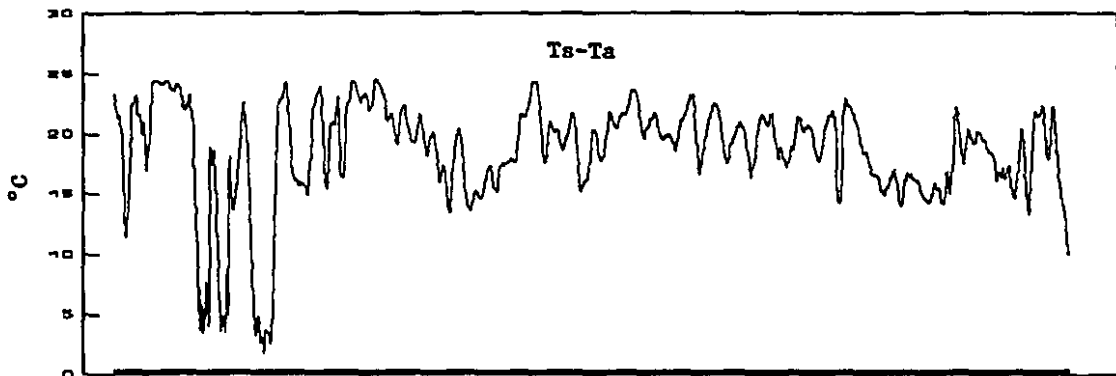
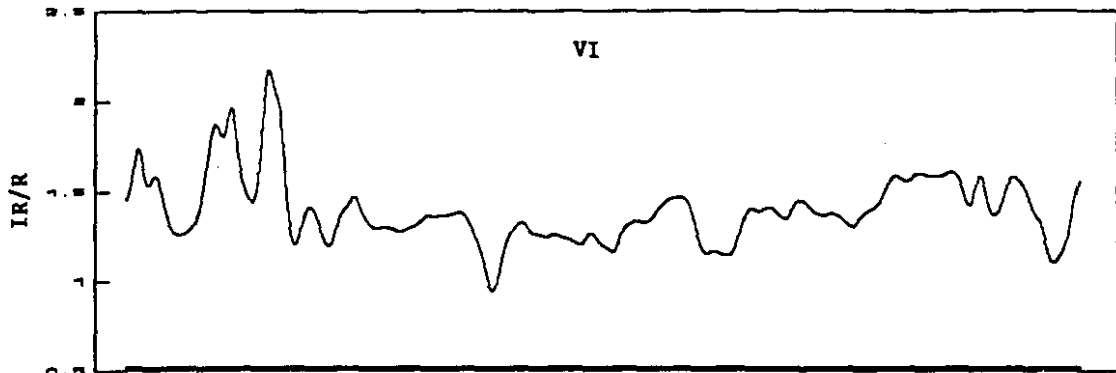


Figure 2.14. Surface characteristics and plume distribution (as defined in Figure 2.13) for a 15-km run over the S end of the FIFE site. Mean flight altitude is 100 m.

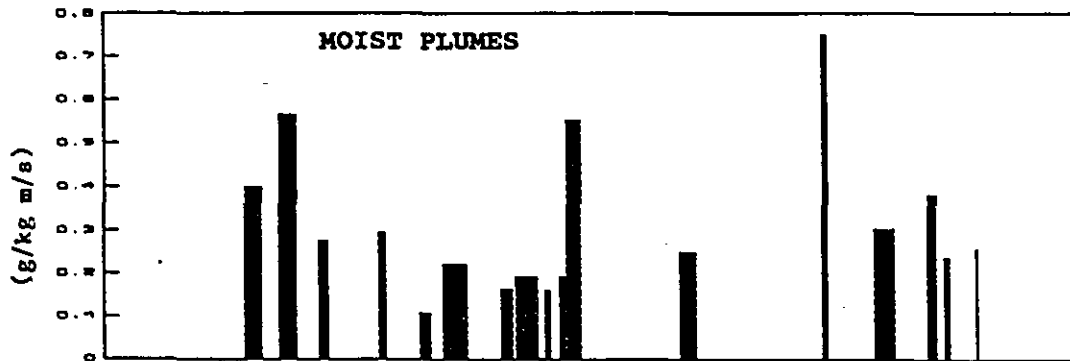
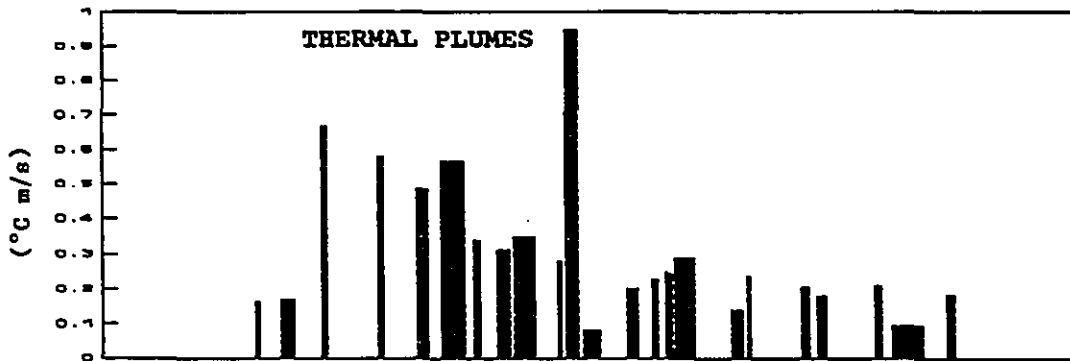
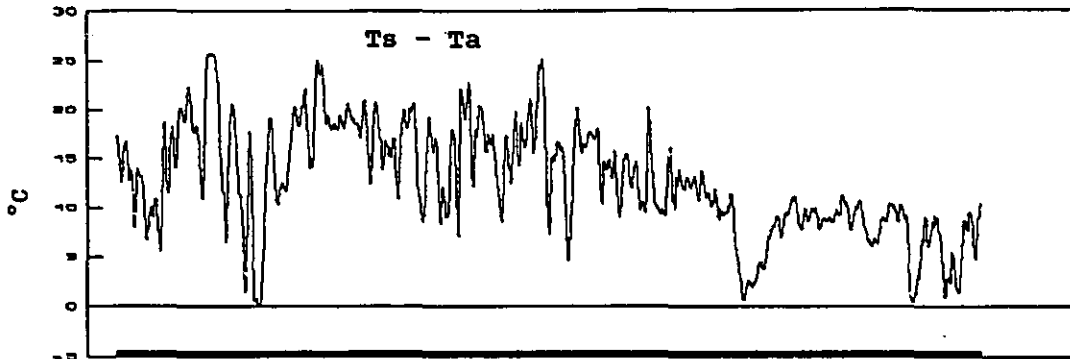
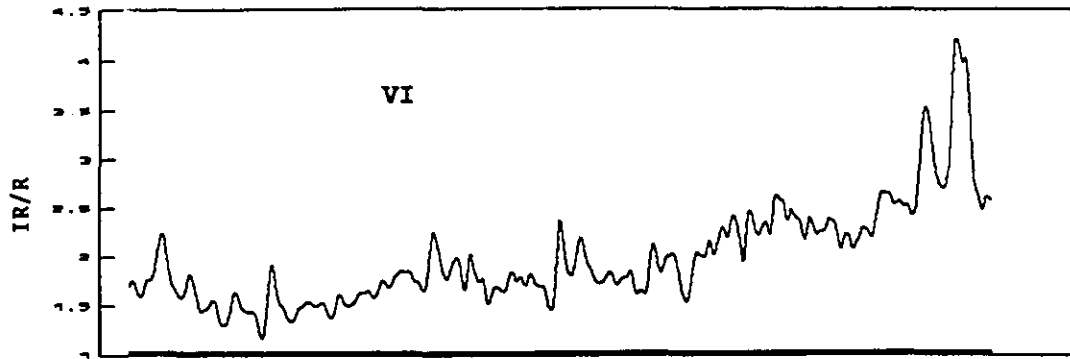


Figure 2.15. Surface characteristics and plume distribution for a 12-km run over the San Joaquin Valley. Mean flight altitude is 30 m.

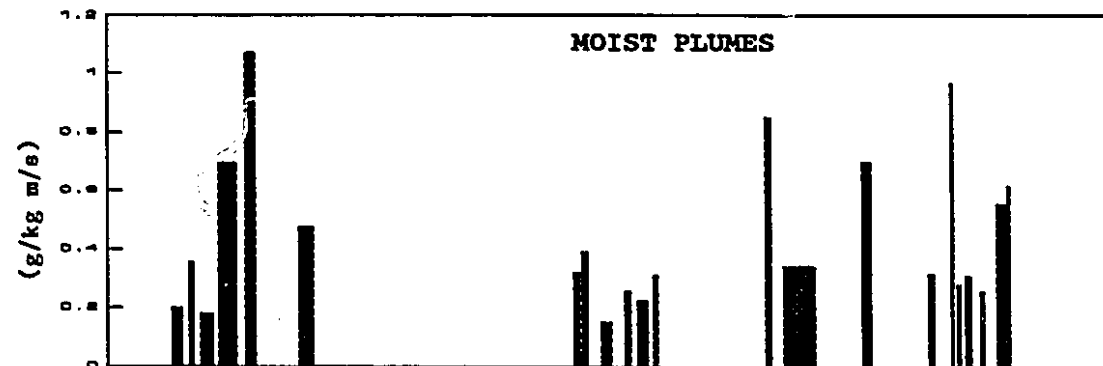
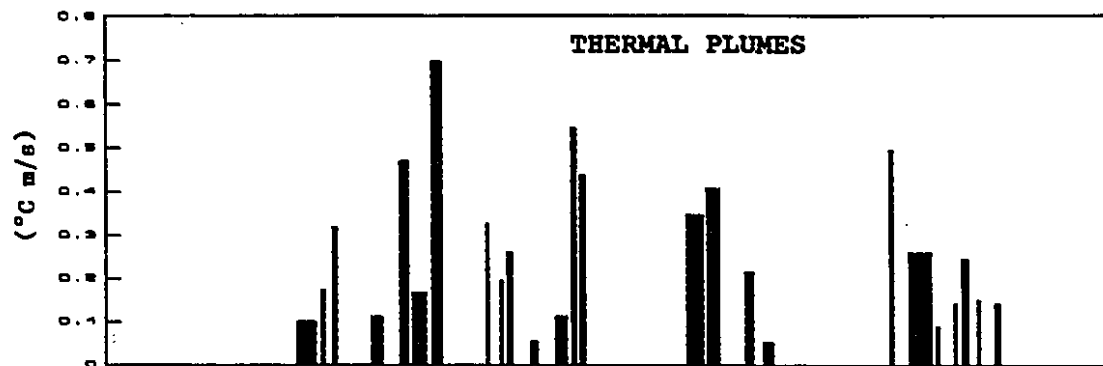
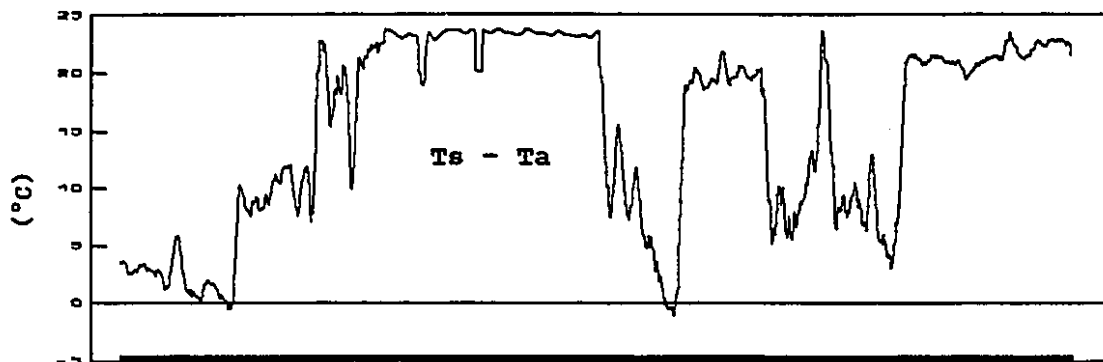
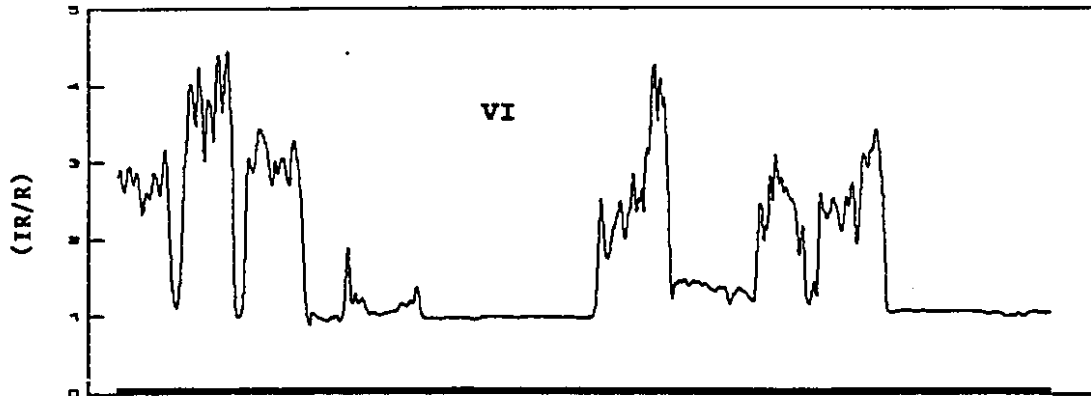


Figure 2.16. Difference between radiative surface temperature and air temperature ($T_s - T_a$), Ratio of Infrared (IR) over Red (R) reflected solar radiation (VI), and distribution of thermal and moist plumes for a 12-km run over the San Joaquin Valley. Mean flight altitude is 30m.

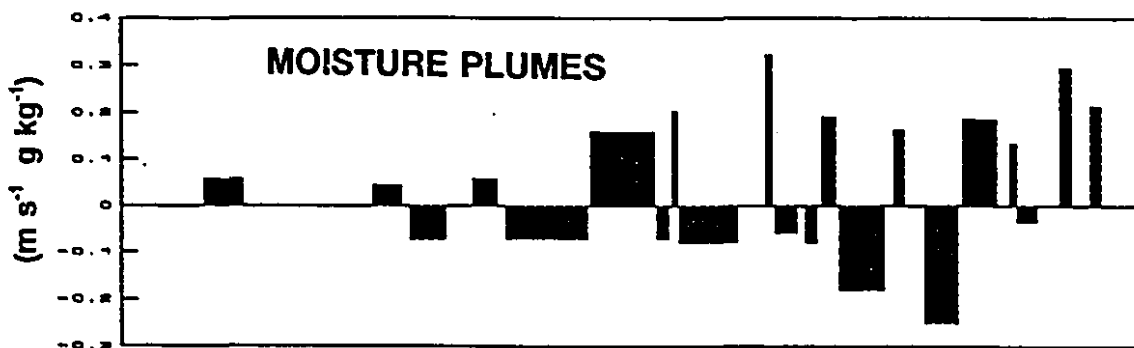
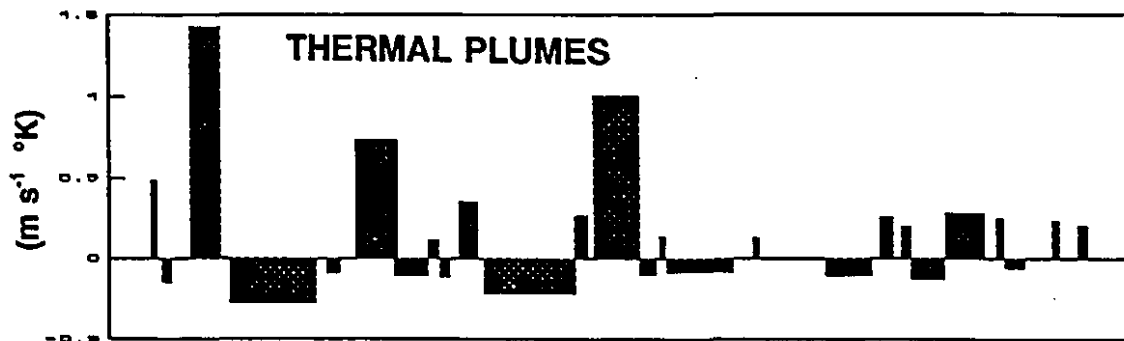
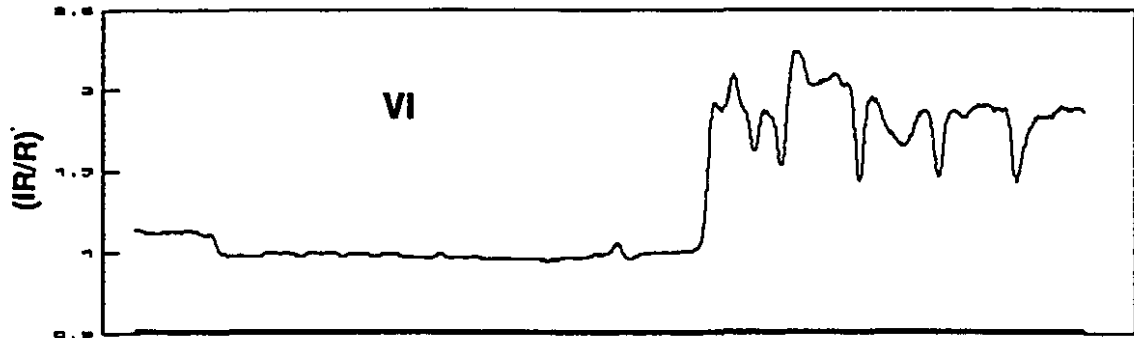
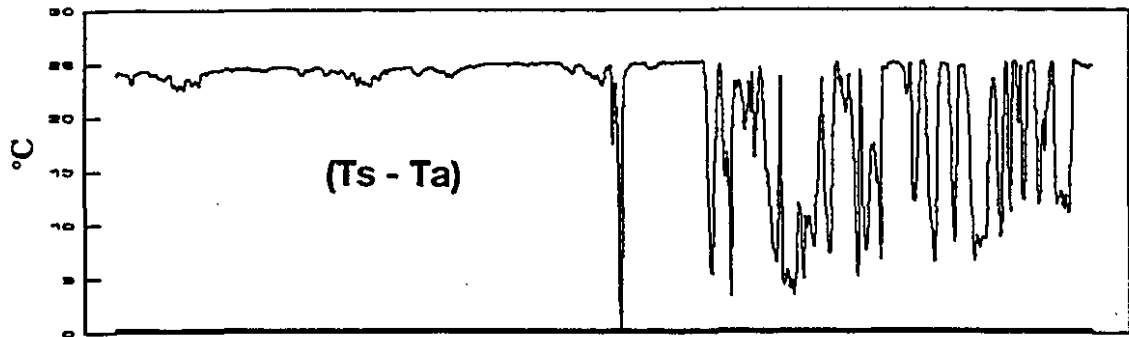
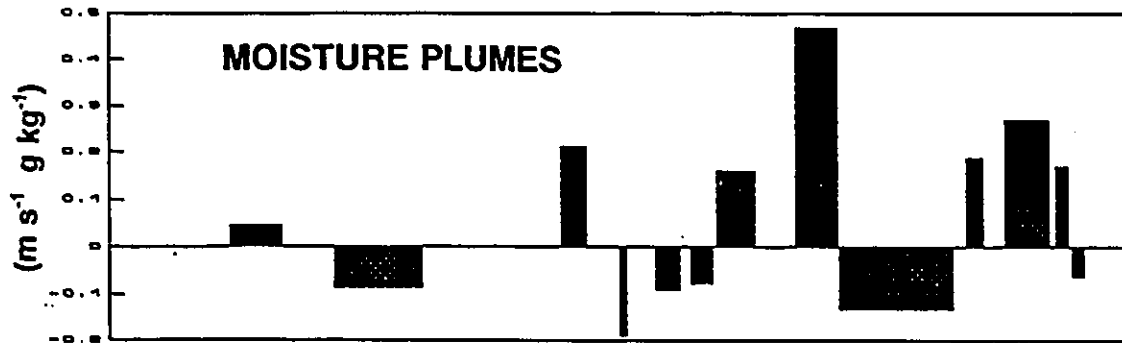
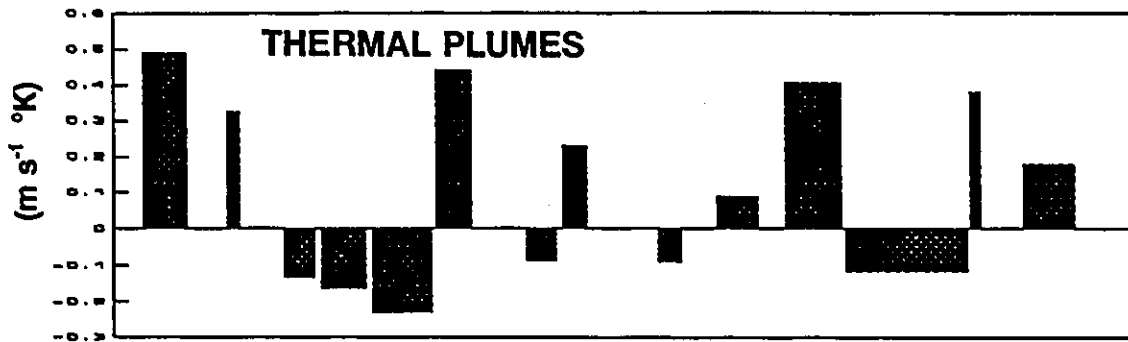
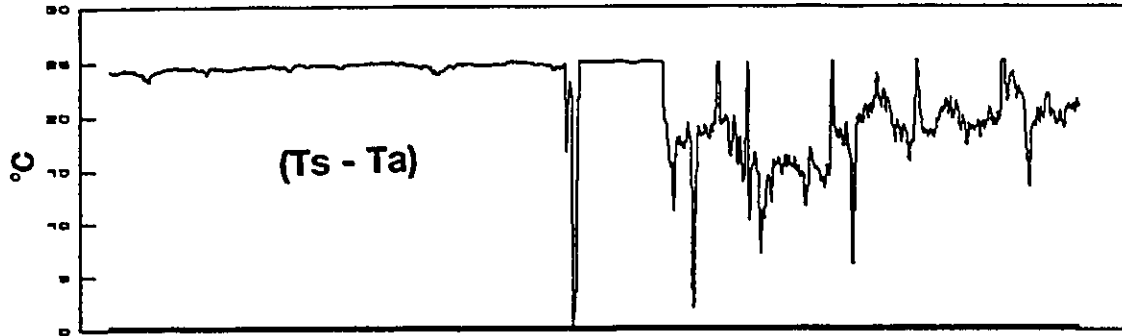


Figure 2.17. Difference between radiative surface temperature and air temperature ($T_s - T_a$), Ratio of Infrared (IR) over Red (R) reflected solar radiation (VI), and distribution of thermal and moist plumes for a 12-km run over the San Joaquin Valley. Mean flight altitude is 100 m.



2.4. SUMMARY AND CONCLUSIONS

Airborne observations of the turbulent fields of velocity, moisture and temperature above three ecosystems have been analyzed in terms of coherent structures. In these structures a non-vanishing covariance can be interpreted as a contribution to the flux of heat or moisture through the eddy correlation technique. The intermittent nature of such structures in time and space is well known. However, a statistical description of their physical characteristics (relative contribution to the flux, spatial extent and spacing) and their dependence on underlying surface features is not yet available.

This work is a compilation of a large set of observations over grassland, wetland and wet and dry agricultural land, about the distribution and relative importance of coherent structures in terms of the four modes of eddy-covariance transfer. These observations are expected to provide a data base against which boundary-layer models could be tested, especially in the interaction between boundary-layer dynamics and surface characteristics. They also form a step in our attempts to link airborne flux observations with surface parameters (such as moisture, greenness and temperature) that could be observed by satellite-based remote sensing.

Our analyses, obtained under conditions of moderate thermal instability, permit the following general observations:

- the distribution of structures along a run, in terms of the four 'quadrant' modes of turbulent transport, depends strongly on the definition of the mean. Non-linear detrending of moisture and temperature signals appears to lead to a physically more reasonable definition of the mean. Although non-linear detrending represents a high-pass filtering procedure, it was shown to lead to an overall increase in the flux estimate compared to linear detrending.

- coherent structures exhibit broadly similar characteristics over the three ecosystems, indicating that boundary-layer dynamics is a strong controlling agent on their formation. Significant differences, primarily in size and relative distribution of flux contribution as a function of size, were observed between wet and dry areas, with a larger number of small structures observed over wet areas. There is strong indication of spatial re-organisation from smaller into larger, more sporadic structures with increasing height, with associated consequences for airborne sampling criteria.

- the spatial organisation of structures (such as moisture or thermal plumes) with heights gradually weakens the correlation between such structures and the physical characteristics of the underlying surface. These observations are in agreement with the concept of a 'blending height' (Wieringa 1986).

2.5. REFERENCES

- Alvo, P., R. L. Desjardins, P. H. Schuepp, and J. I. MacPherson. Aircraft measurements of CO₂ exchange over various ecosystems. Bound.-Layer Meteor., 29(2), 167-183, 1984.
- Antonia, R. A.. Conditional sampling in turbulence measurement. Ann. Rev. Fluid Mech., 13, 131-156, 1981.
- Austin, L. B., P. H. Schuepp, and R. L. Desjardins. The feasibility of using airborne flux measurements for the imaging of the rate of biomass production. Agric. Forest Meteorol., 39, 13-23, 1987.
- Brutsaert, W. and M. Sugita. The extent of the unstable Monin-Obukhov layer for temperature and humidity above complex hilly grassland. Bound.-Layer Meteor., 51, 383-400, 1990.
- Cihlar, J., P. H. Caramori, P. H. Schuepp, R. L. Desjardins, and J. I. Macpherson. Relationship between satellite-derived vegetation index and aircraft-based CO₂ measurements. J. Geophys. Res., 97(d17), 18,515-18,522, 1992.
- Coulman, C. E.. Correlations between velocity, temperature and humidity fluctuations in the air above land and ocean. Bound.-Layer Meteor., 19, 403-420, 1980.
- Desjardins, R. L., J. I. MacPherson, P. H. Schuepp, and F. Karanja. An evaluation of aircraft flux measurements of CO₂, water vapor and sensible heat. Bound.-Layer Meteor., 47, 55-70, 1988.
- Desjardins, R. L., P. H. Schuepp, J. I. MacPherson, and D. J. Buckley. Spatial and temporal variation of the fluxes of carbon dioxide and sensible and latent heat over the FIFE site. J. Geophys. Res., 97(d17), 18467-18476, 1992.
- Duncan, M. R.. Structure and contribution of extreme events in airborne carbon

- dioxide and water vapour flux traces. M.Sc. Thesis, McGill University, Montreal, 1990. 83 pp.
- Duncan, M. R., P. H. Schuepp, J. I. MacPherson, and R. L. Desjardins. Statistical analysis of airborne flux measurements over the FIFE site. 19th. Conf. Agric. and For. Meteor. and Ninth Conf. Biomet. and Aerobiol., Charleston, S. Carolina, Amer. Meteor. Soc., 129-130, 1989.
- Duncan, M. R., and P. H. Schuepp. A method to delineate extreme structures within airborne flux traces over the FIFE site. J. Geophys. Res., 97(d17), 18,487-18,498, 1992.
- Grant, R. H., G. E. Bertolin, and L. P. Herrington. The intermittent vertical heat flux over a spruce forest canopy. Bound.-Layer Meteor., 35, 317-330, 1986.
- Greenhut, G. K., and S. J. S. Khalsa. Updraft and downdraft events in the atmospheric boundary layer over the equatorial Pacific Ocean. J. Atmos. Sci., 39, 1803-1818, 1982.
- Grossman, R. L. Bivariate conditional sampling of moisture flux over a tropical ocean. J. Atmos. Sci., 41, 3227-3253, 1984.
- Horst, T. W., and J. C. Weil. Footprint estimation for scalar flux measurements in the atmospheric surface layer. Bound.-Layer Meteor. (*in press*).
- Leclerc, M. Y., and G. W. Thurtell. Footprint predictions of scalar fluxes using a Markovian analysis. Bound.-Layer Meteor., 52, 247-258, 1990.
- Lenschow, D. H., and B. B. Stankov. Length scales in the convective boundary layer. J. Atmos. Sci., 43(12), 1198-1209, 1986.
- Lenschow, D. H., and P. L. Stephens. The role of thermals in the convective boundary-layer. Bound.-Layer Meteor., 19, 507-532, 1980.

MacPherson, J. I.. NAE Twin Otter operations in FIFE. National Aeronautic Establishment Laboratory Technical Report, Ottawa, 1988, 148 pp.

MacPherson, J. I.. NAE Twin Otter operations in FIFE 1989. Institute for Aerospace Research Laboratory Technical Report, Ottawa, 1990, 80 pp.

MacPherson, J. I.. NRC Twin Otter operations in the 1991 California Ozone Deposition Experiment. National Research Council Canada, Institute for Aerospace Research, Ottawa, 1992, 213 pp.

Mahrt, L.. Intermittency of atmospheric turbulence. J. Atmos. Sci., 46(1), 79-95, 1989.

Mahrt, L., and J. Palmier. Heat transport in the atmospheric boundary layer. J. Atmos. Sci., 21, 3061-3075, 1984.

Manton, M. J.. On the structure of convection. Bound.-Layer Meteor., 12, 491-503, 1977.

Schuepp, P. H., R. L. Desjardins, J. I. MacPherson, J. B. Boisvert, and L. B. Austin. Interpretation of airborne estimates of evapotranspiration. In: Estimation of Areal Evapotranspiration (T.A.Black, D.L. Spittlehouse and M.D. Novak, eds.). Int'l. Assoc. of Hydrol. Sci. Press, Wallingford; Publ. no. 177, pp.185-196, 1989.

Schuepp, P. H., M. Y. Leclerc, J. I. MacPherson, and R. L. Desjardins. Footprint prediction of scalar fluxes from analytical solutions of the diffusion equation. Bound.-Layer Meteor., 50, 355-373, 1990.

Schuepp, P. H., J. I. MacPherson, and R. L. Desjardins. Adjustment of footprint correction for airborne flux mapping over the FIFE site. J. Geophys. Res., 97(d17), 18,455-18,466, 1992.

Schulmann, U., and C. H. Moeng. Plume fluxes in clear and cloudy convective

- boundary layers. J. Atmos. Sci., 48, 1746-1757, 1991.
- Sellers, P. J., F. G. Hall, G. Asrar, D. E. Strebel, and R. E. Murphy. The first ISLSCP field experiment (FIFE). Bull. Amer. Met. Soc. 69(1), 22-27, 1988.
- Shaw, J. W., and Businger, J. A.. Intermittency and the organization of turbulence in the near-neutral marine atmospheric boundary layer. J. Atmos. Sci., 42, 2563-2584, 1985.
- Shaw, R. H.. On diffusive and dispersive fluxes in forest canopies. In: The Forest Atmosphere Interaction, D. Reidel Publ. Co., 1985, pp. 407-419.
- Swinbank, W. C.. The measurement of vertical transport of heat and water vapour by eddies in the lower atmosphere. Meteorol., 6, 135-145, 1951.
- Wieringa, J.. Roughness-dependent geographical interpolation of surface wind speed averages. Quart. J. R. Meteorol. Soc., 112, 867-889, 1986.
- Wilson, J. D., and G. E. Swaters. The source area influencing a measurement in the planetary boundary layer: the "footprint" and the "distribution of contact distance". Bound.-Layer Meteor., 55, 25-46, 1991.
- Wyngaard, J. C.. Lectures on the planetary boundary layer. In: Mesoscale Meteorology - Theories, Observations and Models (D. K. Lilly and T. Gal-Chen, eds.). Reidel Publ., Dordrecht, 1983, pp. 603-650 and pp. 216-224.
- Wyngaard, J. C., W. T. Pennell, D. H. Lenschow, and M. A. LeMone. The temperature-humidity covariance budget in the convective boundary layer. J. Atmos. Sci., 35, 47-58, 1978.

Connecting Statement

In chapter 2 we used conditional analysis to study the turbulent structures that dominate the fluxes of water vapor and sensible heat above wetland, grassland, and irrigated land. Results showed a progressive loss of the flux 'signature' with increasing altitude, suggesting intensive reorganization of the structures near the surface. In chapter 3 we further evaluate this problem, and provide a statistical description of the significant turbulent structures at different heights above the three ecosystems.

Chapter 3:

Characterization of moisture and thermal plumes at different heights over wetland, grassland, and irrigated agricultural land.

Abstract

Aircraft-based observations of velocity fields, temperature, and water vapor concentration were used to study the statistical distributions of diameter and spacing of moisture and thermal plumes above wetland, grassland, and irrigated land alternated with dry land. Fluxes were estimated through the eddy correlation technique and plumes were characterized as updrafts with excess temperature or moisture. Thresholds were applied to eliminate events that did not contribute significantly to the flux. Structures were defragmented to reconstruct their presumed size according to specified criteria. Both plume diameter and spacing, at heights that ranged from the surface layer to about half of the top of the planetary boundary layer, could be approximated by lognormal distributions. Indications were found that stability plays a significant role in plume size, with smaller plume diameter occurring under more unstable conditions. Mean plume diameter and spacing increased with height, while the number of plumes per sampling length decreased as a power function of height. Flux contributions from larger structures become more important with increasing altitude. Comparison

between the three ecosystems showed very similar general characteristics, with differences more likely due to boundary layer than surface characteristics.

3.1. INTRODUCTION

Criteria for adequate sampling of atmospheric boundary layer properties are not easy to define because of the highly intermittent nature of turbulence (Khalsa 1980, Shaw and Businger 1985, Mahrt 1989, Mahrt and Gibson 1992). Estimates based on the Twin Otter observations showed that events that happened only 20% of the time accounted for about 80% of the total flux (Duncan and Schuepp 1989, Duncan 1990). It is not uncommon to observe single, extreme plumes contributing more than 10% of the total flux along a 15km segment at flight altitudes between 100 and 150m. The inclusion or exclusion of such events accounts for much of the observed run-to-run variability in flux estimates. Information about the distribution of these turbulent structures for given atmospheric and surface conditions is important in the modelling of boundary layer transfer process.

In Chapter 2 of this thesis, we analyzed the organization of moisture and thermal plumes over grassland, wetland, and partly irrigated agricultural land, using conditional sampling of aircraft flux observations. Analyses performed at two heights suggested strong reorganization of smaller plumes into larger ones with increasing height, with implications for intercomparison of aircraft and satellite-based estimates (see Figures 2.13 to 2.17). In this chapter, we examine the reorganization of moisture and thermal plumes at different heights over three ecosystems, their statistical distributions, and address the question of their

dependence on local surface characteristics and boundary layer properties. Such information may be useful to establish optimum sampling criteria for aircraft, in validation of satellite-based models of surface exchange or models of boundary layer structure.

3.2. MATERIALS AND METHODS

3.2.1. Aircraft instrumentation and data processing

The present analyses use data obtained with the Canadian Twin Otter Research Aircraft of the Institute for Aerospace Research, which has been successfully used to collect detailed information of the boundary-layer properties over a number of ecosystems (see for example Desjardins et al. 1982, Schuepp et al. 1987, Desjardins et al. 1989, Mack et al. 1990, Schuepp et al. 1992, Desjardins et al. 1992, among others). Three data sets were analyzed: a) The FIFE experiment over grassland in Kansas, in the summer of 1989 (Sellers et al. 1988); b) The Canadian Northern Wetland Study (NOWES) in the Hudson Bay - James Bay lowlands during the summer of 1990; c) The California Ozone Deposition Experiment (CODE) in the San Joaquin Valley during the summer of 1991 (MacPherson, 1992). The parameters relevant to the present study are summarized in Chapter 2 of this thesis and presented in detail in MacPherson (1988, 1990, 1992). The time series of vertical wind, air temperature, and mixing ratio of water vapor were individually inspected, and linear or nonlinear detrending procedures selected according to the trends in flux variables in each case (Caramori et al. 1992, and Chapter 2). Table 3.1 gives a summary of the runs analyzed. The boundary layer top was more variable and generally higher over wetland and positive moisture flux divergence with height was not uncommon. The

approach used to characterize a turbulent coherent event was described in Chapter 2; it is only briefly summarized here. Fluxes of water vapor and sensible heat along run segments were estimated using the eddy correlation technique. Based on the recorded fluctuations of the vertical wind (w') and the concentration of the scalar to be analyzed (q'), each datapoint lies in one of four quadrants: excess-up ($w'+q'+$); excess-down ($w'-q'+$); deficit-down ($w'-q'-$); deficit-up ($w'+q'-$). A coherent turbulent structure is defined as containing at least 8 consecutive datapoints (30m) in the same quadrant, and such a structure in the excess-up quadrant is considered to be a coherent plume. Moisture plumes and thermal plumes were analyzed separately.

Table 3.1. Site, average flight height, combined run length, shortwave solar radiation ($K\downarrow$), sensible heat flux (H), latent heat flux (LE), stability parameter (z/L), and ratio of flight level to boundary layer height (z/z_i). The range of values observed for $K\downarrow$, H , LE , and z/L are given.

Site	Height (m)	Length (km)	$K\downarrow$ ($W\ m^{-2}$)	H ($W\ m^{-2}$)	LE ($W\ m^{-2}$)	z/L	z/z_i
Wetland	40	115.7	703 → 806	105 → 125	169 → 216	-0.19 → -1.73	0.02
	100	108.4	711 → 805	87 → 123	184 → 276	-0.60 → -6.62	0.09
	240	104.2	724 → 815	42 → 164	218 → 368	-1.17 → -2.56	0.21
	780	121.3	759 → 839	-36 → 30	12 → 229	[17.1] → -2.0	0.63
FIFE	100	66.3	685 → 936	135 → 188	139 → 311	-0.51 → -2.7	0.05
	200	63.7	727 → 752	88 → 159	144 → 266	-2.8 → -14.8	0.10
	450	65.8	733 → 931	47 → 115	56 → 362	-3.2 → -16.7	0.24
	780	69.1	708 → 962	-4 → -24	56 → 311	2.2 → -8.9	0.39
San Joaquin Valley	30	69.4	830 → 894	33 → 273	114 → 296	-1.9 → -14.5	0.04
	60	65.3	828 → 896	25 → 258	30 → 252	-1.29 → -16.5	0.08
	100	49.3	847 → 876	12 → 162	132 → 284	-1.57 → -11.1	0.13

3.2.2. Threshold values vs flux

As pointed out in Chapter 2, many of the structures thus defined may not carry much flux, and even the most intensive ones may contain zones of weak signal. Because we are primarily interested in associating the strong plumes with surface characteristics, these weak sections become a complicating factor in the analysis. In previous studies by Duncan and Schuepp (1991), and Caramori et al. (1992), a threshold was applied to the coherent structures as such to eliminate those that were not significantly contributing to the flux, but no attempt was made to eliminate weak signals from the remaining dominant structures. Results presented in Chapter 2 using this approach showed that the flux carried by 20 to 40% of the weaker structures contributed less than 5% to the total flux along a 15 km segment. In the present analysis we evaluate two choices of threshold: (1) elimination of structures that contribute less than a certain fraction to the total flux estimate along a given run segment and (2) application of a threshold to the flux itself, prior to its decomposition into quadrants. Option (1) follows the above-mentioned principle of Duncan and Schuepp (1991) and Chapter 2, where entire structures are either retained, or eliminated if their flux contribution falls below an arbitrary threshold level. Option (2) corresponds to the application of hyperbolic holes to eliminate weak signals from the database prior to their grouping into coherent turbulent structures. Thresholds applied as hyperbolic holes have generally been defined as multiples of the mean flux (e.g. Antonia 1981, Grant et

al. 1986, Shaw 1985), or as fractions of the standard deviation of the analyzed scalar (e.g. Lenschow and Stephens, 1980).

In the present study the standard deviation (rms) of the flux estimates along each individual run was estimated (for all datapoints), and fractions of rms were applied as thresholds to eliminate weaker datapoints. Figure 3.1 illustrates the application of several threshold levels defined as fractions of the standard deviation of the water vapor flux. Notice the progressive elimination of weaker signals, with dominance of excess up and deficit down modes at higher thresholds. Figure 3.2 shows the application of two values of rms along a run segment over the wetland. The solid lines correspond to a threshold of ± 0.2 rms and the dashed lines to ± 1 rms. Any datapoint located between the \pm threshold lines is eliminated. In general, the application of a threshold corresponding to 0.2 rms eliminated weak signals, whereas the threshold of 1 rms retained only the extreme signals associated to the cores of the plumes. The counter-gradient events (excess-down and deficit-up) practically disappeared under the higher threshold. Figure 3.3 illustrates the typical case of a plume with a weak tail under application of two threshold levels. In such cases weak tail eliminated by the lower threshold level may extend for a few hundred meters. This is often the case at higher altitudes where fluxes may become small. Figure 3.4 shows a plume containing many weak signals, non-uniformly distributed in space. The application of thresholds in such cases will cause fragmentation of the structure. It is important to point out that, as

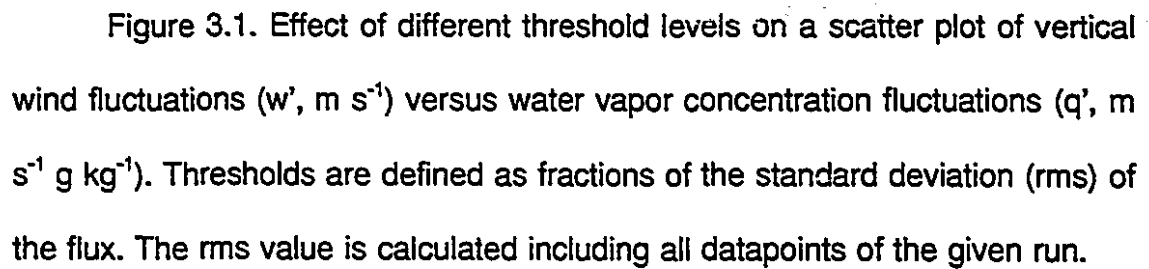
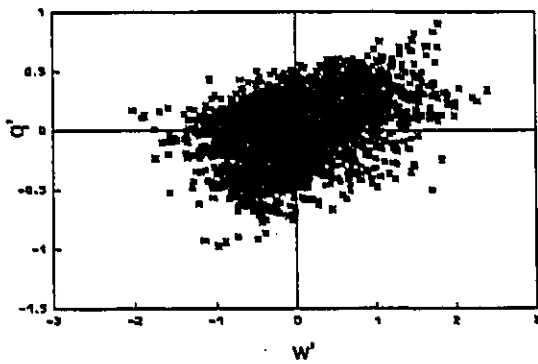
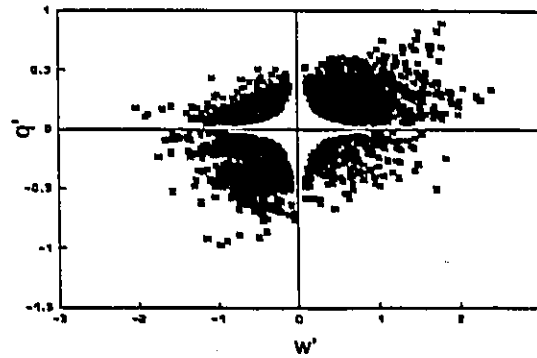


Figure 3.1. Effect of different threshold levels on a scatter plot of vertical wind fluctuations (w' , m s^{-1}) versus water vapor concentration fluctuations (q' , $\text{m s}^{-1} \text{ g kg}^{-1}$). Thresholds are defined as fractions of the standard deviation (rms) of the flux. The rms value is calculated including all datapoints of the given run.

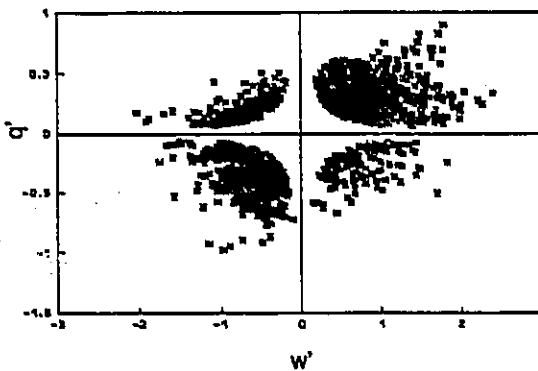
HH = 0.0



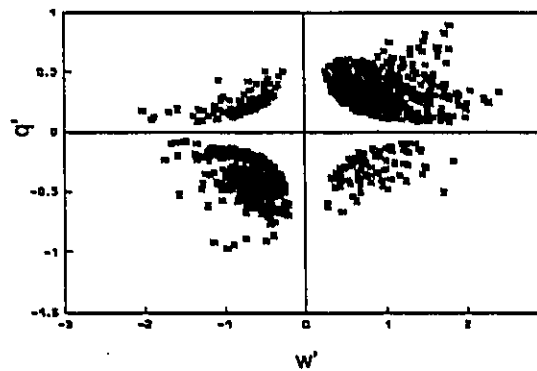
HH = 0.2 RMS



TH = 0.4 RMS



TH = 0.6 RMS



TH = 1.0 RMS

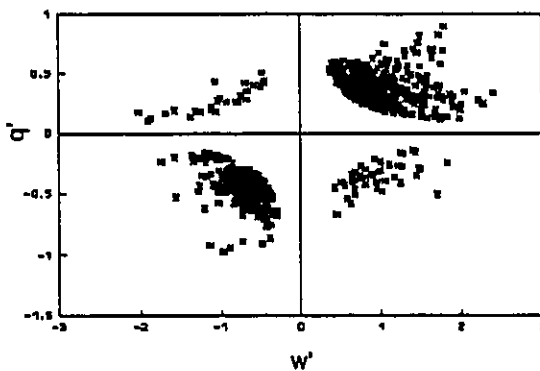


Figure 3.2. Water vapor flux along a run segment over the wetland, showing the threshold of ± 0.2 rms (solid lines) and ± 1 rms (dashed lines). Datapoints within the \pm line for a given threshold level are eliminated.

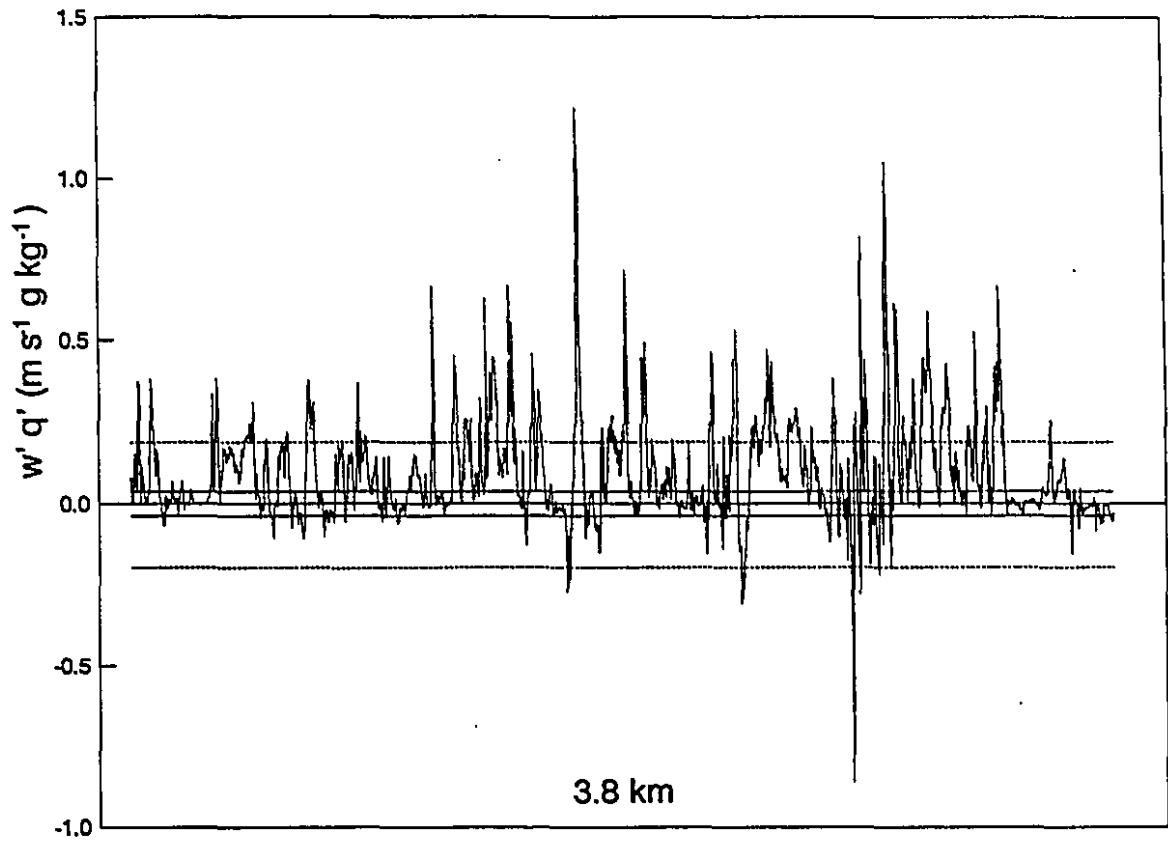


Figure 3.3. A moisture plume with weak tails. The solid lines represent the size of the structure after the application of thresholds equivalent to 0.2 rms and 1 rms.

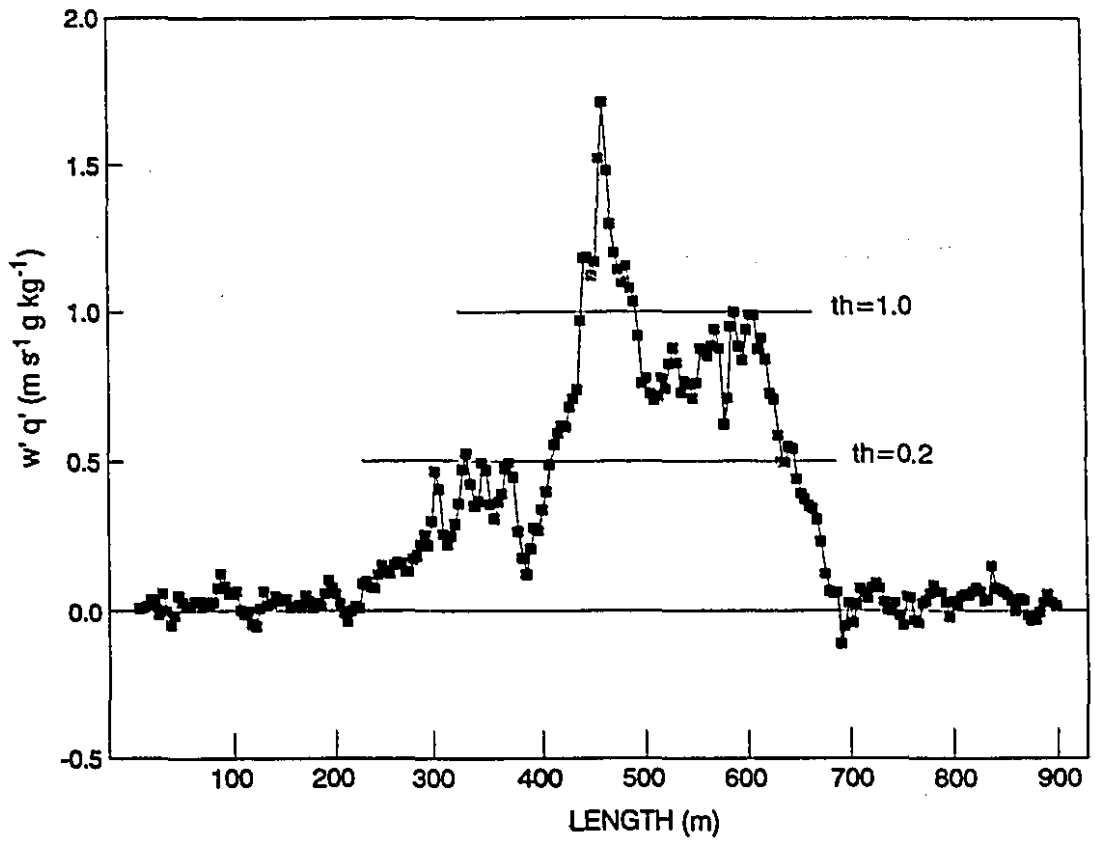
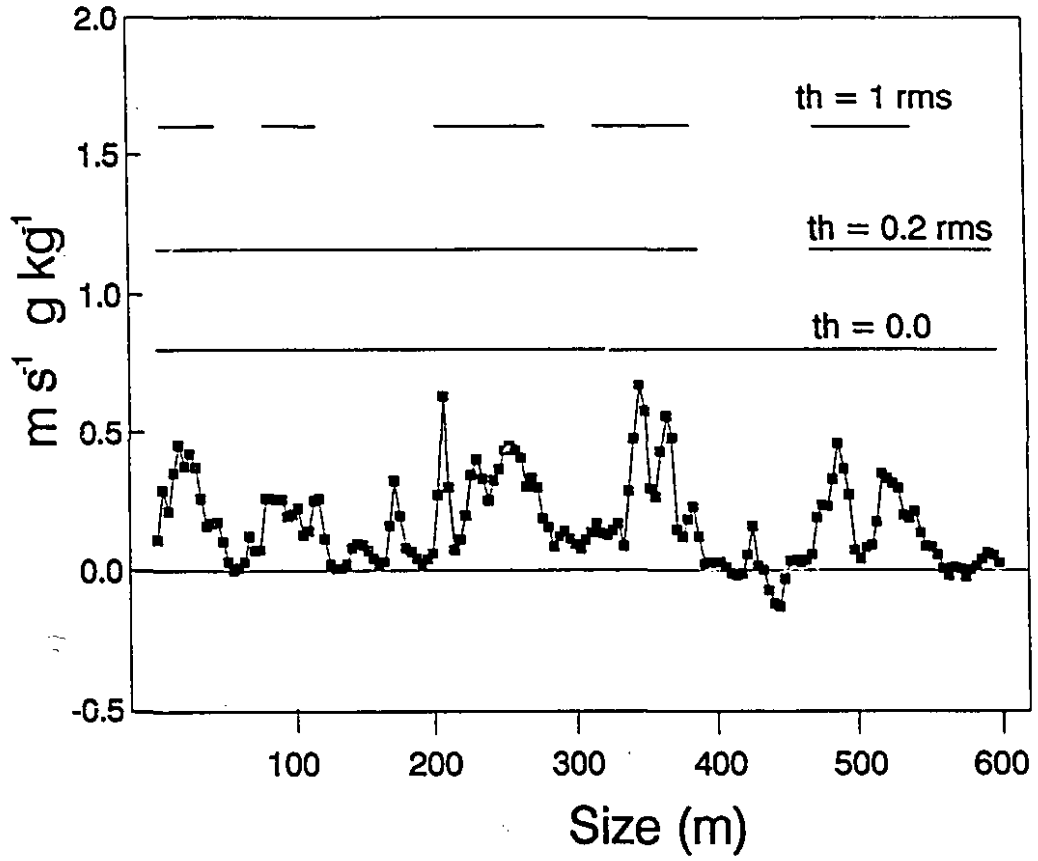


Figure 3.4. A moisture plume with many small flux values. Solid lines represent plume diameter after application of the thresholds of 0.0, 0.2 rms, and 1 rms.



in Chapter 2, the threshold is not applied to gaps of less than 8 datapoints between two sequences of at least 8 datapoints in the same quadrant. This means that some weak signals are retained inside dominant structures, but it assures that local fluctuations that naturally occur within a dominant plume will not break up the structure. On the other hand, the external definition of a dominant structure, which is often ill defined through weak tails in the original data set, becomes much clearer.

3.2.3. Distribution of plume diameter and spacing

The diameter of each plume (L) is defined in terms of the length of the one-dimensional aircraft transect in its arbitrary cut through the structure, and the spacing between plumes (S) as the distance between two consecutive turbulent structures of the excess-up quadrant along the flight line. S will, therefore, include all the datapoints from the other three quadrants between two consecutive plumes, as well as the datapoints from the excess-up quadrant that fall below the threshold level. It must be stressed that these values represent statistical averages, since there is no guarantee that the aircraft is sampling the most active sections of the plumes.

Plume diameters and spacings for several combined flights for each height over the three ecosystems (see Table 3.1) were fitted to lognormal distributions. The selection of this distribution was originally motivated by its successful

application in many areas of environmental and atmospheric sciences. It has been used, for example, in early studies in hydrology, to model daily stream flow, flood peak discharges, annual floods, and rainfall (see Benjamin and Cornell 1971). Kolmogorov (1962) proposed a lognormal distribution for the dissipation of turbulent kinetic energy in the atmosphere. Gurvich and Yaglon (1967) included the lognormal distribution for any non-negative quantity governed by the fine structure of turbulence. Khalsa and Businger (1977) and Khalsa (1978, 1980) observed that the mean dissipation rate of turbulence is bimodal and lognormally distributed, with distinct distribution for the plume and nonplume states. Rao et al. (1971) found that the intervals between 'bursts' sampled by a hot wire anemometer in a wind tunnel experiment are distributed according to the lognormal law, while Shaw and Businger (1985) show the lognormality for both 'bursts' and interval between 'bursts' in the atmospheric boundary layer. The lognormal distribution has the advantage that the log transformation reduces the positive skewness of the data (Chow et al. 1989). A detailed description of the distribution is given in Aitchison and Brown (1957).

3.3. RESULTS AND DISCUSSION

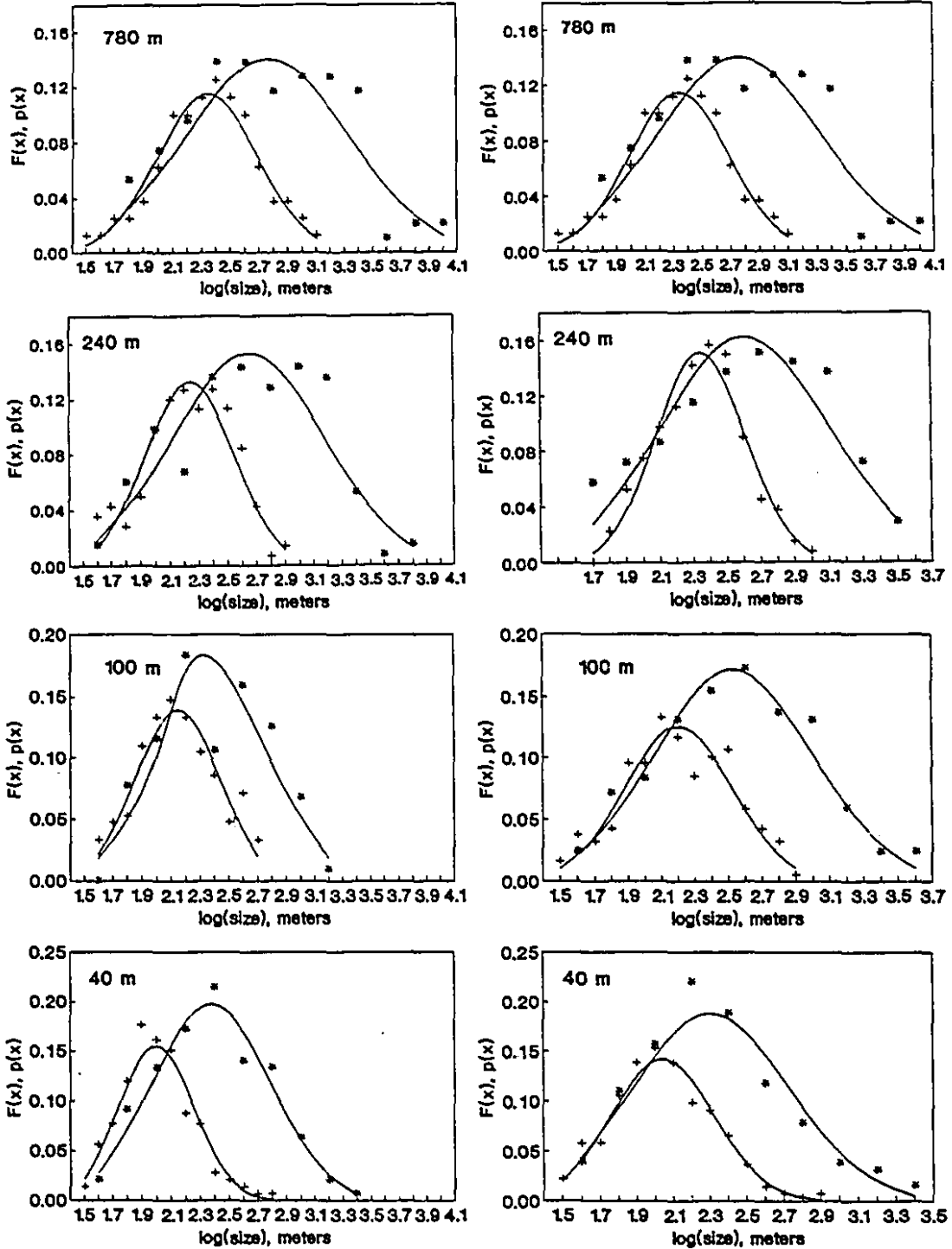
3.3.1. Distributions of plume diameter and spacing - The summary statistics of the distributions of plume diameter and spacing for the original data and the two different threshold procedures are presented in the appendix. Figures 3.5 to 3.7 show the distributions of plume diameter and spacing at different heights over the wetland, FIFE grassland, and San Joaquin Valley agricultural land, after application of a threshold that eliminated individual structures contributing less than 0.2% of the total flux along each run. The distributions of plume diameter and spacing are bimodal lognormal, with distinct distributions for plume size and spacing. Khalsa (1980) also found bimodal lognormal distributions for the dissipation rate of kinetic energy in the atmosphere. Distributions are truncated at 30 m, since this is the minimum plume size considered. All fits were successful in explaining over 95% of the variance in the data. The null hypothesis that the lognormal distribution fits the data could not be rejected at 95% confidence level for all cases according to the chi-square test. The fit was better near the surface, where a larger number of structures are observed. Structure diameter generally showed a better fit than spacing; the poorest fit was obtained for the larger structures due to their sporadic occurrence within each run.

3.3.2. Mean plume diameter versus height - The mean diameter for thermal

Figure 3.5. Lognormal distributions of diameter and spacing of thermal and moisture plumes at different heights above wetland. Structures that contributed less than 0.2% to the total flux within a given run are not included. The relative frequency functions ($F(x)$) are plotted as symbols and the incremental probability functions ($p(x)$) are plotted as solid lines.

THERMAL PLUMES

MOISTURE PLUMES

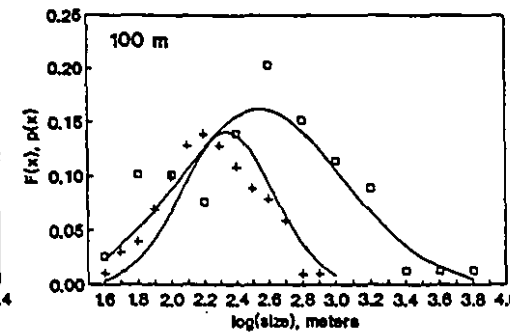
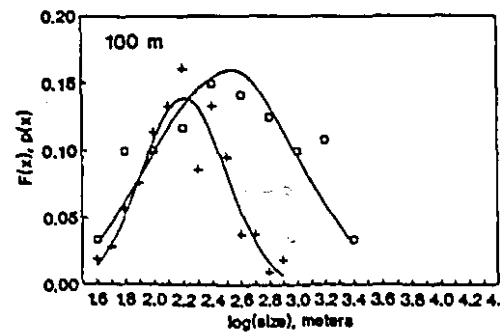
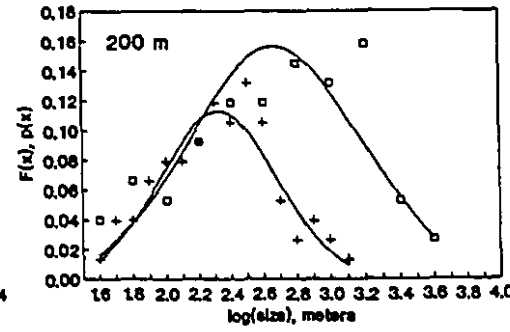
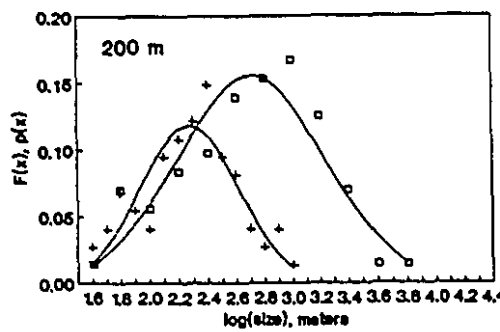
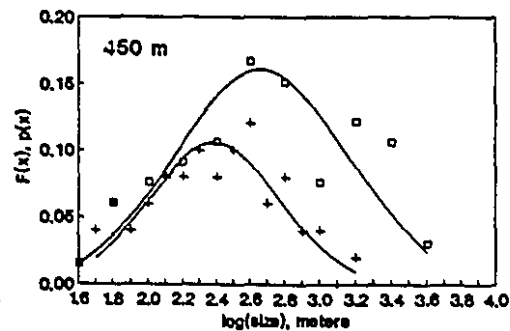
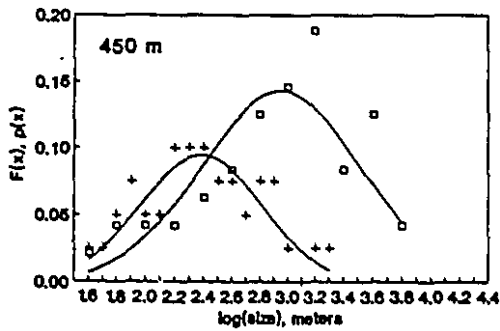
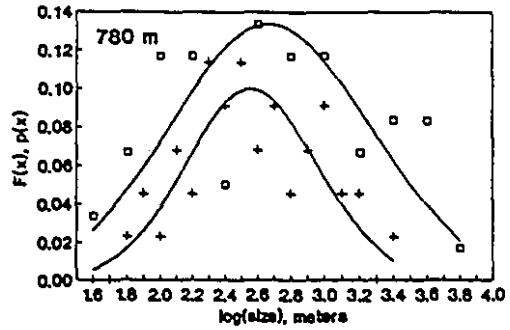
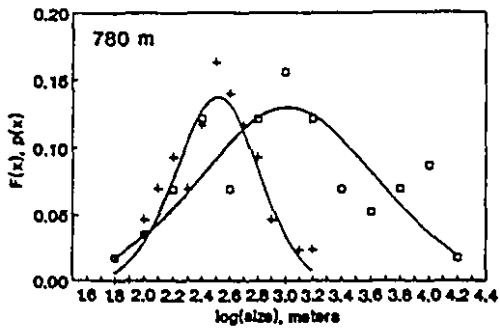


+ DIAMETER * SPACING

Figure 3.6. Lognormal distributions of diameter and spacing of thermal and moisture plumes at different heights above grassland (FIFE). Structures that contributed less than 0.2% to the total flux within a given run are not included. The relative frequency functions ($F(x)$) are plotted as symbols and the incremental probability functions ($p(x)$) are plotted as solid lines.

THERMAL PLUMES

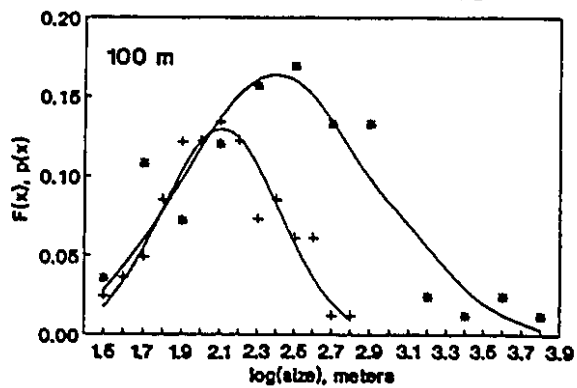
MOISTURE PLUMES



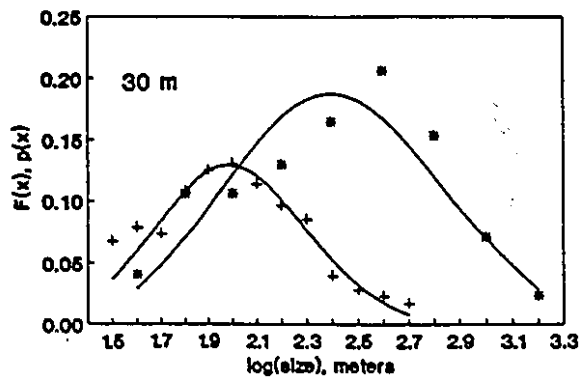
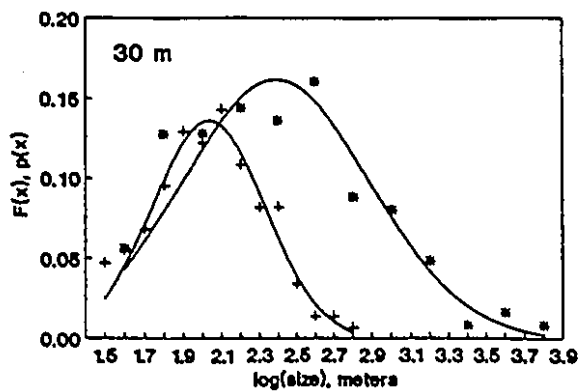
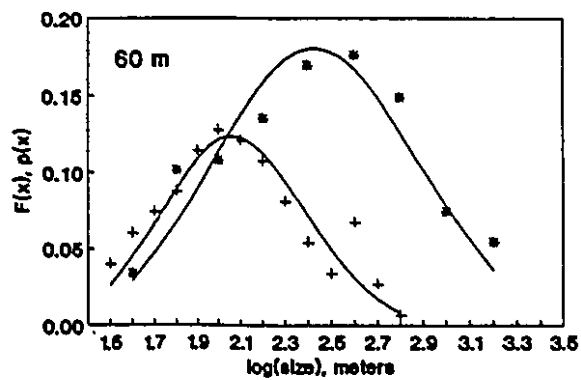
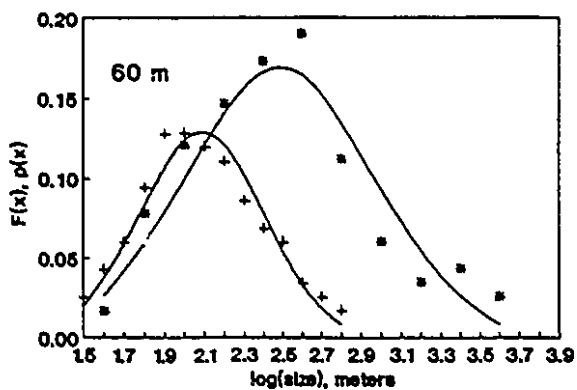
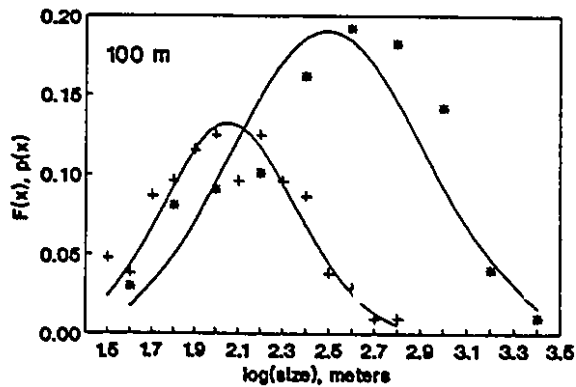
+ DIAMETER □ SPACING

Figure 3.7. Lognormal distributions of diameter and spacing of thermal and moisture plumes at different heights above irrigated and non-irrigated agricultural land. Structures that contributed less than 0.2% to the total flux within a given run are not included. The relative frequency functions ($F(x)$) are plotted as symbols and the incremental probability functions ($p(x)$) are plotted as solid lines.

THERMAL PLUMES



MOISTURE PLUMES



+ DIAMETER * SPACING

Figure 3.8. Mean diameter of thermal and moisture plumes at different heights above wetland.

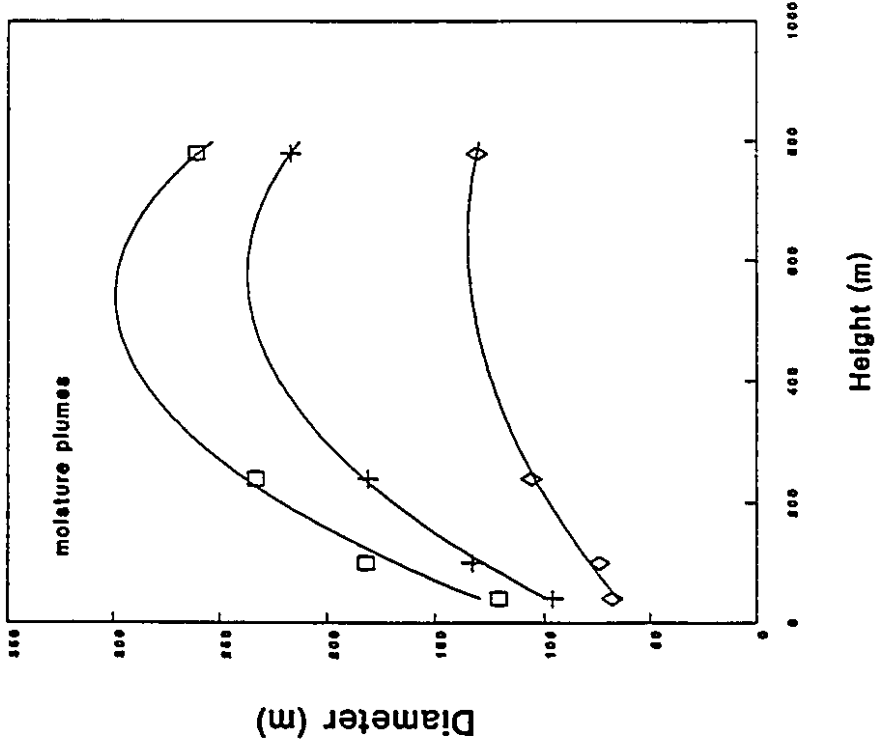
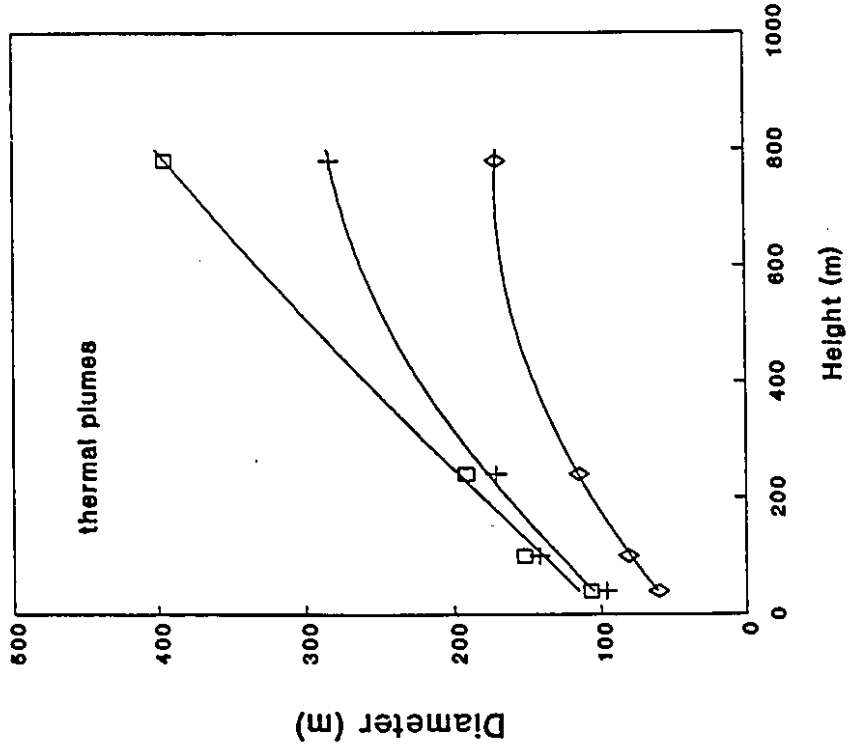
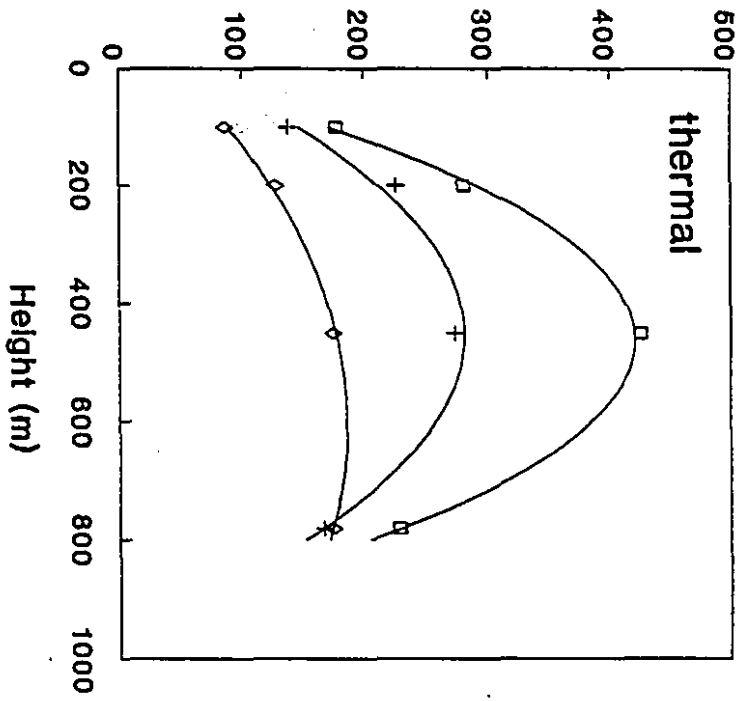
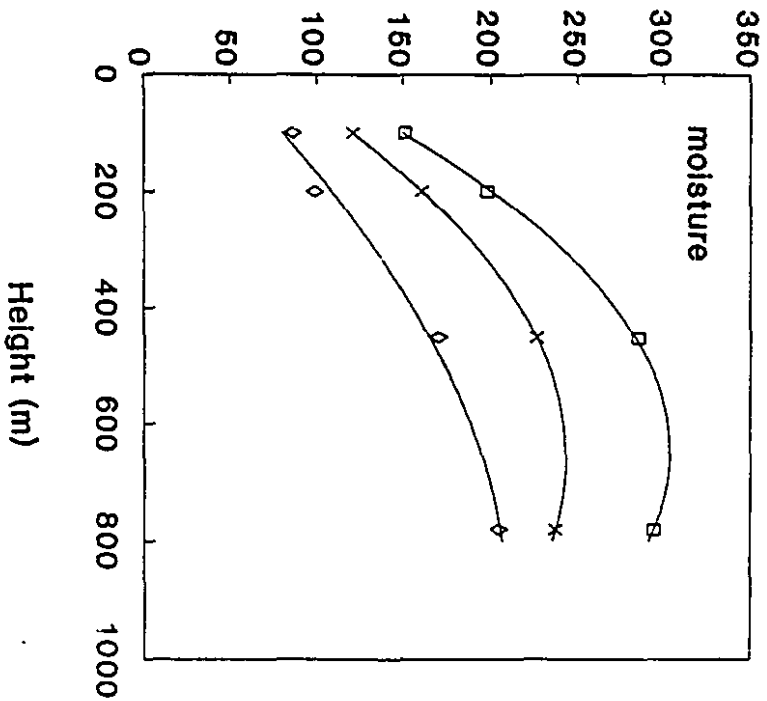
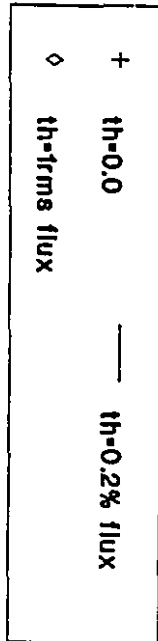


Figure 3.9. Mean diameter of thermal and moisture plumes above grassland (FIFE).

Diameter (m)



Height (m)



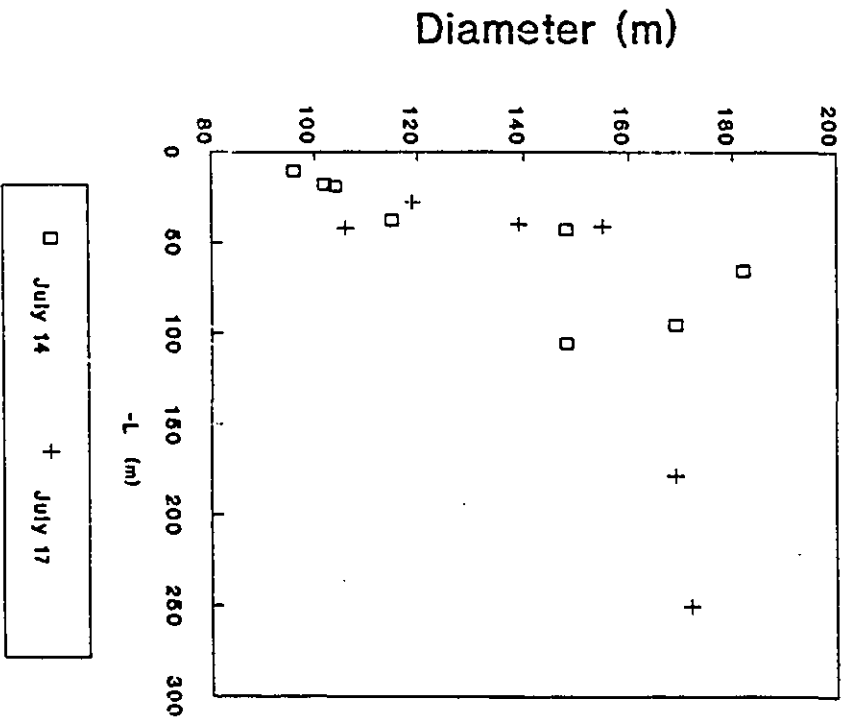
Height (m)

and moisture plumes as a function of height for the wetland and FIFE grasslands is plotted in Figures 3.8 and 3.9, respectively. It can be observed that plumes initially become larger with increasing altitude. As the structures start to break up into smaller ones or dissipate, the average size tends to decrease. This is in agreement with observations made with Lidar (Eloranta and Forrest, 1992). For both wetland and grassland, the average size of the thermal plumes exceeded that of moisture plumes. Comparing the two ecosystems, we observe that both thermal and moisture plumes are within the same size range. The average diameter ranged from 80m to 400m for the thermal plumes and 60 to 300m for the moisture plumes. The evolution of mean plume diameter with height was approximated by a polynomial of second degree. The choices of threshold and threshold level directly affected the average size of the turbulent structures. The threshold that eliminated structures contributing less than 0.2% to the flux resulted in higher average diameter, since a larger number of small structures were eliminated. On the other hand, thresholds represented by fractions of the standard deviation of the flux lead to smaller diameters compared to the original data.

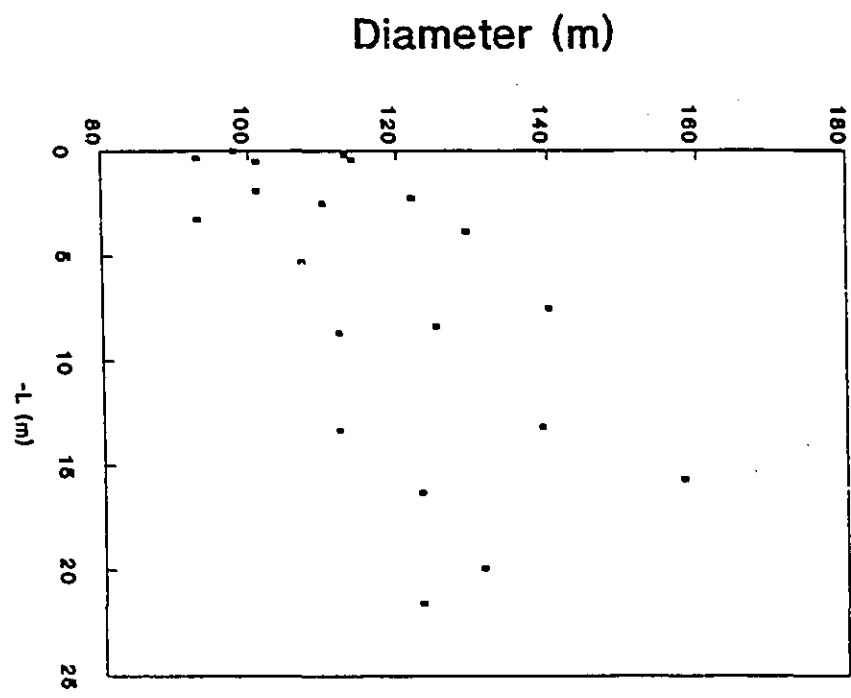
3.3.3. Stability versus plume size - The role of stability conditions is examined in Figure 3.10, where values of mean moisture plume diameter over the wetland and San Joaquin Valley are plotted against the negative Obukhov length (-L). The values of plume diameter were obtained without application of threshold (th=0.0) and only runs within the surface layer are included. The data from the

Figure 3.10. Plume diameter as a function of the negative of the Obukhov length (-L) for wetland and irrigated agricultural land.

WETLAND



SAN JOAQUIN VALLEY



wetland shows a wider range of stability. On both cases it is possible to see the increase of plume diameter for higher values of $-L$. The results from the wetland are very similar to those presented by Khalsa (1980), who observed increases in plume diameter within the surface layer for values of $-L$ up to about 80, with no response detected beyond this value.

3.3.4. Line Density of Plumes - The mean number of plumes per sampling length is calculated as the number of plumes found in all the runs combined for a given height, divided by the total run length (km). The results for wetland and FIFE grasslands (Figures 3.11 and 3.12, respectively) show that the number of plumes decreased as a power function of height. Previous results (e.g. Grant 1965, Lenschow and Stephens 1978) have also shown a decrease in the number of plumes with increasing height, while the average size of the remaining plumes tended to increase. For the Wetland the number of plumes decreased by about 50% between 40m and 150m. The significant decrease of plume number with increasing altitude near the surface is evidence for a great level of reorganization. This is the reason why sampling at higher altitudes will not likely be successful in reflecting the 'surface signature' in terms of flux, since a single plume may contain information from several plumes originating from different sources at the surface. These findings certainly help to explain some of the poor correlations obtained in Chapter 1, where measurements were taken at 150m. When compared at the

Figure 3.11. Line density of thermal and moisture plumes as a function of height above wetland.

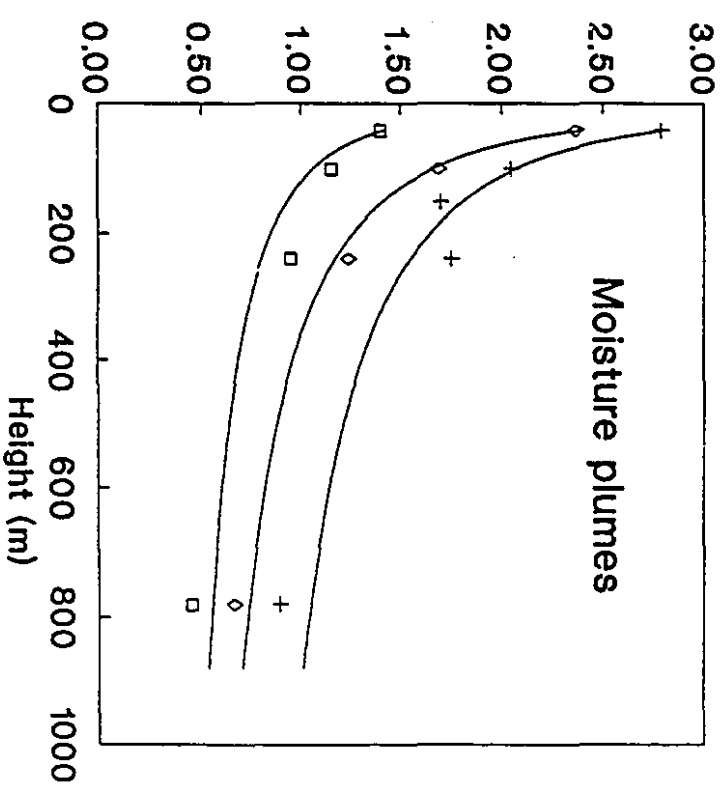
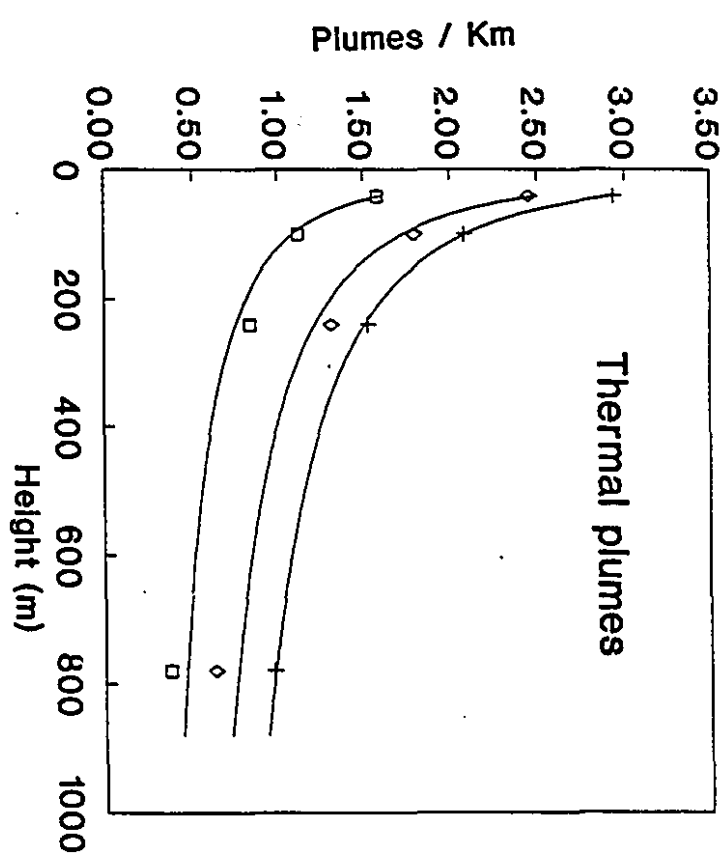
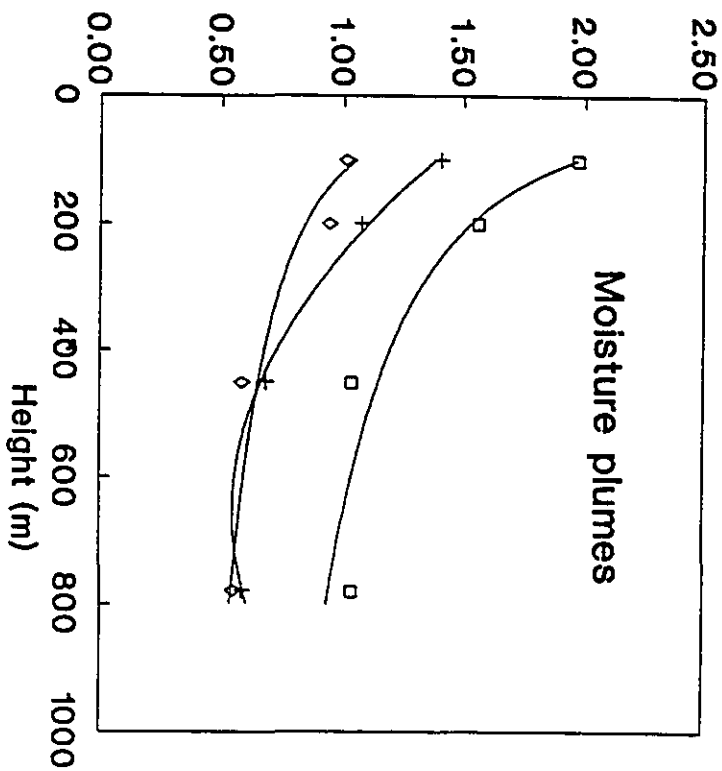
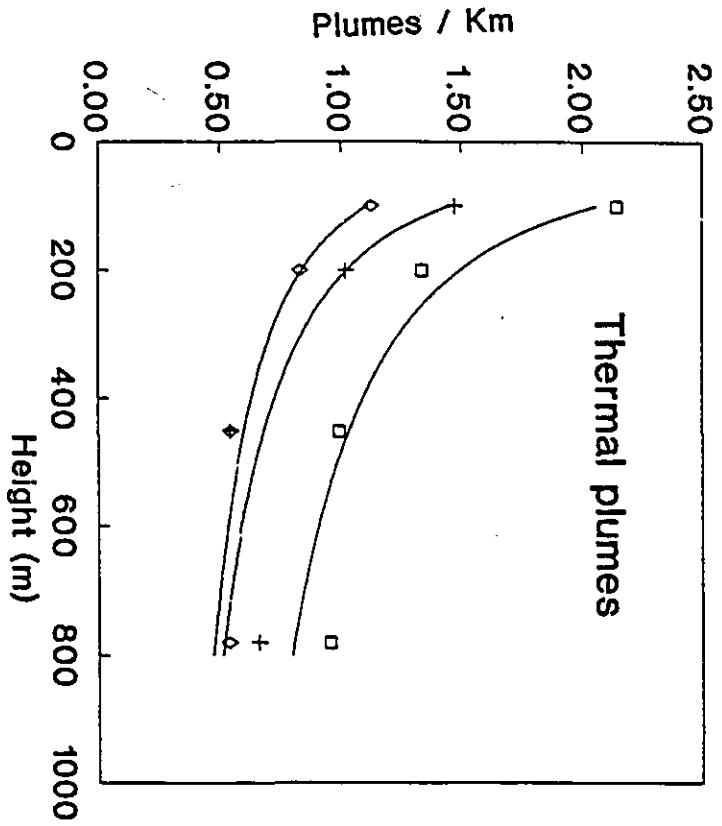


Figure 3.12. Line density of thermal and moisture plumes as a function of height above grassland.



+ th=0.2% flux □ TH=0.0
 ◇ TH=1.0

same height (100m and above), both ecosystems show very similar values. Considering that the surface conditions in terms of moisture availability and vegetation are completely different, it seems that boundary layer dynamics is playing a major role in the reorganization of these turbulent structures.

3.3.5. Mean spacing versus height - The mean spacing of thermal and moisture plumes for both wetland and FIFE grasslands generally increased with altitude (Figures 3.13 and 3.14). Wetland data (Figure 3.13) show nonlinear response near the surface. The same could not be detected over the FIFE site, probably because fewer measurements were taken near the surface. The spacing of thermal plumes was more affected by the threshold of 1 rms, due to the large number of weak datapoints within the structures at higher altitudes. The shape of the curves changed with the choice of threshold for the same reason. Comparison between the ecosystems show the same overall pattern, with the exception of the spacing of moisture plumes after application of the 1 rms threshold. In this case, the wetland data show closer plume spacing near the surface, but the opposite is true at higher altitudes. Two factors seem to be responsible for such scenarios. The higher moisture availability at the surface of the Wetland will provide more moisture excess to the rising air, but less unstable conditions will constrain these plumes to lower altitudes compared to FIFE.

3.3.6. Flux contribution versus height - The relative contributions to the total flux from different classes of plume size are presented in Figures 3.15 and 3.16,

for the wetland and FIFE grasslands, respectively. Near the surface (e.g. wetland at 40m) there is a more significant contribution from smaller turbulent structures. With increasing altitude the larger structures become more important. This has a significant effect on the aircraft sampling criteria at different heights. Longer runs would be required at higher altitudes in order to obtain convergent mean fluxes.

Figure 3.13. Mean spacing of thermal and moisture plumes at different heights above wetland.

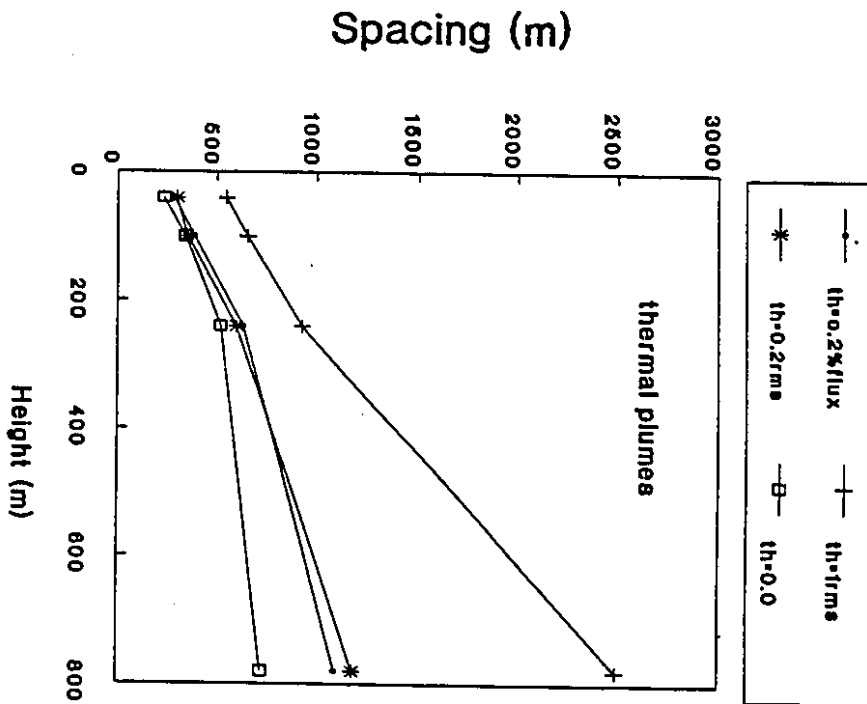
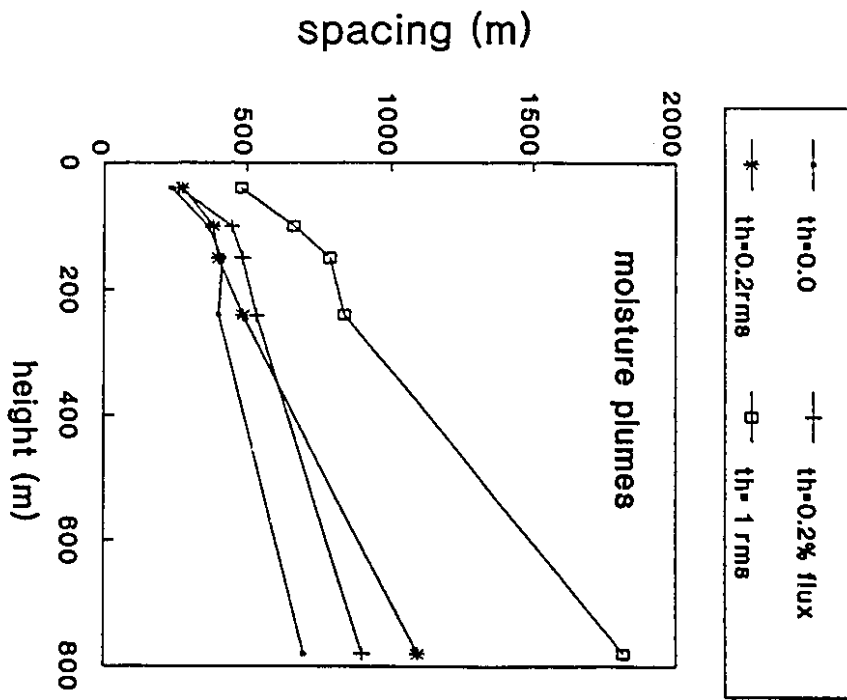


Figure 3.14. Mean spacing of thermal and moisture plumes at different heights above grassland.

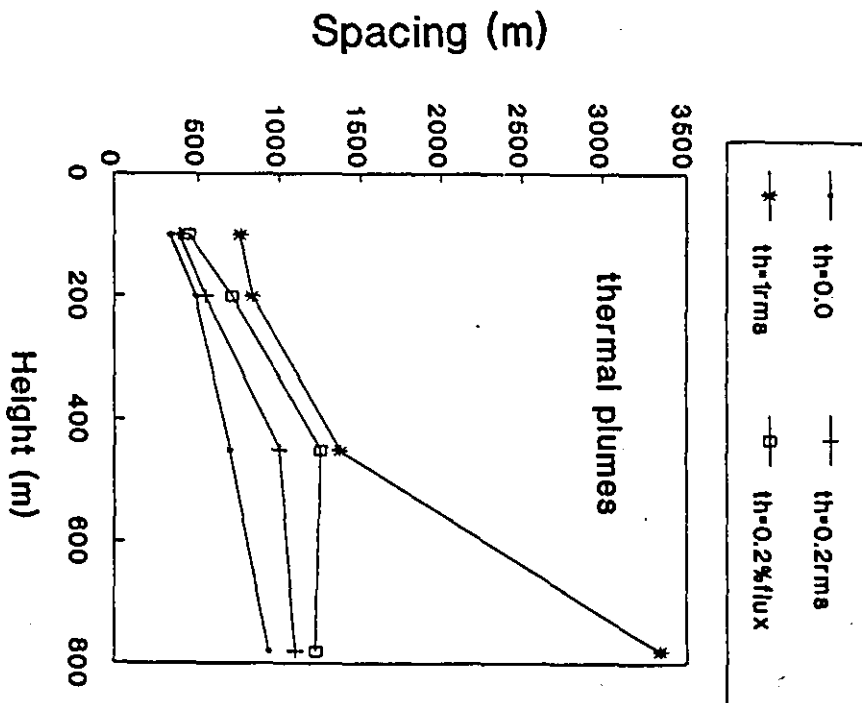
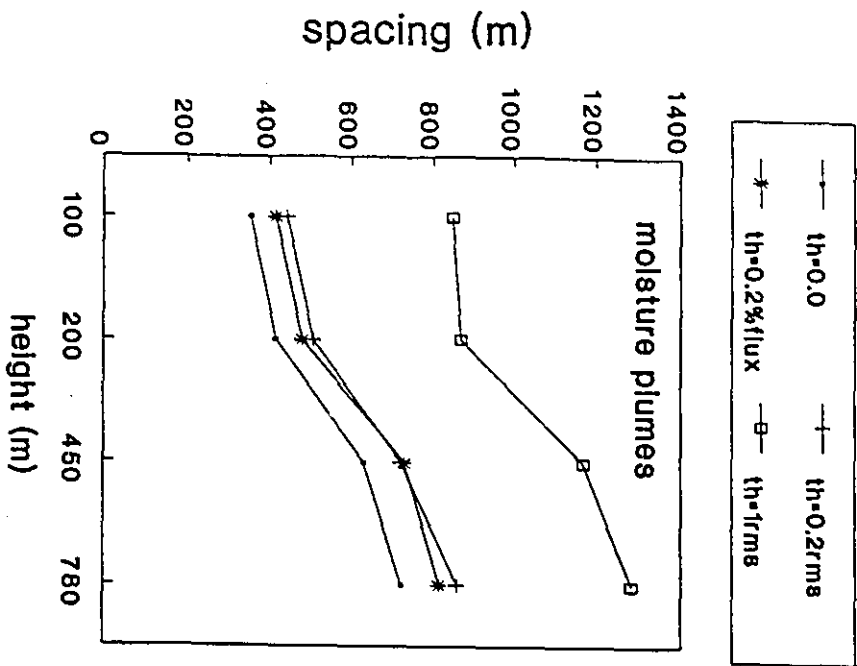


Figure 3.15. Flux contributions from different classes of diameter of thermal and moisture plumes, at four heights above wetland.

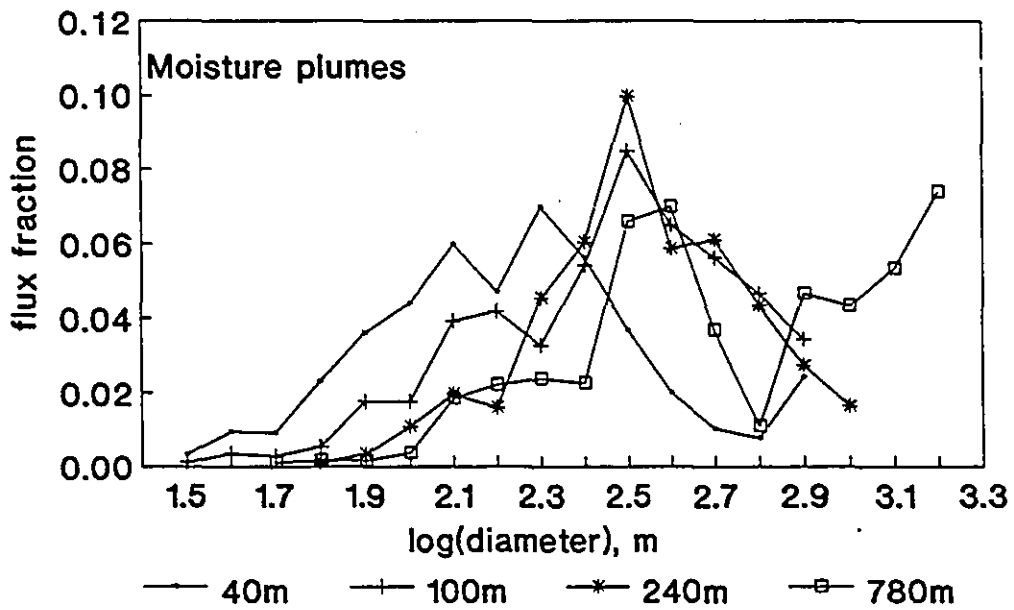
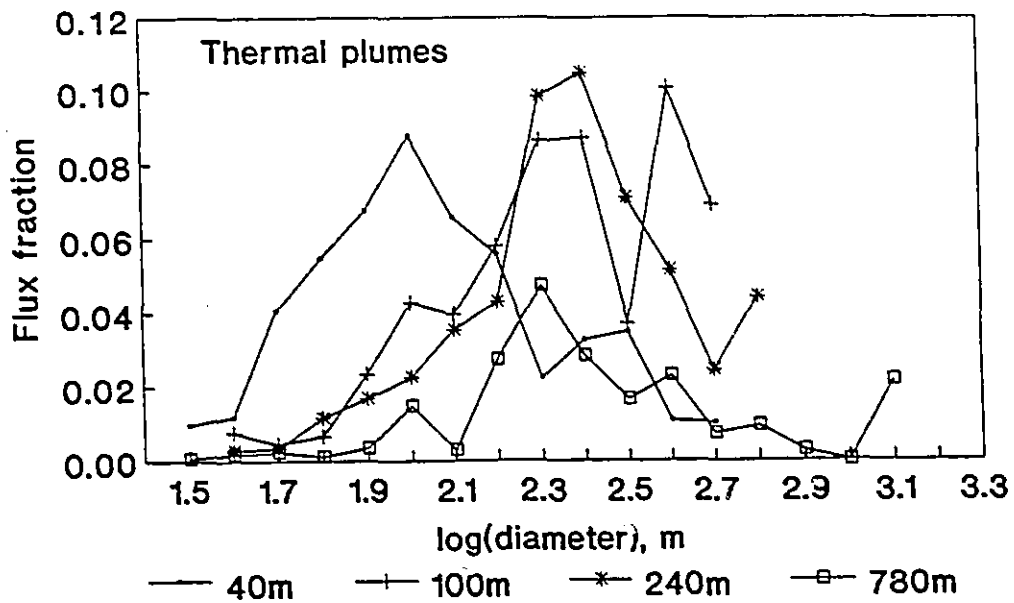
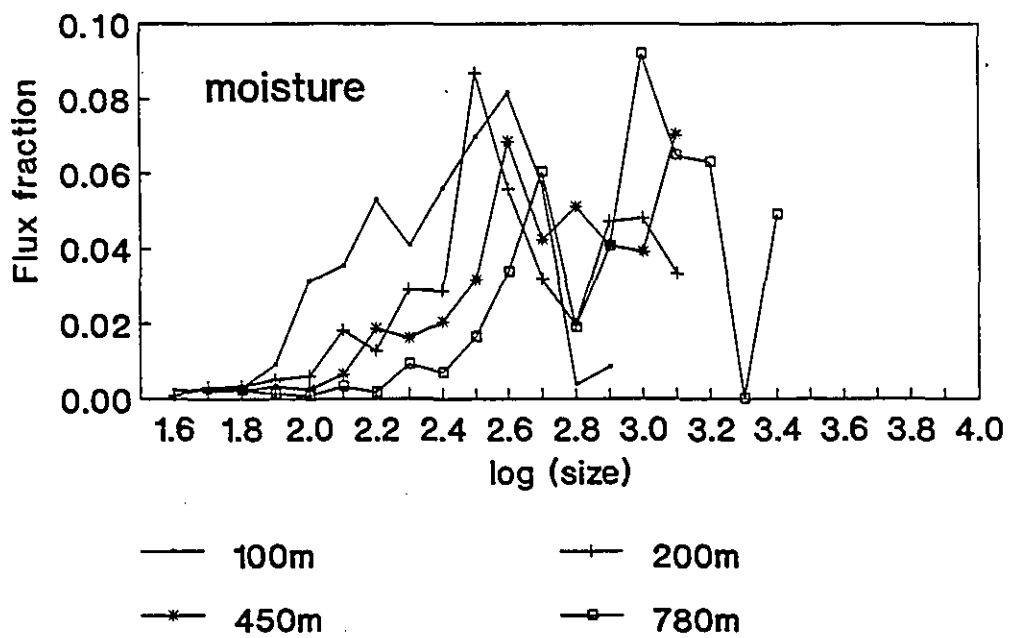
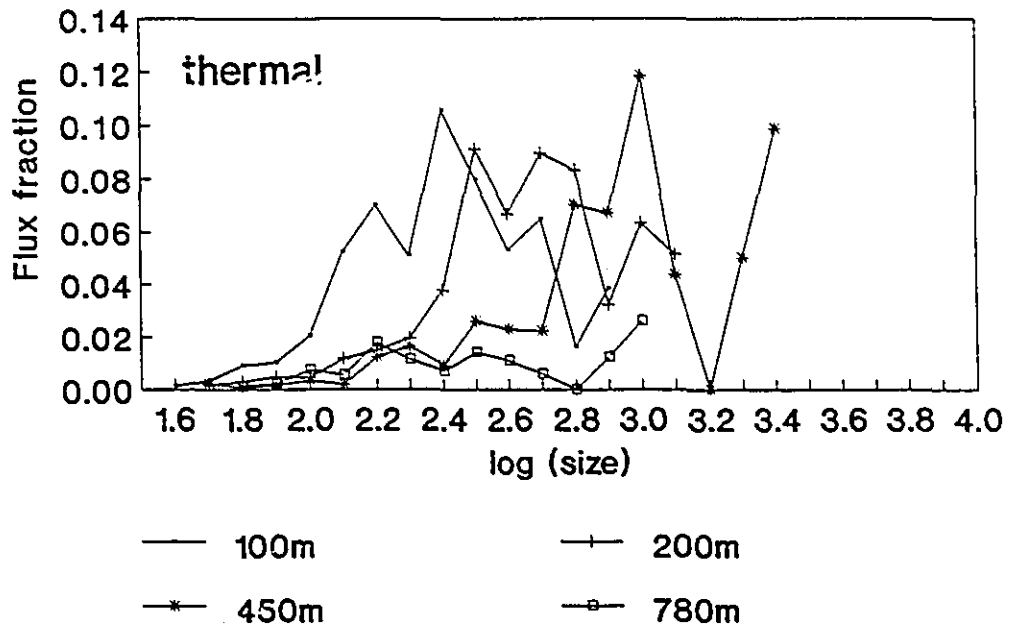


Figure 3.16. Flux contributions from different classes of diameter of thermal and moisture plumes, at four heights above grassland.



3.4. SUMMARY AND CONCLUSIONS

Airborne observations of turbulent fields of velocity, temperature and moisture above wetland, grassland, and irrigated agricultural land have been used to identify coherent thermal and moisture plumes. Sensible heat and water vapor fluxes are estimated through the eddy correlation technique, and the turbulent structures are isolated into the four modes of transport (excess up/down, deficit up/down). The excess-up mode is used to characterize the thermal and moisture plumes, with the other three modes included in the spacing between plumes. Two choices of thresholds are evaluated: (1) a fraction of the flux contribution from entire structures, and (2) a fraction of the standard deviation of the flux prior to the grouping of events into coherent turbulent structures.

These analyses represent a first attempt to statistically describe plume distributions at different heights over varying surface conditions. The results obtained under moderately unstable to stable conditions permit the following general conclusions:

- Plume diameter and spacing from near the surface up to about half of the top of the boundary layer was approximated by distinct lognormal distributions.
- The mean plume diameter and spacing increased with height. The line density of plumes decreased as a power function of height. Flux contribution shifted towards larger turbulent structures with increasing altitude. These findings

suggest the need to define better criteria for aircraft sampling at different heights and for studies relating flux signatures to the surface.

- Despite very different surface conditions, the results of these statistical analyses are very similar over the different ecosystems, suggesting that boundary layer dynamics is playing the major role in the reorganization of the turbulent structures.

3.5. REFERENCES

- Aitchison, J. and J. A. C. Brown. The lognormal distribution. Cambridge University Press, Cambridge, England, 1957.
- Antonia, R. A.. Conditional sampling in turbulence measurement. Ann. Rev. Fluid Mech., 13, 131-156, 1981.
- Benjamin, J. R. and C. A. Cornell. Probability, Statistics, and Decision for Civil Engineers. McGrall-Hill Co., New York, 1971, 684pp.
- Caramori, P. H., P. H. Schuepp, R. L. Desjardins, and J. I. MacPherson. Structural analysis of airborne flux estimates over a region. Submitted to J. Climate.
- Chow, V. T., D. R. Maidment, and L. W. Mays. Applied Hydrology, McGraw Hill, New York, 1988, 572pp.
- Desjardins, R. L., E. J. Brach, P. Alvo, and P. H. Schuepp. Aircraft monitoring of surface CO₂ exchange. Science, 216, 733-735, 1982.
- Desjardins, R. L., J. I. MacPherson, P. H. Schuepp, and F. Karanja. An evaluation of aircraft flux measurements of CO₂, water vapor and sensible heat. Bound.-Layer Meteor., 47, 55-69, 1989.
- Desjardins, R. L., P. H. Schuepp, J. I. MacPherson, and D. J. Buckley. Spatial and temporal variation of the fluxes of carbon dioxide and sensible and latent heat over the FIFE site. J. Geophys. Res., 97(d17), 18,467-18,476, 1992.
- Duncan, M. R.. Structure and contribution of extreme events in airborne carbon dioxide and water vapour flux traces. M.Sc. Thesis, McGill University, Montreal, 1990, 83 pp.
- Duncan, M. R., P. H. Schuepp, J. I. MacPherson, and R. L. Desjardins. Statistical analysis of airborne flux measurements over the FIFE site. 19th. Conf. Agric. and For. Meteor. and Ninth Conf. Biomet. and Aerobiol., Charleston, S. Carolina, Amer. Met. Soc., 129-130, 1989.
- Duncan, M. R., and P. H. Schuepp. A method to delineate extreme structures within airborne flux traces over the FIFE site. J. Geophys. Res., 97(d17), 18,487-18,498, 1992.

- Eloranta, E. W., and D. K. Forrest. Volume-imaging Lidar observations of the convective structure surrounding the flight path of a flux-measuring aircraft. J. Geophys. Res., 97(d17), 18,383-18,394, 1992.
- Grant, D. R.. Some aspects of convection as measured by aircraft. Quart. J. Roy. Meteor. Soc., 91, 268-281, 1965.
- Grant, R.H., G.E. Bertolin, and L.P. Herrington. The intermittent vertical heat flux over a spruce forest canopy. Bound.-Layer Meteor., 35, 317-330, 1986.
- Gurvich, A. S., and A. M. Yaglon. Breakdown of eddies and probability distributions for small scale turbulence. Phys. Fluids Suppl., 10, s59-s65, 1967.
- Khalsa, S. J. S.. The intermittent structure of surface-layer convection over the Tropical Ocean and its significance in the parameterization of turbulent fluxes. Ph.D. Thesis, University of Washington, 1978, 174 pp.
- Khalsa, S. J. S.. Surface-layer intermittency investigated with conditional sampling. Boundary-Layer Meteorol., 19, 135-153, 1980.
- Khalsa, S. J. S. and Businger, J. A.. The drag coefficient as determined by the dissipation method and its relation to Meteorol., 12, 273-297, 1977.
- Kolmogorov, A. N.. A refinement of previous hypotheses concerning the local structure of turbulence in a viscous incompressible fluid at high Reynolds number. J. Fluid Mech., 13, 82-85, 1962.
- Lenschow, D. H., and Stephens, P. L.. Airborne measurements of the structure of thermals. Paper presented at XVI OSTIV Congress 20-29 July 1978, Châteauroux, France.
- Lenschow, D. H., and P. L. Stephens. The role of thermals in the convective boundary-layer. Bound.-Layer Meteorol., 19, 507-532, 1980.
- Mack, A. R., R. L. Desjardins, J. I. MacPherson, and P. H. Schuepp. Relative photosynthetic activity of agricultural lands from airborne carbon dioxide and satellite data. Ins. J. Remote Sens., 11(2), 237-251, 1990.
- MacPherson, J.I.. NAE Twin Otter operations in FIFE. National Aeronautic Establishment Laboratory Technical Report, Ottawa, 1988, 148 pp.
- MacPherson, J.I.. NAE Twin Otter operations in FIFE 1989. Institute for Aerospace

- Research Laboratory Technical Report, Ottawa, 1990, 80 pp.
- MacPherson, J. I.. NRC Twin Otter operations in the 1991 California Ozone deposition experiment. National Research Council Canada, Institute for Aerospace Research, Ottawa, 1992, 213pp.
- Mahrt, L.. Intermittency of atmospheric turbulence. J. Atmos. Sci., 46(1), 79-75, 1989.
- Mahrt, L. and Gibson, W.. Flux decomposition into coherent structures. Boundary-Layer Meteorol., 60, 143-168, 1992.
- Rao, K. N., R. Narashima, and M. A. B. Narayanan. The 'bursting' phenomenon in a turbulent boundary layer. J. Fluid Mech., 48(Part 2), 339-352, 1971.
- Schuepp, P. H., R. L. Desjardins, J. I. MacPherson, J. B. Boisvert, and L. B. Austin. Airborne determination of regional water use efficiency and evapotranspiration: present capabilities and initial field tests. Agric. For. Meteorol., 41, 1-19, 1987.
- Schuepp, P. H., J. I. MacPherson, and R. L. Desjardins. Adjustment of footprint correction for airborne flux mapping over the FIFE site. J. Geophys. Res., 97(d17), 18,455-18,466, 1992.
- Sellers P. J., F. G. Hall, G. Asrar, D. E. Strebel, and R. E. Murphy. The first ISLSCP field experiment (FIFE). Bull. Amer. Meteor. Soc., 69(1), 22-27, 1988.
- Shaw, R.H.. On diffusive and dispersive fluxes in forest canopies. In: The Forest-Atmosphere Interaction, D. Reidel Publ. Co., 1985, pp. 407-419.
- Shaw, W. J., and Businger, J. A.. Intermittency and the organization of turbulence in the near-neutral marine atmospheric boundary layer. J. Atmos. Sci., 42, 2563-2584, 1985.

General Conclusions

In the first Chapter of the thesis, the possibility of using single aircraft overpasses to fit satellite-based models was explored. Data obtained over a mixed of grassland and agricultural land showed a highly nonlinear seasonal relationship between satellite-derived vegetation indices and aircraft-based CO₂ flux estimates. A strong seasonal relationship between NDVI and sensible heat flux was also detected. Overall the data showed appreciable scatter, which was partly attributed to boundary-layer intermittency. Conditional sampling pursued in Chapter 2 revealed that a few extreme events were responsible for a significant fraction of the flux. The detrending procedure affected the flux magnitude and the distribution of plumes along a given run, with consequences for the detection of surface 'signatures'. The analyses also showed that a much clearer signature of the surface emerged when measurements were taken near the surface due to the reorganization that takes place with increasing height. Chapter 3 provides a statistical analysis of moisture and thermal plumes at different heights above grassland, wetland, and partly irrigated agricultural land. The distribution of plumes and spacing between plumes could be approximated by lognormal distributions. It was found that stability plays a major role in plume size, with smaller plumes generally occurring under more unstable conditions. The average number of plumes decreased with height, whereas the number of plumes per sampling length

decreased as a power function of height. As the sampling altitude increased, larger structures became responsible for a more significant fraction of the flux. This shows again the intensive reorganization that takes place near the surface, with weak plumes dissipating or being incorporated into larger ones. Measurements taken at higher altitudes will contain information originated from different sources at the surface, which are difficult to be assigned to a given satellite pixel. This helps to explain some of the poor correlations obtained in Chapter 1 of this thesis. Comparison of the three ecosystems showed very similar general characteristics, suggesting that boundary layer dynamics is playing a major role in the reorganization of the turbulent structures.

Suggestions for future studies

The effect of the windspeed on the surface 'signature' of the plumes should be evaluated. It is expected that as the windspeed increases, lateral mixing will cause a decrease on the correspondence between detected plumes and surface characteristics.

The correspondence between thermal and moisture plumes is another topic that should be investigated. The hypothesis is that the thermal plumes work as a driving force for the moisture plumes, since heating at the surface is the starting mechanism for buoyant rising of air parcels. The geographic location and persistence of the plumes can provide information about existence of preferable surface conditions generating such turbulent structures.

The level up to which a correspondence between surface inhomogeneities and boundary layer structure can be seen could be studied as a function of the dimension of such inhomogeneities and as a function of surface source strength.

The use of other techniques, such as wavelet transforms, could also provide elements for comparison of different methods used to isolate turbulent structures, particularly over conditions where there are non-linear trends of the property being investigated. Fractal analysis might provide a further tool for the description of the spatial relationships between the turbulent structures isolated in this study, and contribute with an alternative description of their statistical properties.

Appendix - Parameters of the lognormal distributions for FIFE, Northern Wetlands, and San Joaquin Valley: mean, standard deviation (STD), variance (VAR), skewness (SKEW), and kurtosis (KURT). Data are presented for different heights and threshold levels.

SITE: FIFE

HEIGHT: 100 m

THRESHOLD	0.0	0.2RMS	1.0RMS	0.2%FLUX
-----------	-----	--------	--------	----------

DIAMETER THERMAL PLUMES

MEAN	2.0083	1.9689	1.8643	2.1579
STD	0.3420	0.3123	0.2390	0.2826
VAR	0.1170	0.0975	0.0571	0.0798
SKEW	0.3072	0.2044	0.3152	0.1351
KURT	-0.6128	-0.8046	-0.3049	-0.2039

DIAMETER MOISTURE PLUMES

MEAN	2.0563	1.9844	1.8507	2.1938
STD	0.3399	0.2777	0.2514	0.2765
VAR	0.1155	0.0770	0.0630	0.0764
SKEW	0.1489	0.1029	0.5321	-0.0305
KURT	-0.8264	-0.7056	-0.2433	-0.4558

SPACING THERMAL PLUMES

MEAN	2.3088	2.4240	2.6415	2.3954
STD	0.4486	0.4831	0.5183	0.4870
VAR	0.2012	0.2333	0.2686	0.2372
SKEW	0.1328	-0.0829	-0.2727	-0.0098
KURT	-0.8684	-0.9684	-0.9347	-1.0480

SPACING MOISTURE PLUMES

MEAN	2.2989	2.3769	2.6600	2.4708
STD	0.4542	0.4886	0.5003	0.4910
VAR	0.2063	0.2388	0.2503	0.2411
SKEW	0.3735	0.0106	-0.2456	0.0153
KURT	-0.1001	-0.8212	-0.4057	-0.3820

SITE: FIFE

HEIGHT: 200 m

THRESHOLD	0.0	0.2RMS	1.0RMS	0.2%FLUX
-----------	-----	--------	--------	----------

DIAMETER THERMAL PLUMES

MEAN	2.1815	2.0919	2.0119	2.3272
STD	0.3921	0.3552	0.3106	0.3337
VAR	0.1537	0.1262	0.0965	0.1113
SKEW	0.0255	0.3333	0.3948	-0.1465
KURT	-0.9669	-0.3740	0.5204	-0.4268

DIAMETER MOISTURE PLUMES

MEAN	2.1331	2.0729	1.9008	2.2716
STD	0.3693	0.3549	0.2979	0.3462
VAR	0.1364	0.1259	0.0887	0.1198
SKEW	0.1797	0.2693	0.3254	-0.0186
KURT	-0.7194	-0.6820	-0.4020	-0.5111

SPACING THERMAL PLUMES

MEAN	2.4722	2.4835	2.6551	2.6283
STD	0.4543	0.5116	0.5434	0.5071
VAR	0.2064	0.2617	0.2953	0.2572
SKEW	-0.2695	-0.1030	-0.4554	-0.3521
KURT	-0.8330	-0.9181	-0.7384	-0.5772

SPACING MOISTURE PLUMES

MEAN	2.3366	2.4686	2.6213	2.5258
STD	0.4967	0.4986	0.6157	0.4847
VAR	0.2467	0.2486	0.3791	0.2349
SKEW	0.1555	-0.1079	-0.2288	-0.0837
KURT	-1.1111	-0.7779	-1.2706	-0.2178

SITE: FIFE

HEIGHT: 450 m

THRESHOLD	0.0	0.2RMS	1.0RMS	0.2%FLUX
-----------	-----	--------	--------	----------

DIAMETER THERMAL PLUMES

MEAN	2.1744	2.1067	2.1201	2.4412
STD	0.4502	0.3824	0.3705	0.4181
VAR	0.2027	0.1463	0.1373	0.1748
SKEW	0.4087	0.2758	-0.0876	0.0220
KURT	-0.5386	-0.8388	-0.7526	-0.5879

DIAMETER MOISTURE PLUMES

MEAN	2.2544	2.1773	2.1129	2.4379
STD	0.4446	0.4022	0.3138	0.3752
VAR	0.1977	0.1617	0.0984	0.1408
SKEW	0.2766	-0.0746	0.2383	-0.0856
KURT	-0.6514	-1.1549	-0.4966	-0.6192

SPACING THERMAL PLUMES

MEAN	2.5756	2.6864	2.8210	2.8802
STD	0.5338	0.5775	0.5989	0.5292
VAR	0.2849	0.3335	0.3586	0.2800
SKEW	-0.0256	-0.2296	-0.4816	-0.7080
KURT	-0.9916	-0.9627	-0.6262	-0.1034

SPACING MOISTURE PLUMES

MEAN	2.4887	2.4532	2.7432	2.6185
STD	0.5506	0.6379	0.6311	0.5111
VAR	0.3031	0.4069	0.3983	0.2613
SKEW	0.0511	0.2398	-0.0644	-0.1661
KURT	-1.1281	-1.4883	-1.4516	-0.7377

SITE: FIFE

HEIGHT: 780 m

THRESHOLD	0.0	0.2RMS	1.0RMS	0.2%FLUX
-----------	-----	--------	--------	----------

DIAMETER THERMAL PLUMES

MEAN	2.0650	2.0697	2.1201	2.0581
STD	0.3632	0.3673	0.3705	0.3627
VAR	0.1319	0.1349	0.1373	0.1316
SKEW	0.1135	0.4798	-0.0876	0.4411
KURT	-0.6073	-0.2599	-0.7526	-0.3484

DIAMETER MOISTURE PLUMES

MEAN	2.2166	2.1186	2.1569	2.511
STD	0.4854	0.4769	0.3777	0.3824
VAR	0.2356	0.2274	0.1462	0.1462
SKEW	0.4791	0.5240	0.1508	0.0963
KURT	-0.6424	-0.9352	-0.9551	-0.7853

SPACING THERMAL PLUMES

MEAN	2.5433	2.5068	3.179	2.7349
STD	0.6711	0.7119	0.9633	0.6072
VAR	0.4503	0.5068	0.9279	0.3687
SKEW	0.1573	0.3897	-1.2319	0.0712
KURT	-1.1367	-1.1938	0.0100	-0.9580

SPACING MOISTURE PLUMES

MEAN	2.4288	2.3905	2.6231	2.5855
STD	0.5306	0.6318	0.6698	0.5993
VAR	0.2816	0.3991	0.4486	0.3591
SKEW	0.2242	0.3488	0.1290	0.0705
KURT	-0.9693	-1.2623	-1.2549	-1.1722

SITE: NORTHERN WETLANDS

HEIGHT: 40 m

THRESHOLD	0.0	0.2RMS	1.0RMS	.2%FLUX
-----------	-----	--------	--------	---------

DIAMETER THERMAL PLUMES

MEAN	1.8905	1.8328	1.7259	1.9490
STD	0.2662	0.2346	0.1881	0.2492
VAR	0.0709	0.0550	0.0354	0.0621
SKEW	0.5720	0.4825	0.6579	0.5350
KURT	0.0961	-0.1579	-0.1816	0.3263

DIAMETER MOISTURE PLUMES

MEAN	1.9419	1.8854	1.7703	1.9907
STD	0.2891	0.2812	0.2299	0.2733
VAR	0.0836	0.0791	0.0599	0.0747
SKEW	0.4832	0.4590	0.6929	0.3905
KURT	0.0128	0.9417	-0.0940	0.0142

SPACING THERMAL PLUMES

MEAN	2.2186	2.2993	2.5706	2.2784
STD	0.3624	0.4017	0.3962	0.3839
VAR	0.1313	0.1614	0.1570	0.1474
SKEW	0.1404	-0.0186	-0.1540	0.2249
KURT	-0.8163	-0.7416	-0.2917	-0.4410

SPACING MOISTURE PLUMES

MEAN	2.1669	2.2459	2.4654	2.2044
STD	0.3959	0.3897	0.4274	0.4060
VAR	0.1567	0.1518	0.1827	0.1649
SKEW	0.5511	0.3902	0.3049	0.5185
KURT	-0.0234	-0.1848	-0.3953	-0.2392

SITE: NORTHERN WETLANDS

HEIGHT: 100 m

THRESHOLD	0.0	0.2RMS	1.0RMS	.2%FLUX
-----------	-----	--------	--------	---------

DIAMETER THERMAL PLUMES

MEAN	2.0242	1.9594	1.8453	2.0959
STD	0.2978	0.2735	0.2336	0.2801
VAR	0.0887	0.0748	0.0545	0.0785
SKEW	0.2301	0.2605	0.2733	0.1223
KURT	-0.6606	-0.6980	-0.7622	-0.6480

DIAMETER MOISTURE PLUMES

MEAN	2.0691	2.0016	1.8035	2.1499
STD	0.3452	0.2797	0.2063	0.3140
VAR	0.1192	0.0782	0.0426	0.0986
SKEW	0.1626	-0.0079	0.1011	-0.0305
KURT	-0.8196	-0.6316	-1.0442	-0.5995

SPACING THERMAL PLUMES

MEAN	2.3595	2.3562	2.6075	2.4038
STD	0.3936	0.4193	0.4663	0.4120
VAR	0.1549	0.1758	0.2175	0.1698
SKEW	0.0876	0.0780	-0.3645	0.0096
KURT	-0.7641	-0.9076	-0.7198	-1.0392

SPACING MOISTURE PLUMES

MEAN	2.3563	2.3751	2.4629	2.4286
STD	0.4254	0.4977	0.5029	0.4464
VAR	0.1810	0.2477	0.2529	0.1993
SKEW	0.1225	-0.1233	0.0178	0.0636
KURT	-0.6689	-1.0350	-0.7383	-0.5084

SITE: NORTHERN WETLANDS

HEIGHT: 240 m

THRESHOLD	0.0	0.2RMS	1.0RMS	.2%FLUX
-----------	-----	--------	--------	---------

DIAMETER THERMAL PLUMES

MEAN	2.1177	2.0552	1.9912	2.1906
STD	0.3325	0.3311	0.2763	0.2954
VAR	0.1106	0.1096	0.0764	0.0873
SKEW	-0.2010	0.1451	-0.0963	-0.2973
KURT	-0.7427	-0.7815	-1.2408	0.3205

DIAMETER MOISTURE PLUMES

MEAN	2.1191	2.0736	1.9307	2.2940
STD	0.3642	0.3469	0.2993	0.2568
VAR	0.1327	0.1203	0.0896	0.0659
SKEW	-0.1525	0.0516	0.2199	-0.1024
KURT	-0.9027	-0.8489	-1.2469	-0.3524

SPACING THERMAL PLUMES

MEAN	2.4377	2.5119	2.6505	2.5508
STD	0.5152	0.5103	0.6039	0.4981
VAR	0.2655	0.2604	0.3647	0.2481
SKEW	0.0493	-0.1765	-0.2576	-0.1732
KURT	-1.0578	-0.9947	-1.0770	-0.7701

SPACING MOISTURE PLUMES

MEAN	2.3816	2.4147	2.7058	2.5069
STD	0.4706	0.5304	0.5809	0.4791
VAR	0.2214	0.2813	0.3375	0.2295
SKEW	-0.1474	-0.1342	-0.6444	-0.2858
KURT	-1.0212	-1.1190	-0.7037	-0.9104

SITE: NORTHERN WETLANDS

HEIGHT: 780 m

THRESHOLD	0.0	0.2RMS	1.0RMS	.2%FLUX
-----------	-----	--------	--------	---------

DIAMETER THERMAL PLUMES

MEAN	2.2059	2.2075	2.0832	2.4255
STD	0.4411	0.4079	0.3881	0.3904
VAR	0.1946	0.1664	0.1506	0.1524
SKEW	0.1915	0.3397	0.1525	0.0895
KURT	-0.6604	-1.1091	-0.9145	-0.2037

DIAMETER MOISTURE PLUMES

MEAN	2.1652	2.1745	1.9678	2.2949
STD	0.4053	0.3653	0.3681	0.3316
VAR	0.1643	0.1334	0.1355	0.1099
SKEW	-0.0028	-0.0350	0.3765	-0.1763
KURT	-0.8098	-0.6258	-1.0109	-0.2341

SPACING THERMAL PLUMES

MEAN	2.5142	2.6787	3.2324	2.7262
STD	0.5762	0.6414	0.4887	0.5752
VAR	0.3320	0.4114	0.2388	0.3308
SKEW	0.0041	-0.0687	0.3247	-0.4391
KURT	-1.0516	-0.9832	-1.1182	-0.7389

SPACING MOISTURE PLUMES

MEAN	2.6053	2.6915	2.8631	2.6485
STD	0.4485	0.6160	0.6192	0.5435
VAR	0.2012	0.3794	0.3834	0.2954
SKEW	-0.0553	0.1523	-0.2529	0.0235
KURT	-0.7942	-0.6248	-1.1446	-0.6349

SITE: SAN JOAQUIN VALLEY

HEIGHT: 30m

THRESHOLD	0.0	0.2RMS	1.0RMS	0.2%FLUX
-----------	-----	--------	--------	----------

DIAMETER THERMAL PLUMES

MEAN	1.9531	1.8837	1.7991	1.9853
STD	0.2874	0.2969	0.2520	0.2872
VAR	0.0826	0.0881	0.0635	0.0825
SKEW	0.1440	0.4749	0.7248	0.1714
KURT	-0.699	-0.604	-0.377	-0.5200

DIAMETER MOISTURE PLUMES

MEAN	1.9066	1.8551	1.7473	1.9423
STD	0.3086	0.265	0.2269	0.2987
VAR	0.0952	0.0703	0.0515	0.0892
SKEW	0.4007	0.4198	1.025	0.3233
KURT	-0.6565	-0.4842	0.6386	-0.4876

SPACING THERMAL PLUMES

MEAN	2.2358	2.339	2.5777	2.2452
STD	0.4627	0.4614	0.5436	0.5316
VAR	0.2141	0.2129	0.2955	0.2826
SKEW	0.317	0.2911	0.0461	0.5579
KURT	-0.4065	-0.1954	-0.1491	-0.4138

SPACING MOISTURE PLUMES

MEAN	2.3039	2.3271	2.553	2.3142
STD	0.4041	0.3868	0.4665	0.3858
VAR	0.1633	0.1496	0.2177	0.1488
SKEW	-0.2508	-0.1958	-0.309	-0.3727
KURT	-0.8167	-0.7736	-0.5311	-0.6888

SITE: SAN JOAQUIN VALLEY

HEIGHT: 60m

THRESHOLD	0.0	0.2RMS	1.0RMS	0.2%FLUX
-----------	-----	--------	--------	----------

DIAMETER THERMAL PLUMES

MEAN	1.9765	1.9143	1.8572	2.0391
STD	0.3125	0.3111	0.2969	0.3039
VAR	0.0976	0.0968	0.0881	0.0924
SKEW	0.3561	0.4735	0.6916	0.2721
KURT	-0.472	-0.6702	-0.3659	-0.522

DIAMETER MOISTURE PLUMES

MEAN	1.9413	1.9101	1.8176	2.0119
STD	0.3619	0.2961	0.2599	0.3175
VAR	0.131	0.0877	0.0675	0.1008
SKEW	0.4857	0.521	0.7446	0.2768
KURT	-0.8428	-0.2622	0.1155	-0.61

SPACING THERMAL PLUMES

MEAN	2.3373	2.4572	2.6505	2.394
STD	0.42	0.4745	0.5552	0.4639
VAR	0.1764	0.2252	0.3082	0.2152
SKEW	0.4581	0.1182	0.1755	0.6062
KURT	-0.0895	-0.2081	-0.5499	0.2494

SPACING MOISTURE PLUMES

MEAN	2.2773	2.3494	2.5973	2.3242
STD	0.4093	0.4261	0.4494	0.4091
VAR	0.1675	0.1816	0.202	0.1674
SKEW	-0.0664	-0.1687	-0.3424	-0.1202
KURT	-0.9267	-0.8622	-0.6125	-0.8782

SITE: SAN JOAQUIN VALLEY

HEIGHT: 100m

THRESHOLD	0.0	0.2RMS	1.0RMS	0.2%FLUX
-----------	-----	--------	--------	----------

DIAMETER THERMAL PLUMES

MEAN	2.0216	1.8632	1.8459	2.058
STD	0.3026	0.2914	0.2844	0.3013
VAR	0.0915	0.0849	0.0809	0.0908
SKEW	0.0475	0.8303	0.7748	0.0949
KURT	-0.7886	0.0499	0.1895	-0.737

DIAMETER MOISTURE PLUMES

MEAN	2.0436	1.8713	1.8302	2.0037
STD	0.2986	0.2939	0.2351	0.2966
VAR	0.0892	0.0864	0.0553	0.088
SKEW	-0.2026	0.5847	0.5044	0.1443
KURT	-0.8406	-0.6295	-0.234	-0.632

SPACING THERMAL PLUMES

MEAN	2.3448	2.4639	2.6482	2.394
STD	0.4854	0.4778	0.5632	0.458
VAR	0.2356	0.2283	0.3172	0.2097
SKEW	0.2812	0.1141	-0.1258	0.07
KURT	-0.2747	-0.3966	-0.7736	-0.2829

SPACING MOISTURE PLUMES

MEAN	2.3305	2.4162	2.6477	2.4046
STD	0.4004	0.4147	0.4808	0.4026
VAR	0.1603	0.172	0.2312	0.1621
SKEW	-0.0599	-0.3184	-0.5974	-0.318
KURT	-0.7223	-0.6535	-0.4545	-0.5513
